# EFFECTS OF AXONAL MISROUTING AT THE OPTIC CHIASM ON MOTOR BEHAVIOR IN ZEBRAFISH LARVAE

---

**DISSERTATION**

**ZUR**

**ERLANGUNG DER NATURWISSENSCHAFTLICHEN DOKTORWÜRDE**
**(DR. SC. NAT.)**

**VORGELEGT DER**

**MATHEMATISCH-NATURWISSENSCHAFTLICHEN FAKULTÄT**

**DER**

**UNIVERSITÄT ZÜRICH**


VON

**SABINA HUBER-REGGI**

VON

MADISWIL BE, RIEHEN BS, LUGANO TI


PROMOTIONSKOMITEE

PROF. DR. STEPHAN C. F. NEUHAUSS (LEITUNG DER DISSERTATION)
PROF. DR. CHRISTIAN GRIMM
PROF. DR. DOMINIK STRAUMANN
PROF. DR. MAARTEN FRENS

**ZÜRICH, 2014**

„…domandato come si generavano i suoni, generosamente rispondeva di sapere alcuni modi, ma che teneva per fermo potervene essere cento altri incogniti ed inopinabili.“

Galileo Galilei,
“Favola dei suoni” dal Saggiatore, 1623

# I TABLE OF CONTENT

# II SUMMARY

A central goal of modern neuroscience is to understand how sensory inputs are decoded and integrated in the brain to produce an appropriate behavior in real time. Sensory information about changes in the environment such as motions, odors or touching objects, is constantly integrated and compared with information on self-generated sensory stimuli such as self-motion in order to constantly adapt behavior. Miswiring of any involved neural circuit disrupts the complex feedback loops and inserts misleading and contradictory information, which may lead to instabilities in motor behavior. In the present PhD Thesis I studied how miswiring of the visual pathways affects ocular motor and postural control of zebrafish larvae.

In the zebrafish mutant *belladonna* (*bel*) pathfinding of optic nerve fibers at the optic chiasm is affected, resulting in a variable fraction of fibers projecting to the wrong brain hemisphere. Whereas in wild-type zebrafish larvae all fibers cross at the optic chiasm and project to the contralateral brain hemisphere, in *bel* some or all fibers project in the wrong hemisphere but to the right topographic place. Additionally, various subtle morphological eye defects and two abnormal ocular motor phenotypes (reversed optokinetic response and spontaneous eye oscillations) have been previously described. The optokinetic response (OKR), an ocular motor behavior that stabilizes the image of a moving visual environment on the retina, is reversed in some larvae as the eyes are moving in the opposite direction to the environment. Moreover, larvae with a reversed OKR additionally display spontaneous eye oscillations (SOs) in the absence of movement in the surroundings. The observed ocular motor behavior abnormalities closely resemble those occurring in human patients suffering from Infantile Nystagmus Syndrome (INS), as shown in Chapter 3 of this thesis. Therefore, *bel* larvae may be a valuable model to study possible mechanisms leading to INS.

In chapter 4 we performed a correlation study between the percentage of misrouting optic nerve fibers and ocular motor behavior. We found a reduction of eye velocity during OKR in larvae with few misprojecting fibers and both a reversed OKR and SOs in larvae with a substantial fraction of misprojecting fibers. A stronger reversed OKR correlated with more frequent SOs. In contrast, additional morphological eye defects did not affect ocular motor behavior although they impaired visual performance. These results confirmed that misrouting of most optic nerve fibers to the wrong hemisphere turns a negative feedback loop, which would aim at stabilizing a moving environment on the retina, into a positive feedback loop which increases motion perception. Motion perception is maintained by the positive feedback loop even if real motion of the environment is discontinued, leading to SOs. In contrast, few misprojecting fibers insert some misleading information into an otherwise still working feedback system, which leads to a reduction of eye velocity during OKR, but not to a positive destabilizing feedback loop.

SOs can assume several different waveforms both in human INS patients and in *bel* larvae. The etiology of single waveforms is unclear and a matter of debate. In Chapter 5 we investigated a possible correlation between individual waveforms and the severity of the morphological phenotype. We found waveforms not to be predictors of the extent of fibers misprojections because most individual larvae displayed all waveforms over a given time span. Instead, we found that waveforms were influenced by viewing conditions.

In Chapter 6 we described a so far not reported deficit in postural control in a subset of *bel* larvae. These larvae display balance defects on the longitudinal body axis during swimming, a condition that had been

previously related to vestibular and somatosensory deficits in other mutants, but never directly to visual defects. Nevertheless, postural control in vertebrates is achieved by integration of inputs originating from different sensory systems, including the visual system. Here, we showed that the behavior is visually-driven in *bel* and occurs in larvae in which more fibers project to one brain hemisphere than to the other. We proposed that asymmetric innervations might lead to imbalance in outputs from the two hemispheres upon visual stimulation and thus to an imbalance of motor commands to the muscles during swimming. These findings may provide the basis for the identification of the circuits involved in visual-postural control in zebrafish. Towards this long-term aim, we worked at establishing calcium imaging in our laboratory to quantify neuronal activity.

# III ZUSAMMENFASSUNG

Ein zentrales Ziel der modernen Neurowissenschaften ist es zu verstehen, wie sensorische Informationen im Gehirn entziffert und integriert werden, um eine angemessene Verhaltensreaktion in Echtzeit zu erzeugen. Sensorische Informationen über Veränderungen in der Umwelt (zum Beispiel Bewegungen, neue Gerüche oder Berührungen) werden kontinuierlich integriert und mit Informationen aus selbsterzeugten Sinnesreizen (zum Beispiel Eigenbewegungen) verglichen. Auf diese Weise wird das Verhalten ständig an die neuen Bedingungen angepasst. Falsche Verknüpfungen in den beteiligten neuronalen Schaltkreisen können die komplexen Rückkopplungen beeinträchtigen, indem irreführende oder widersprüchliche Informationen eingefügt werden. Dies kann zu einer Instabilität des motorischen Verhaltens führen. In der vorliegenden Dissertation untersuchte ich die Auswirkungen von falschen Verknüpfungen der Sehbahn auf die Augenbewegung und die Gleichgewichtskontrolle bei Zebrafischlarven.

In der Zebrafischmutante *belladonna* (*bel*) ist das Wachstum der Sehnervenfasern durch die Sehnervenkreuzung (*chiasma opticum*) beeinträchtigt, was zu einer abnormalen Projektion eines variablen Anteils der Fasern zur falschen Hirnhemisphäre führt. Während in Wildtyp Zebrafischlarven alle Fasern am *chiasma opticum* kreuzen und zur kontralateralen Hirnhemisphäre projizieren, projizieren einige oder alle Fasern in *bel* Larven in die falsche Hemisphäre, dort aber an die korrekte topographische Stelle. Zusätzlich wurden subtile morphologische Augendefekte sowie zwei Augenbewegungsstörungen in *bel* Larven beschrieben. Die erste Augenbewegungsstörung ist eine Seitenverkehrung des optokinetischen Nystagmus (OKN), eine normalerweise kompensatorische Augenbewegung in die Richtung eines sich bewegenden Umfelds, die das Bild auf der Netzhaut stabilisiert. Bei einigen *bel* Larven bewegen sich die Augen in die entgegengesetzte Richtung, was als seitenverkehrter OKN bezeichnet wird. Larven mit einem seitenverkehrten OKN zeigen zudem in Abwesenheit eines bewegten Umfelds spontane Augenoszillationen (Spontannystagmus). Diese Augenbewegungsstörungen ähneln jenen, die in Patienten mit Kongenitalem Nystagmus (KN) beobachtet werden, wie im Kapitel 3 dieser Arbeit gezeigt wird. Auf Grund dieser Ähnlichkeit könnte die *bel* Zebrafischmutante ein wertvolles Modell sein, um mögliche Mechanismen zu untersuchen, die zu den Augenoszillationen bei Patienten mit KN führen.

Das vierte Kapitel dieser Dissertation befasst sich mit einer Korrelationsstudie zwischen der Anzahl der falsch projizierenden Sehnervenfasern und dem Ausmass der Augenbewegungsstörungen bei *bel* Larven. Wir fanden eine Reduktion der Augengeschwindigkeit während des OKN in Larven mit wenigen falsch projizierenden Fasern und sowohl einen seitenvekehrten OKN wie auch Spontannystagmus in Larven mit einem erheblichen Anteil falsch projizierender Fasern. Zudem wurde eine positive Korrelation zwischen der Stärke des inversen OKN und der Anzahl an spontanen Augenbewegungen in einer definierten Zeitspanne gefunden. Wir konnten ebenso zeigen, dass zusätzliche morphologische Augendefekte keinen Einfluss auf Augenbewegungen haben, obwohl sie die Sehleistung beeinträchtigen. Diese Ergebnisse bestätigen, dass die Projektion der Mehrheit der Sehnervenfasern zur falschen Hirnhemisphäre die normalerweise negative Rückkopplungsschleife, die zur Stabilisierung eines sich bewegenden Umfelds auf der Netzhaut zielen würde, in eine positive Rückkopplungsschleife umwandelt. Die positive Rückkopplungsschleife führt dazu, dass die Wahrnehmung einer Bewegung erhalten bleibt auch nachdem die reale Bewegung des Umfelds beendet wurde, was den

Spontannystagmus erklärt. Dagegen fügen wenige falsch projizierende Fasern irreführende Informationen in ein ansonsten funktionierendes Rückkopplungssystem ein. Dies führt zu einer verminderten Stabilisierung des sich bewegenden Umfelds auf der Netzhaut aber nicht zu einer positiven Rückkopplungsschleife.

Die Augenoszillationen können sowohl bei Patienten mit KN wie auch bei *bel* Larven verschiedene Wellenformen annehmen. Die Ätiologie der einzelnen Wellenformen ist unklar und umstritten. In Kapitel 5 untersuchten wir eine mögliche Korrelation zwischen den verschiedenen Wellenformenarten und dem Schweregrad des morphologischen Phänotyps. Wir konnten zeigen, dass die Wellenformen vermutlich nicht den Prozentsatz der falsch projizierenden Sehnervenfasern widerspiegeln, weil die meisten untersuchten einzelnen Larven während einer gewissen Zeitspanne alle Wellenformen zeigten. Stattdessen fanden wir, dass die Wellenformen durch die Sehbedingungen beeinflusst werden.

In Kapitel 6 wird eine bisher nicht beschriebene Gleichgewichtsstörung geschildert, die bei einigen *bel* Larven vorkommt. Diese Larven können das Gleichgewicht bezogen auf ihre longitudinalen Körperachse während des Schwimmens nicht beibehalten. Solch ein Zustand wurde in anderen Zebrafischmutanten auf vestibuläre oder somatosensorische Dysfunktionen zurückgeführt, aber nie direkt mit Fehlsichtigkeit in Verbindung gebracht, obwohl bekannt ist, dass visuelle Informationen die Gleichgewichtskontrolle bei Wirbeltieren stark beeinflussen. Wir konnten zeigen, dass die Gleichgewichtstörung in *bel* visuell bedingt ist und dass sie in Larven vorkommt, in denen die Sehnervenfasern asymmetrisch zu den Hirnhemisphären projizieren. Wir postulieren, dass eine asymmetrische Innervierung der beiden Hemisphären zu einem Ungleichgewicht bei der Efferenz aus den beiden Hemisphären nach einer visuellen Stimulation führen kann. Dies führt dann zu einem Ungleichgewicht bei der Weitergabe des Reizes zu den Muskeln während des Schwimmens. Diese Befunde können als Grundlage für die Ermittlung der Nervenschaltkreise dienen, die an der Gleichgewichtskontrolle mittels visueller Information beteiligt sind. Im Hinblick auf dieses langfristige Ziel haben wir erste Schritte unternommen, um eine Messung der neuronalen Aktivität in unserem Laboratorium zu ermöglichen. Diese Experimente sind am Ende des Kapitels 6 zusammengefasst.

# Chapter 1

# General Introduction

## 1.1 The zebrafish as a model organism in vision research

The zebrafish (*Danio rerio*), a small freshwater teleost native to the Indian subcontinent, was introduced to the scientific world as a vertebrate model organism by George Streisinger with the idea to use it at the larval stage for developmental genetics (Streisinger et al., 1981). Streisinger and colleagues recognized the potential of this little animal, which combines many advantages of vertebrates with amenabilities of invertebrate organisms, such as the possibility to keep it in large numbers with little costs and the ability to produce hundreds of fast developing offsprings every week. 5 days post fertilization (dpf), zebrafish embryos have already developed to freely swimming larvae with a good functioning visual system and a rich repertoire of reflexive behaviors. This allows researchers to study genetic mechanisms and neural circuits regulating behavior without the influence of experience-based behavior and of individual variability inherent of adult stages. Moreover, the embryo develops extra-corporeal and is transparent allowing experimental manipulations and observations. For reviews on the advantages of zebrafish larvae for research on behavioral genetics see (Neuhauss, 2003) and (Wolman and Granato, 2012).

### 1.1.1 The zebrafish visual system

The visual system of the zebrafish consists of the eyes with the retina, the retinofugal projections of the retinal ganglion cells (optic nerve) crossing at the optic chiasm and the visual centers of the brain, which integrate visual inputs (Fig. 1.1). For a review on the zebrafish visual system see (Neuhauss, 2010).

Development of the retina is very fast. At about 28 hours post fertilization (hpf) the first postmitotic retinal cells appear (Nawrocki, 1985), at about 30 hpf the first fibers of the optic nerve appear and reach the visual centers in the brain at about 48 hpf (Burrill and Easter 1994). Signal transmission within the retina is fully functional at 5 dpf (Easter and Nicola, 1996), reviewed in (Neuhauss, 2010).

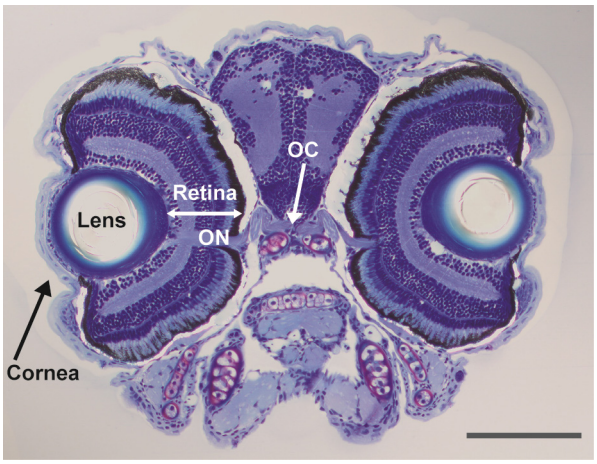


***Figure 1.1: The visual system morphology of a 6-day-old larva.***
*Histological cross section of the forebrain through the eyes. Eye structures, optic nerve and optic chiasm are visible. The optic tectum in the midbrain is not visible in this section. OC, optic chiasm; ON, optic nerve. Scale bar, 100 µm. Adapted from (Neuhauss, 2010).*

The larval retina consists of all typical cell types of a vertebrate retina (Fig. 1.2). As an adaptation to the diurnal life style in slow-moving, stagnant water, zebrafish display an excellent color vision and possess, beside rod photoreceptors (high sensitive photoreceptors working under dim light conditions), cones photoreceptors that absorb light in the red, green, blue and ultraviolet range. Photoreceptors build the outer nuclear layer. The inner nuclear layer contains cell bodies of bipolar, horizontal and amacrine interneurons and of Mueller glial cells, in analogy to the human retina. Those cells form synaptic contacts with photoreceptors in the outer plexiform layer. The last layer closest to the lens consists of displaced amacrine cells and of cell bodies of retinal ganglion cells (RGC), whose dendrites build connections to inner nuclear cells in the inner plexiform layer and whose axons form the optic nerve and leave the retina (reviewed in (Neuhauss, 2010)).

Light enters the eye through the lens and is focused on the photoreceptor outer segments, located on the back of the eye enclosed by the retinal pigment epithelium (RPE, *see* Fig. 1.2), which shields and supports photoreceptors in their function (reviewed in (Strauss, 2005)). In the human retina, cone photoreceptors are densely packed in a central region of the retina, the fovea, onto which the image is focused (Kolb, 2013). In contrast, zebrafish are afoveate animals and cones are distributed in a cone mosaic all over the retina (Lyall, 1957). Photoreceptors hyperpolarize upon light photon absorption and reduce the release of glutamate. Glutamate released into the synaptic cleft causes depolarization of OFF-bipolar cells and hyperpolarization of ON-bipolar cells. Thus, OFF-bipolar cells pass the signal further to RGC when light is reduced (higher amount of glutamate is released by the photoreceptors) and ON-bipolar cells signal an increase in light (a reduced amount of glutamate is released by the photoreceptors). An horizontal network of horizontal and amacrine cells form lateral connections and modulate the signal for contrast enhancement or light adaptation (reviewed in (Neuhauss, 2010)). The fourth cell type in the inner nuclear layer, Mueller glial cells, are essential for retinal development and function (reviewed in (Bringmann et al., 2006)). Recently, Mueller glia have been shown to function as retinal stem cells in response to damage in zebrafish (Bernardos et al., 2007). Axons of RGC form the optic nerve and project to 10 arborization fields in the larval brain (Burrill and Easter, 1994).

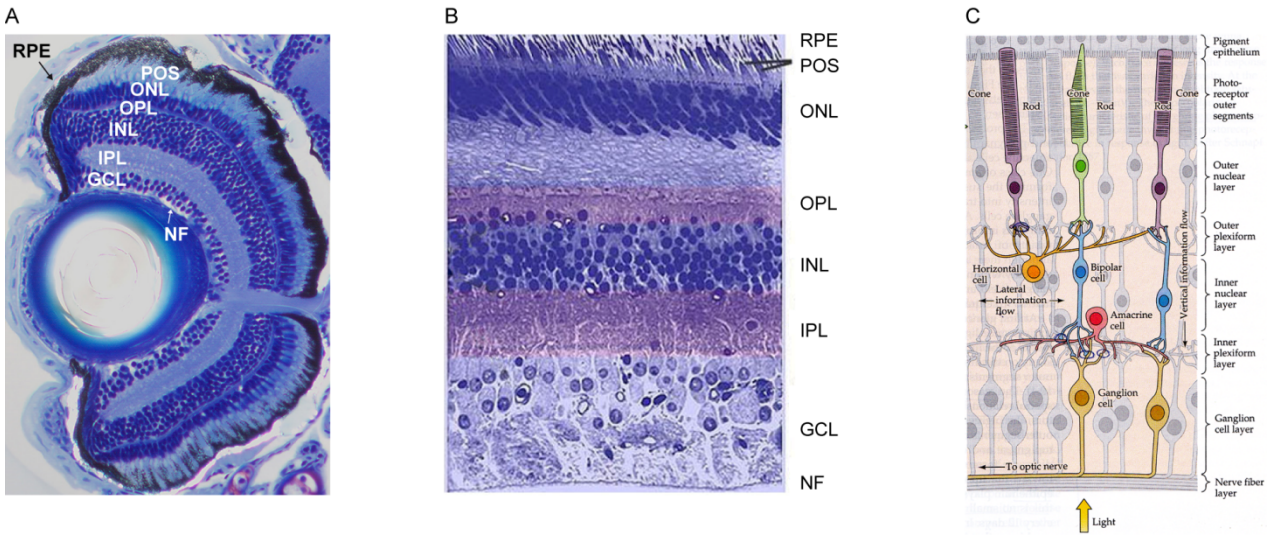


***Figure 1.2: Structure of the retina***
***A, B,*** *Histological sections through the retina of a 6-day-old larval zebrafish (**A**) and through a human retina (**B**). Both retina show a similar layered structure.* ***C****, Schematic drawing of a section showing retinal cell types and circuits. Mueller glial cells, spanning through all retinal layers, are not shown. GCL, ganglion cell layer; INL, inner nuclear layer; IPL, inner plexiform layer; NF, nerve fibers; ONL, outer nuclear layer; OPL, outer plexiform layer; POS, photoreceptor outer segments; RPE, retinal pigment epithelium. (**A,** adapted from (Neuhauss, 2010),* ***B,*** *http://webvision.med.utah.edu/sretina.html (accessed October 31, 2013),* ***C,*** *(Purves et al., 2004)).*

In zebrafish, all optic nerve fibers grow across the midline building a complete optic chiasm. This is different from the projection of optic nerve fibers in humans, where only fibers originating from the nasal retina are crossing, whereas fibers originating from the temporal retina are projecting ipsilaterally (Fig. 1.3) (reviewed in (Williams et al., 2004)). However, this difference is only apparent, since in both cases the visual field is mapped on the contralateral brain hemisphere. The real difference is the position of the eyes: Lateral in zebrafish, frontal in humans. In animals with lateral eyes the visual field is typically projected on the ipsilateral eye and the complete optic nerve needs to cross at the optic chiasm, whereas the more the eyes are shifted to the front, the bigger the portion of visual field that is projected on the temporal retina of the contralateral eye. The fibers originating from this portion of the retina do not cross at the chiasm.

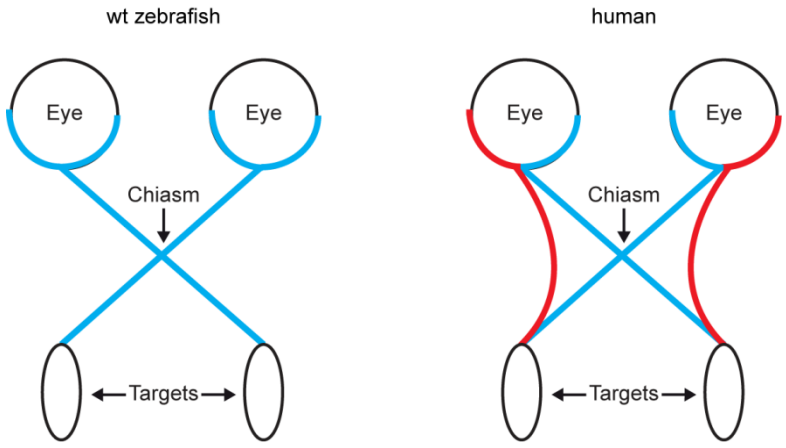


***Figure 1.3: Schematic representation of the projection of optic nerve fibers at the chiasm in zebrafish and humans.***
*In wild type (wt) zebrafish all fibers (blue) cross at the optic chiasm and project to targets in the contralateral brain hemisphere. In humans, fibers originating in the nasal retina (blue) cross at the chiasm, whereas fibers originating in the temporal retina (red) do not cross at the chiasm and project to targets in the ipsilateral brain hemisphere.*

The main target in the brain is the optic tectum, homologous to the superior colliculus, which plays an important role in the control of eye movements (Hall and Moschovakis, 2003). The optic tectum, with a more complex architecture than its mammalian counterpart, receives and integrates different sensory inputs (Hall and Moschovakis, 2003) and mediates a number of complex behaviors such as prey capture. It is likely that the tectum fulfills many integrating tasks that in mammals have been taken over by the neocortex (Friedrich et al., 2010). Terminal arborization in the tectum is topographic with retinal nasal axons terminating in the posterior tectum and temporal axons terminating in the anterior tectum. Analogously, ventral axons terminate in the dorsal tectum and dorsal axons terminate in the ventral tectum (Stuermer, 1988). The tectum consists of a neuropil, the region in which retinal axons project and make connections with dendrites from tectal cells, and the stratum periventriculare (SPV), the region where most of the tectal cells bodies reside (Nevin et al., 2010).

Laser ablation experiments have shown that the tectum is not involved in stereotypical behaviors in response to whole field motion stimuli (Roeser and Baier, 2003). Those behaviors are most likely controlled by one of the nine additional arborization fields of optic nerve projections. Except for one, they are all contralateral and build the pretectal region rostrally to the tectum (Burrill and Easter, 1994).

Pretectum and tectum receive visual inputs from the retina and send motor outputs to several premotor nuclei of the reticulospinal system in the hindbrain via the tectobulbar tract (Wurtz and Albano, 1980; Sato et al., 2007). The zebrafish hindbrain is organized in segments, called rhombomeres, and there is evidence that neurons originating from a specific tectal region project to different segments, suggesting that one visual input could be transformed in several motor outputs (Sato et al. 2007).

The axon guidance mechanisms involved in the control of proper pathfinding of the optic nerve are complex and still not well understood but it is likely that several mechanisms are involved. After exit from the eye, each RGC extends an axon with a motile growth cone at the tip, which senses the environment and finds its way across the optic chiasm to finally reach its target (reviewed in (Tessier-Lavigne and Goodman, 1996; Petros et al., 2008)). Several attractive and repellent guidance molecules and their receptors - expressed by RGCs themselves and by supporting cells such as other neurons or glial cells - may be involved (reviewed in (Petros et al., 2008)) (Dell et al., 2013). The absence or downregulation of some of them can lead to RGCs misrouting (reviewed in (Hutson and Chien, 2002)) (Dell et al., 2013). Recently, Pittman et al. could show that axon-axon interactions with early-born RGCs (pioneer axons) are necessary for later axons to exit the eye and to correctly project to the contralateral brain hemisphere. How pioneer axons lead later axons is still unclear, but cell-adhesion molecules or secretion of attractants could play a role (Pittman et al., 2008). Glial cells have been found in the chiasm (Marcus et al., 1995) and may work as a cellular substrate to build the way for the projecting axons.

Large-scale forward genetic screens coupled with behavioral assays have enabled researchers to isolate mutants with defects in the visual system (reviewed in (Baier, 2000)) and, more specifically, in optic nerve pathfinding (Baier et al., 1996), paving the way to many years of discoveries about development and function of the visual system.

### 1.1.2 Forward genetic screens

In a classical forward genetic screens, spermatogonia of male zebrafish are randomly mutagenized by exposure to N-ethyl-N-nitrosurea (ENU), a potent mutagen. The mutagenized males are then crossed to wild-

type (wt) females, resulting in F1 offspring carrying various mutations. Crossing single members of F1 with wt fish gives raise to strains heterozygous carriers of specific mutations (F2 generation). Inbreeding of F2 carriers gives rise to homozygous mutants that can be screened for specific recessive phenotypes. If two carriers are crossed, around 25 % of the offspring displays the phenotype and can be further analyzed to shed light on the function of the mutated gene (Mullins et al., 1994).

The first pilot screens adapted the approaches already used in invertebrate organisms and isolated mutagenized lines in which homozygous embryos displayed general developmental defects (Mullins et al., 1994; Haffter et al., 1996). Further screenings selected more specific phenotypes affecting several different organs. One of them screened for defective pathfinding of the optic nerve by means of an axon tracing assay (Baier et al., 1996; Karlstrom et al., 1996; Trowe et al., 1996). Fluorescent lipophilic dyes, injected in the eyes of fixed larvae, are taken up by the neurons and transported along the axons so that the labeled projections can be observed a few hours later in a wholemount preparation (Baier et al., 1996).

The screenings described above were mainly based on a morphological characterization of the mutant phenotype and did not allow functional classification. The development of functional assays made it possible to screen for functional visual defects (Brockerhoff et al., 1995; Neuhauss et al., 1999; Muto et al., 2005). In the next section the most important assays are summarized.

### 1.1.3 Functional assays

Functional assays for screening of visual defects make use of innate, i.e. reflexive, responses to visual stimuli. Pioneer work was done by John Clark, a student of George Streisinger, who already described many of the behavioral assays in his doctoral thesis (Clark, 1981).

One of the most robust innate behaviors is the optokinetic response (OKR) (reviewed in (Huang and Neuhauss, 2008)), which is elicited by whole field movement of the environment and is characterized by stereotypic compensating tracking eye movements intercalated by resetting fast movements in the opposite direction, called saccades. In a laboratory environment, the OKR is elicited by a rotating grating pattern around the immobilized larva (Fig. 1.4*A*). Several properties of the pattern - such as contrast, spatial frequency, temporal frequency and color - can be changed to test different aspects of vision, e.g. visual acuity (Haug et al., 2010) or color blindness (Brockerhoff et al., 1997). When only one eye is presented with the moving stimulus, the unstimulated eye will move in the same direction as the stimulated one, although at a lower velocity, indicating that optokinetic eye movements are coupled in zebrafish larvae (Beck et al., 2004; Rinner et al., 2005). This behavioral assay has been successfully applied in several screens (reviewed in (Neuhauss, 2003)), but can be used as well to study how motion is decoded (reviewed in (Maurer et al., 2011)). A review of the main applications of this assay as well as a detailed protocol is found in Chapter 2 of this Thesis.

A similar behavior based on visual motion detection is the optomotor response (OMR) (Fig. 1.4*B*), characterized by a tendency to swim in the direction of a moving whole field environment. In the laboratory, the OMR can be evoked by placing free-swimming larvae in a container with transparent bottom, through which a moving pattern is presented. If larvae can see the moving pattern, they will swim in the direction of the perceived motion and collect at one end of the container (reviewed in (Neuhauss, 2003; Orger et al., 2004)).

OKR and OMR are both based on motion detection. A motion independent visual assay has been developed more recently (Emran et al., 2008). It is based on the visual startle reflex, a motor response to fast changes in illumination. Larval movement during changes in light intensity can be monitored by an automated tracking system (Fig. 1.4*C*). The assay of this behavior, called visual motor response (VMR), has the advantage that allows testing of motion independent visual performance. Moreover, it allows to distinguish ON and OFF responses. On the other hand, VMR is quite unspecific as light can be detected by photoreceptors located outside of the retina (Fernandes et al., 2012) and the behavioral response can be affected by locomotion defects.

The electroretinogram (ERG) allows recording of electrical activity in the outer retina in response to a light flash but independently from behavior. A light stimulation leads to recording of an a- a b-, and a d-wave reflecting responses generated by photoreceptors, ON-bipolar cells, and OFF-bipolar cells, respectively (Fig. 1.4*D*).

Genetic screenings have employed a combination of different assays leading to characterization of the main behavioral properties of zebrafish vision mutants. In one of those screenings, the mutant *belladonna* (*bel*) was characterized (Neuhauss et al., 1999).

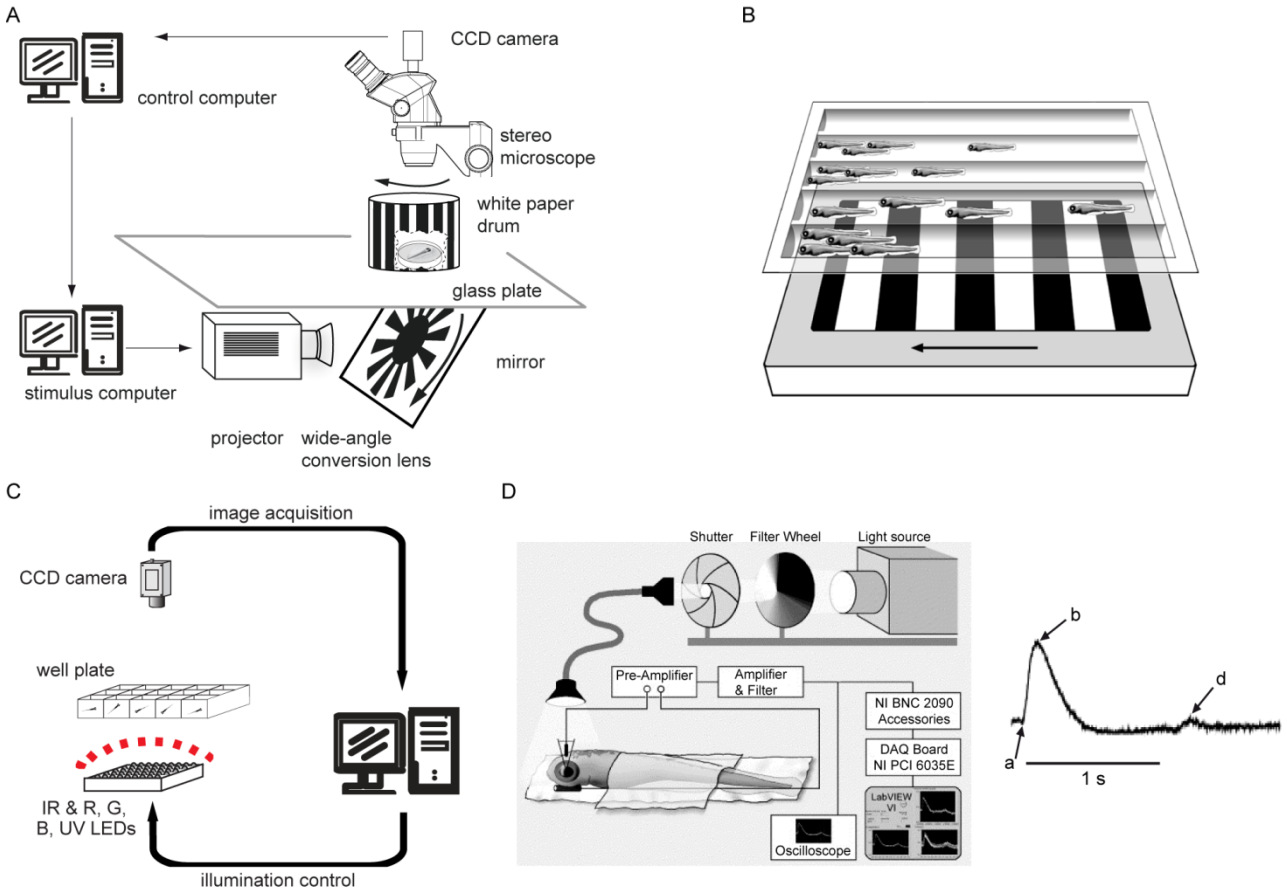


***Figure 1.4: Assays for testing visual performance in zebrafish larvae.***
***A,*** *Setup to elicit and record the optokinetic response (OKR).* ***B,*** *Screening of optomotor response (OMR) in groups of larvae.* ***C,*** *Setup for testing visual motor responses (VMR) in several larvae simultaneously.* ***D,*** *Schema of the working method to measure the electroretinogram (ERG). The light flash triggers an electrical response in the retina characterized by an a-, a b-, and a d-wave reflecting responses generated by photoreceptors, ON-bipolar cells and OFF-bipolar cells, respectively. (**A,** Adapted from (Mueller and Neuhauss, 2010);* ***B,*** *from (Neuhauss, 2003);* ***C,*** *by K. Müller, adapted from (Haug, 2012);* ***D,*** *adapted from (Makhankov et al., 2004)).*

## 1.2 The mutant *belladonna*

The *bel* mutant was first identified in a screening of mutations affecting optic nerve pathfinding (Karlstrom et al., 1996). The mutant was named for an abnormal gap between the lens and the pigmented epithelium causing the pupil to appear dilated, a well known effect of extracts from the plant *atropa belladonna* after ingestion (Feinsod, 2000; Duncan and Collison, 2003). In *bel* larvae a variable fraction of optic nerve fibers did not cross the midline and instead projected to the topographically correct position in the ipsilateral tectum. In contrast to other mutants with a similar phenotype, *bel* larvae did not show general midline defects (Karlstrom et al., 1996).

The *bel* mutant carries a recessive mutation in the zebrafish *lhx2* homolog (Seth et al., 2006), a Lim domain homeobox transcription factor, member of a transcription factor family that is involved in neural patterning, cell fate determination and axon pathfinding (Sockanathan, 2003). Detailed analysis of eye and forebrain morphology displayed acellular aggregates near the lens, slightly disorganized Mueller glial cells, forebrain

patterning defects and highly disorganized glial bridges at the chiasm at 21 hpf (thus prior to optic nerve patterning). Expression analysis of guidance molecules revealed that some of them (*sema3d*, *netrin1a* and *slit2*) are mis-expressed in the chiasm region but others are not affected (Seth et al., 2006). Taken together, these data indicate that *lhx2* in zebrafish is involved in eye morphogenesis and midline pathfinding by regulating some aspects of axon guidance (Seth et al., 2006).

Functional analysis revealed that *bel* larvae displayed OMR and an ERG response, indicating that those mutants do have a functional visual system. Intriguingly, a subset of *bel* larvae displayed a peculiar reversal of the OKR that had never been observed in wt or in other mutants. The tracking eye movements looked normal but the direction was opposite to the direction of the visual stimulus (Neuhauss et al., 1999). After that a correlation study showed that achiasmatic larvae (i.e. larvae in which all optic nerve fibers do not cross the chiasm) presented a reversed OKR, the authors suggested that misrouting of optic nerve projections may reverse a controlling negative feedback loop, which normally would have the function to regulate compensatory eye movements in order to stabilize the retinal slip, i.e. the moving image on the retina (Neuhauss et al., 1999; Rick et al., 2000).

A few years later a new study in our group described spontaneous eye oscillations (SOs) in the absence of environmental motion in *bel* mutants with a reversed OKR. In this study, both OKR reversal and SOs were shown to depend on vision and to be contrast sensitive. A quantitative mathematical model was able to simulate the observed SOs by reversing the signal of the retinal slip velocity, adding evidence to the hypothesis that misrouting of the optic nerve fibers may affects the sensorimotor feedback loop. In larvae with ipsilateral projections, the visual input reaches the wrong brain hemisphere, leading to an inverted perception of motion. The attempt to compensate the retinal slip actually results in its increase. Thus, a normally negative feedback loop is turned into a positive one (Huang et al., 2006).

The observed SOs closely resembled spontaneous eye movements displayed by human patients with Infantile Nystagmus Syndrome (INS). Since reversed OKR and misrouting of optic nerve fibers have been observed in some INS patients, *bel* was suggested as a putative animal model to study the etiology of this syndrome (Rick et al., 2000; Huang et al., 2006).

## 1.3 Infantile Nystagmus Syndrome

INS is a congenital ocular motor disorder characterized by involuntary conjugate, predominantly horizontal oscillations of the eyes. In contrast to acquired nystagmus, which arises later in life as a consequence of an accompanying neurological disorder (Stahl et al., 2000), infantile nystagmus is already present at birth or arises during the first months of life (Gresty et al., 1984; Maybodi, 2003). Prevalence is around 2 per 1000 individuals (Sarvananthan et al., 2009). INS leads to a decreased motion perception, reduced visual acuity, and, in some cases, postural control problems (Dell'Osso, 1991), affecting visual performance (incl. reading performance), the ability to drive a car, and general occupational and social functioning (Pilling et al., 2005; McLean et al., 2012; Barot et al., 2013). Moreover, INS is often associated with visuosensory abnormalities affecting the cornea, lens, retina or optic nerve, such as aniridia, fovea hypoplasia and misprojection of optic nerve fibers. However, in many cases no abnormalities besides eye oscillations have been found and patients have been classified as idiopathic (Khanna and Dell'Osso, 2006).

The etiology of INS is poorly understood but the broad range of accompanying symptoms suggests that eye oscillations may be provoked by different mechanisms. Varying hypotheses circulate in the field (reviewed in (Abadi, 2002)) and it may well be that many of them are explaining different etiologies of eye oscillations. However, most hypotheses are based on mathematical modeling and the lack of a suitable animal model makes their validation difficult.

Recently, genetic analysis of affected families has helped toward a better biological understanding of the syndrome. Mutations in the gene encoding FERM domain-containing 7 protein (*FRMD7*) have been related to idiopathic forms of INS (Tarpey et al., 2006; Watkins et al., 2012). FRMD7 is involved in neuronal outgrowth and development, suggesting a role in neuronal network formation (Betts-Henderson et al., 2010). Moreover, several genes associated to accompanying disorders such as albinism, fovea hypoplasia and achromatopsia have been discovered (reviewed in (Proudlock and Gottlob, 2011)).

In a recent large-scale survey, albinism was found to be the most common nystagmus-associated condition among children younger than 18 with a prevalence of 3.2 per 10000 (Sarvananthan et al., 2009). Albinism is a group of inherited disorders in which melanin production is affected. Oculocutaneus albinism is characterized by the absence of pigment in skin, hairs and iris and by several ocular phenotypes. In contrast, in ocular albinism only the eyes are affected. Ocular findings include iris transillumination defects, high refractive error, strabismus, fundal hypopigmentation, foveal hypoplasia and excessive crossing of optic nerve fibers at the optic chiasm (reviewed in (Summers, 2009)). The etiology of spontaneous eye oscillations in albinism is still not known but misrouting of the optic nerve fibers could play a role (Collewijn et al., 1978; Winterson and Collewijn, 1981). Optic nerve misrouting is also associated to other forms of infantile nystagmus, such as Congenital Stationary Night Blindness (Tremblay et al., 1996), achiasmia (Apkarian et al., 1994) or other forms of chiasmal misrouting not related to albinism (McCarty et al., 1992; van Genderen et al., 2006). Misrouting of the optic nerve is not diagnosed routinely in INS patients and, if so, mostly by means of Visual Evoked Potentials (VEP), electrical potentials in the visual cortex that are triggered by short visual stimuli. VEP is an indirect way of detecting misrouting of the optic nerve and its efficacy is controversial (von dem Hagen et al., 2008) making misrouting of the optic nerve a possibly under-diagnosed condition in INS patients.

Eye oscillations in human INS can assume different waveforms, which have been classified by Dell'Osso and Daroff (Dell'Osso and Daroff, 1975). Decades of debates followed about the importance of those waveforms for determination of their cause (Optican and Zee, 1984; Hertle and Dell'Osso, 1999; Jacobs and Dell'Osso, 2004; Dell'Osso, 2006; Dell'Osso et al., 2007; Akman et al., 2012). Some researchers suggested that different waveforms could be correlated to different underlying conditions (Thomas et al., 2008; Kumar et al., 2011), but others did not find such a correlation (Yee et al., 1976; Abadi and Bjerre, 2002).

## 1.4 Aims of this thesis

This thesis aimed at using the zebrafish mutant *belladonna* to study the effects of optic nerve miswiring on behavior, whereby two aspects were investigated: Ocular motor behavior and postural control. These data not only help giving new insights in a possible mechanism underlying INS but may be also of interest for studies on how the brain deals with and adapts to conflicting inputs.

As mentioned above, ocular motor behavior can be quantified in a laboratory setting. In Chapter 2 the characteristics of ocular motor behavior are summarized and detailed procedures to elicit, influence, and quantify eye movements are explained. This chapter was published as a book section in *Methods in Molecular Biology*.

In order to establish *bel* mutant as a model to study possible mechanisms underlying INS, waveform characteristics of SOs needed to be described and compared to eye oscillations in human patients. In Chapter 3 we qualitatively compared waveforms recorded in zebrafish and human and show that zebrafish waveforms include all features typical of INS. This chapter is an adapted version of a publication in the *Annals of the New York Academy of Science*, resulting from a joint work with the Neurology Department of the University Hospital Zurich.

*bel* homozygous mutants display a variety of ocular motor phenotypes as well as a variable number of misrouting optic nerve fibers (Rick et al., 2000; Huang et al., 2006). Therefore, the mutant may be suitable to study how misrouting of the optic nerve fibers affects ocular motor behavior. In chapter 4, we studied the etiology of SOs and we performed a correlation study between fraction of misrouting optic nerve fibers, OKR characteristics and occurrence of SOs. This work was published in *Journal of Neuroscience*. In chapter 5, we quantified the occurrence of different SOs waveforms in single fish under different conditions to answer the question whether different waveforms mirror a specific morphological phenotype or are influenced by environmental factors. This manuscript has been submitted for publication to *Investigative Ophthalmology & Visual Sciences*.

In chapter 6 a so far not reported deficit in postural control in a subset of *bel* mutants is described. Those larvae show deficits in postural control on the longitudinal body axis, a condition that had been previously related to vestibular deficits (Whitfield et al., 1996) but never directly to visual defects. Here, we aimed at studying the influence of vision and misrouting optic nerve fibers on postural control. This work may provide the basis for the identification of the circuit involved in visual-postural control in zebrafish. As such studies would benefit from calcium imaging experiments to quantify neural activity, the principal steps toward the implementation of this technique in our laboratory are presented in the second part of chapter 6.

## 1.5 References

Abadi RV (2002) Mechanisms underlying nystagmus. J R Soc Med 95:231–234.

Abadi RV, Bjerre A (2002) Motor and sensory characteristics of infantile nystagmus. Br J Ophthalmol 86:1152–1160.

Akman OE, Broomhead DS, Abadi RV, Clement RA (2012) Components of the neural signal underlying congenital nystagmus. Exp Brain Res 220:213–221.

Apkarian P, Bour L, Barth PG (1994) A unique achiasmatic anomaly detected in non-albinos with misrouted retinal-fugal projections. Eur J Neurosci 6:501–507.

Baier H (2000) Zebrafish on the move: towards a behavior-genetic analysis of vertebrate vision. Curr Opin Neurobiol 10:451–455.

Baier H, Klostermann S, Trowe T, Karlstrom RO, Nusslein-Volhard C, Bonhoeffer F (1996) Genetic dissection of the retinotectal projection. Development 123:415–425.

Barot N, McLean RJ, Gottlob I, Proudlock FA (2013) Reading performance in infantile nystagmus. Ophthalmology 120:1232–1238.

Beck JC, Gilland E, Tank DW, Baker R (2004) Quantifying the ontogeny of optokinetic and vestibuloocular behaviors in zebrafish, medaka, and goldfish. J Neurophysiol 92:3546–3561.

Bernardos RL, Barthel LK, Meyers JR, Raymond PA (2007) Late-stage neuronal progenitors in the retina are radial Müller glia that function as retinal stem cells. J Neurosci 27:7028–7040.

Betts-Henderson J, Bartesaghi S, Crosier M, Lindsay S, Chen HL, Salomoni P, Gottlob I, Nicotera P (2010) The nystagmus-associated FRMD7 gene regulates neuronal outgrowth and development. Hum Mol Genet 19:342–351.

Bringmann A, Pannicke T, Grosche J, Francke M, Wiedemann P, Skatchkov SN, Osborne NN, Reichenbach A (2006) Müller cells in the healthy and diseased retina. Prog Retin Eye Res 25:397–424.

Brockerhoff SE, Hurley JB, Janssen-Bienhold U, Neuhauss SC, Driever W, Dowling JE (1995) A behavioral screen for isolating zebrafish mutants with visual system defects. Proc Natl Acad Sci U S A 92:10545–10549.

Brockerhoff SE, Hurley JB, Niemi GA, Dowling JE (1997) A new form of inherited red-blindness identified in zebrafish. J Neurosci 17:4236–4242.

Burrill JD, Easter, S. S., Jr. (1994) Development of the retinofugal projections in the embryonic and larval zebrafish (Brachydanio rerio). J Comp Neurol 346:583–600.

Clark DT (1981) Visual responses in developing zebrafish (Brachydanio rerio). PhD Thesis. University of Oregon.

Collewijn H, Winterson BJ, Dubois MF (1978) Optokinetic eye movements in albino rabbits. inversion in anterior visual field. Science 199:1351–1353.

Dell AL, Fried-Cassorla E, Xu H, Raper JA (2013) cAMP-induced expression of neuropilin1 promotes retinal axon crossing in the zebrafish optic chiasm. J Neurosci 33:11076–11088.

Dell'Osso LF (1991) Eye movements, visual acuity and spatial constancy. Acta Neurol Belg 91:105–113.

Dell'Osso LF (2006) Biologically relevant models of infantile nystagmus syndrome. the requirement for behavioral ocular motor system models. Semin Ophthalmol 21:71–77.

Dell'Osso LF, Daroff RB (1975) Congenital nystagmus waveforms and foveation strategy. Doc Ophthalmol 39:155–182.

Dell'Osso LF, Hertle RW, Daroff RB (2007) "Sensory" and "motor" nystagmus. erroneous and misleading terminology based on misinterpretation of David Cogan's observations. Arch Ophthalmol 125:1559–1561.

Duncan G, Collison DJ (2003) Role of the non-neuronal cholinergic system in the eye: a review. Life Sci 72:2013–2019.

Easter SS Jr, Nicola GN (1996) The development of vision in the zebrafish (Danio rerio). Dev Biol 180:646–663.

Emran F, Rihel J, Dowling JE (2008) A behavioral assay to measure responsiveness of zebrafish to changes in light intensities. J Vis Exp 20: e923.

Feinsod M (2000) The blind beautiful eye. J Neuroophthalmol 20:22–24.

Fernandes AM, Fero K, Arrenberg AB, Bergeron SA, Driever W, Burgess HA (2012) Deep brain photoreceptors control light-seeking behavior in zebrafish larvae. Curr Biol 22:2042–2047.

Friedrich RW, Jacobson GA, Zhu P (2010) Circuit neuroscience in zebrafish. Curr Biol 20:R371-81.

Gresty M, Page N, Barratt H (1984) The differential diagnosis of congenital nystagmus. J Neurol Neurosurg Psychiatry 47:936–942.

Haffter P, Granato M, Brand M, Mullins MC, Hammerschmidt M, Kane DA, Odenthal J, van Eeden, F. J., Jiang YJ, Heisenberg CP, Kelsh RN, Furutani-Seiki M, Vogelsang E, Beuchle D, Schach U, Fabian C, Nusslein-Volhard C (1996) The identification of genes with unique and essential functions in the development of the zebrafish, Danio rerio. Development 123:1–36.

Hall WC, Moschovakis AK (2003) The Superior Colliculus. New Approaches for Studying. London: CRC Press.

Haug MF (2012) Molecular Dissection of Light Perception in Zebrafish. PhD Thesis. Zurich.

Haug MF, Biehlmaier O, Mueller KP, Neuhauss SC (2010) Visual acuity in larval zebrafish. behavior and histology. Front Zool 7:8.

Hertle RW, Dell'Osso LF (1999) Clinical and ocular motor analysis of congenital nystagmus in infancy. J AAPOS 3:70–79.

Huang YY, Neuhauss SC (2008) The optokinetic response in zebrafish and its applications. Front Biosci 13:1899–1916.

Huang YY, Rinner O, Hedinger P, Liu SC, Neuhauss SC (2006) Oculomotor instabilities in zebrafish mutant belladonna. a behavioral model for congenital nystagmus caused by axonal misrouting. J Neurosci 26:9873–9880.

Hutson LD, Chien C (2002) Wiring the zebrafish: axon guidance and synaptogenesis. Curr Opin Neurobiol 12:87–92.

Jacobs JB, Dell'Osso LF (2004) Congenital nystagmus. hypotheses for its genesis and complex waveforms within a behavioral ocular motor system model. J Vis 4:604–625.

Karlstrom RO, Trowe T, Klostermann S, Baier H, Brand M, Crawford AD, Grunewald B, Haffter P, Hoffmann H, Meyer SU, Muller BK, Richter S, van Eeden, F. J., Nusslein-Volhard C, Bonhoeffer F (1996) Zebrafish mutations affecting retinotectal axon pathfinding. Development 123:427–438.

Khanna S, Dell'Osso LF (2006) The diagnosis and treatment of infantile nystagmus syndrome (INS). ScientificWorldJournal 6:1385–1397.

Kolb H (2013) Simple Anatomy of the Retina. http://webvision.med.utah.edu/book/part-i-foundations/simple-anatomy-of-the-retina/. Accessed Oct 31, 2013.

Kumar A, Gottlob I, McLean RJ, Thomas S, Thomas MG, Proudlock FA (2011) Clinical and oculomotor characteristics of albinism compared to FRMD7 associated infantile nystagmus. Invest Ophthalmol Vis Sci 52:2306–2313.

Lyall AH (1957) Cone Arrangements in Teleost Retinae. Quarterly Journal of Microscopical Science s3-98:189–201.

Makhankov YV, Rinner O, Neuhauss SC (2004) An inexpensive device for non-invasive electroretinography in small aquatic vertebrates. J Neurosci Methods 135:205–210.

Marcus RC, Blazeski R, Godement P, Mason CA (1995) Retinal axon divergence in the optic chiasm: uncrossed axons diverge from crossed axons within a midline glial specialization. J Neurosci 15:3716–3729.

Maurer CM, Huang YY, Neuhauss SC (2011) Application of zebrafish oculomotor behavior to model human disorders. Rev Neurosci 22:5–16.

Maybodi M (2003) Infantile-onset nystagmus. Curr Opin Ophthalmol 14:276–285.

McCarty JW, Demer JL, Hovis LA, Nuwer MR (1992) Ocular motility anomalies in developmental misdirection of the optic chiasm. Am J Ophthalmol 113:86–95.

McLean RJ, Windridge KC, Gottlob I (2012) Living with nystagmus. a qualitative study. Br J Ophthalmol 96: 981-986.

Mueller KP, Neuhauss SC (2010) Quantitative measurements of the optokinetic response in adult fish. J Neurosci Methods 186:29–34.

Mullins MC, Hammerschmidt M, Haffter P, Nusslein-Volhard C (1994) Large-scale mutagenesis in the zebrafish. in search of genes controlling development in a vertebrate. Curr Biol 4:189–202.

Muto A, Orger MB, Wehman AM, Smear MC, Kay JN, Page-McCaw PS, Gahtan E, Xiao T, Nevin LM, Gosse NJ, Staub W, Finger-Baier K, Baier H (2005) Forward genetic analysis of visual behavior in zebrafish. PLoS Genet 1:e66.

Nawrocki LW (1985) Development of the neural retina in the zebrafish, Brachydanio rerio. PhD Thesis. Eugene.

Neuhauss SC (2003) Behavioral genetic approaches to visual system development and function in zebrafish. J Neurobiol 54:148–160.

Neuhauss SC (2010) Zebrafish Vision. Structure and Function of the Zebrafish Visual System. In: Zebrafish (Perry S, Ekker M, Farrell A, Brauner C, eds): Elsevier.

Neuhauss SC, Biehlmaier O, Seeliger MW, Das T, Kohler K, Harris WA, Baier H (1999) Genetic disorders of vision revealed by a behavioral screen of 400 essential loci in zebrafish. J Neurosci 19:8603–8615.

Nevin LM, Robles E, Baier H, Scott EK (2010) Focusing on optic tectum through the lens of genetics. BMC Biol 8:126–135.

Optican LM, Zee DS (1984) A hypothetical explanation of congenital nystagmus. Biol Cybern 50:119–134.

Orger MB, Gahtan E, Muto A, Page-McCaw P, Smear MC, Baier H (2004) Behavioral screening assays in zebrafish. Methods Cell Biol 77:53–68.

Petros TJ, Rebsam A, Mason CA (2008) Retinal axon growth at the optic chiasm: to cross or not to cross. Annu Rev Neurosci 31:295–315.

Pilling RF, Thompson JR, Gottlob I (2005) Social and visual function in nystagmus. Br J Ophthalmol 89:1278–1281.

Pittman AJ, Law M, Chien C (2008) Pathfinding in a large vertebrate axon tract: isotypic interactions guide retinotectal axons at multiple choice points. Development 135:2865–2871.

Proudlock F, Gottlob I (2011) Foveal development and nystagmus. Ann N Y Acad Sci 1233:292–297.

Purves D, Augustine G, Fitzpatrick D, Hall WC, LaMantia A, McNamara JO, Williams SM (2004) Neuroscience. Sunderland: Sinauer Associates, Inc.

Rick JM, Horschke I, Neuhauss SC (2000) Optokinetic behavior is reversed in achiasmatic mutant zebrafish larvae. Curr Biol 10:595–598.

Rinner O, Rick JM, Neuhauss SC (2005) Contrast sensitivity, spatial and temporal tuning of the larval zebrafish optokinetic response. Invest Ophthalmol Vis Sci 46:137–142.

Roeser T, Baier H (2003) Visuomotor behaviors in larval zebrafish after GFP-guided laser ablation of the optic tectum. J Neurosci 23:3726–3734.

Sarvananthan N, Surendran M, Roberts EO, Jain S, Thomas S, Shah N, Proudlock FA, Thompson JR, McLean RJ, Degg C, Woodruff G, Gottlob I (2009) The prevalence of nystagmus. the Leicestershire nystagmus survey. Invest Ophthalmol Vis Sci 50:5201–5206.

Sato T, Hamaoka T, Aizawa H, Hosoya T, Okamoto H (2007) Genetic single-cell mosaic analysis implicates ephrinB2 reverse signaling in projections from the posterior tectum to the hindbrain in zebrafish. J Neurosci 27:5271–5279.

Seth A, Culverwell J, Walkowicz M, Toro S, Rick JM, Neuhauss SC, Varga ZM, Karlstrom RO (2006) belladonna/(Ihx2) is required for neural patterning and midline axon guidance in the zebrafish forebrain. Development 133:725–735.

Sockanathan S (2003) Towards cracking the code: LIM protein complexes in the spinal cord. Trends Neurosci 26:57–59.

Stahl JS, Averbuch-Heller L, Leigh RJ (2000) Acquired nystagmus. Arch Ophthalmol 118:544–549.

Strauss O (2005) The retinal pigment epithelium in visual function. Physiol Rev 85:845–881.

Streisinger G, Walker C, Dower N, Knauber D, Singer F (1981) Production of clones of homozygous diploid zebra fish (Brachydanio rerio). Nature 291:293–296.

Stuermer CA (1988) Retinotopic organization of the developing retinotectal projection in the zebrafish embryo. J Neurosci 8:4513–4530.

Summers CG (2009) Albinism: classification, clinical characteristics, and recent findings. Optom Vis Sci 86:659–662.

Tarpey P et al. (2006) Mutations in FRMD7, a newly identified member of the FERM family, cause X-linked idiopathic congenital nystagmus. Nat Genet 38:1242–1244.

Tessier-Lavigne M, Goodman CS (1996) The molecular biology of axon guidance. Science 274:1123–1133.

Thomas S, Proudlock FA, Sarvananthan N, Roberts EO, Awan M, McLean R, Surendran M, Kumar AS, Farooq SJ, Degg C, Gale RP, Reinecke RD, Woodruff G, Langmann A, Lindner S, Jain S, Tarpey P, Raymond FL, Gottlob I (2008) Phenotypical characteristics of idiopathic infantile nystagmus with and without mutations in FRMD7. Brain 131:1259–1267.

Tremblay F, Becker I de, Cheung C, LaRoche GR (1996) Visual evoked potentials with crossed asymmetry in incomplete congenital stationary night blindness. Invest Ophthalmol Vis Sci 37:1783–1792.

Trowe T, Klostermann S, Baier H, Granato M, Crawford AD, Grunewald B, Hoffmann H, Karlstrom RO, Meyer SU, Muller B, Richter S, Nusslein-Volhard C, Bonhoeffer F (1996) Mutations disrupting the ordering and topographic mapping of axons in the retinotectal projection of the zebrafish, Danio rerio. Development 123:439–450.

van Genderen, M M, Riemslag, F C C, Schuil J, Hoeben FP, Stilma JS, Meire FM (2006) Chiasmal misrouting and foveal hypoplasia without albinism. Br J Ophthalmol 90:1098–1102.

von dem Hagen, E. A., Hoffmann MB, Morland AB (2008) Identifying human albinism. a comparison of VEP and fMRI. Invest Ophthalmol Vis Sci 49:238–249.

Watkins RJ, Thomas MG, Talbot CJ, Gottlob I, Shackleton S (2012) The Role of FRMD7 in Idiopathic Infantile Nystagmus. J Ophthalmol.

Whitfield TT, Granato M, van Eeden, F. J., Schach U, Brand M, Furutani-Seiki M, Haffter P, Hammerschmidt M, Heisenberg CP, Jiang YJ, Kane DA, Kelsh RN, Mullins MC, Odenthal J, Nusslein-Volhard C (1996) Mutations affecting development of the zebrafish inner ear and lateral line. Development 123:241–254.

Williams SE, Mason CA, Herrera E (2004) The optic chiasm as a midline choice point. Curr Opin Neurobiol 14:51–60.

Winterson BJ, Collewijn H (1981) Inversion of direction-selectivity to anterior fields in neurons of nucleus of the optic tract in rabbits with ocular albinism. Brain Res 220:31–49.

Wolman M, Granato M (2012) Behavioral genetics in larval zebrafish: learning from the young. Dev Neurobiol 72:366–372.

Wurtz RH, Albano JE (1980) Visual-motor function of the primate superior colliculus. Annu Rev Neurosci 3:189–226.

Yee RD, Wong EK, Baloh RW, Honrubia V (1976) A study of congenital nystagmus waveforms. Neurology 26:326–333.

# Chapter 2

## Analysis of Optokinetic Response in Zebrafish by Computer Based Eye Tracking

**Sabina P. Huber-Reggi[1], Kaspar P. Mueller[1], Stephan C.F. Neuhauss[1δ]**

[1]Institute of Molecular Life Sciences, University of Zurich, Zurich, Switzerland

[δ] corresponding author

**Article published as a book chapter in** *Retinal Degeneration: Methods and Protocols, in Methods in Molecular Biology*, **935:** 139-160 (2013).

**Personal contribution**

Writing of the manuscript with the help of KM. Preparation of all figures (figure 7 was prepared in collaboration with KM).

## 2.1 Abstract

Large-field movements in the visual surround trigger spontaneous, compensatory eye movements known as optokinetic response (OKR) in all vertebrates. In zebrafish (*Danio rerio*) the OKR is well developed at 5 days post fertilization and can be used in the laboratory for screening of visual performance following genetic manipulations or pharmaceutical treatments. Several setups for measurement of the zebrafish OKR have been described. All of them are based on the presentation of moving gratings to the larva or to the adult fish. However, they differ in the way of presenting gratings and in the method of analysis. Here, we describe a detailed protocol for our newest software that enables computer-generation of the moving stripes and automatic tracking of eye movement. This protocol makes it possible to quantitatively measure OKR in both larvae and adult fish in a fast and reliable way.

## 2.2 Introduction

Eye movements occur in all vertebrates and in some invertebrates and are thought to be required for high resolution vision. Two main groups of eye movements exist. Gaze shifting eye movements aim at shifting of the eyes toward an object of interest and include saccadic movements, smooth pursuit and vergence movements. Gaze stabilizing eye movements include the vestibular ocular reflex (VOR) and the optokinetic response (OKR) and aim at stabilization of a relative movement of the image on the retina, the retinal slip. Retinal slip is caused by either self-motion or motion of the surround and results in a blurred image. VOR and OKR are involuntary compensatory eye movements restoring high visual acuity. When the environment is continuously moving in one direction, the OKR produces a nystagmus composed of cycles of a slow eye movement in the direction of the stimulus and a fast resetting movement, called saccade, in the opposite direction. The OKR is triggered by a velocity and direction input coming from the retina and encoded by a neural circuit involving pretectal nuclei (Huang and Neuhauss, 2008; Maurer et al., 2011).

In a laboratory setting, an OKR can be easily elicited by a striped drum rotating around the subject. The OKR has been measured in a number of model organisms, incl. monkey, rabbit, mouse and fish (e.g. goldfish, medaka and zebrafish) (e.g. (Henderson and Crosby, 1952; Bergmann et al., 1963; Easter, 1972; Mitchiner et al., 1976; Easter and Nicola, 1997; Carvalho et al., 2002)). The combination of high fecundity, extra corporally developing embryos and rapid development of most functions, incl. the visual system, has made zebrafish a model organism of increasing importance for studying visual function. Zebrafish are afoveate animals and therefore, in contrast to humans, do not display gaze shifting eye movements. Another difference between the human and fish visual system is the position of the eyes and the anatomy of the optic nerve. Zebrafish are lateral eyed, and binocular overlap is minimal since all axons from the optic nerve cross at the optic chiasm and project to the contralateral brain side. Humans have frontally positioned eyes and binocular vision, since around half of the axons project to the ipsilateral brain side (Maurer et al., 2011). These differences allow us to study the OKR in zebrafish without the complications of smooth pursuit and binocular vision.

Several setups for measurement of the zebrafish OKR have been described. All of them are based on the presentation of moving gratings to the larva or, more recently, to the adult fish. However, different approaches exist for presenting the gratings and analyzing data. In initial experiments, the larva was placed inside a rotating drum equipped with vertical black-and-white stripes. The rotational speed of the drum was changed mechanically (Brockerhoff et al., 1995). In order to change the properties of the visual stimulus, different drums with stripes of different contrast or width can be used. Although this method is still widely used (Brockerhoff, 2006), computer-generated moving gratings are to our mind more convenient, since they allow to continuously change different parameters, such as contrast, spatial frequency and/or angular velocity, direction of rotation and any other stimulus parameter of choice. In order to project the gratings onto the drum, a digital light projector is placed either on the plane of the subject (linear projection) or below the subject. Using linear projection, only monocular stimulation is possible (Rinner et al., 2005). When the projector is placed below the subject, the gratings are projected via a mirror to the whole drum enabling binocular stimulation (Roeser and Baier, 2003; Mueller and Neuhauss, 2010). In order to avoid visible light from the projector influencing the

recording, the animal is illuminated from below with infrared emitting diodes. An infrared-pass filter in front of the camera ensures selective transmission of the infrared light to the camera.

In initial experiments, analysis of eye movement was performed by visual inspection and by counting the number of saccades occurring. Although this qualitative method - first described for zebrafish by Clark (Clark, 1981) - has been very convenient for a rapid screening of vision mutants, a quantitative approach is needed for uncovering more subtle oculomotor defects. This has been achieved by computer-based tracking of eye position and subsequent quantitative analysis of changes in eye position over time. For this method - first described by Roeser&Baier (Roeser and Baier, 2003) - image series are acquired by an infrared-sensitive CCD camera mounted onto a dissecting microscope. Custom-made tracking software extracts information about eye position from the acquired images.

Most OKR setups described in the literature are built for measurement of eye movements in larvae. OKR testing in adult fish is more challenging, mainly because of the difficulty of restraining body movements of the fish. We were able to solve this problem and published a working method for OKR measurement in the adult (Mueller and Neuhauss, 2010). In the same year, an alternative setup has been described by Zou et al. (Zou et al., 2010). In this paper, however, eye movements are only qualitatively analyzed through visual inspection instead of software-based tracking of eye position.

Here, we describe a detailed protocol for the custom-made setup currently used in our laboratory. The animal is stimulated binocularly by computer-generated gratings and the eye position over time is automatically tracked. The resulting eye velocity is calculated in real time. We describe the detailed procedure for recording OKR in larvae as well as in adult fish. We then describe our standard eye movement quantification approach which allows for detection of subjects with vision defects as well as for investigation of the OKR behavior itself. Since our system is under continuous development (Rinner et al., 2005; Huang et al., 2006; Huang and Neuhauss, 2008; Haug et al., 2010; Mueller and Neuhauss, 2010; Maurer et al., 2011), some of the details described in the protocol may change over time. However, our detailed protocol should enable the reader to apply the methodology of quantitative OKR measurements. Recently, a commercial instrument based on the described setup has become available (VisioTracker by TSE-Systems).

Additionally, we present here a simple assay that enables a non-automated qualitative analysis of OKR performance in larvae without the need of a computer-based setup. This methodology is suited for those researchers that do not have access to a computer-based setup and are interested in a rapid qualitative screening of vision mutants.

## 2.3 Materials

### 2.3.1 Reagents

1. 3% methylcellulose in water: Boil 100 ml dd$H_2O$ in a beaker, then start stirring. Add 3 g methylcellulose (while the hot water is stirring vigorously). Continue to stir till the methylcellulose is dispersed into the liquid. Pour the dispersion quickly into two 50 ml Falcon Tubes and rotate (360 deg) at 4°C overnight. The

day after, spin the clear viscous solution at 4°C, 179 g for ca. 10 min, in order to remove air bubbles. Store at 4°C for long term use. Incubate the solution at 28°C for about a day before use (*see* **Note 1**).

2. Tricaine methanesulfonate solution (MS-222; Sigma E10521): Dissolve 300 mg Tricaine methanesulfonate in 1 L fish system water.

### 2.3.2 Equipment for OKR recording

1. Serum pipette
2. Dissecting needle
3. Forceps
4. Thin wooden stick
5. OKR setup for larvae comprised of (Fig. 2.1):
   (a) a dissecting microscope (e.g. SZH-10, *Olympus Corporation*, Japan).
   (b) an infrared-sensitive CCD-camera (e.g. Guppy F-038B NIR, *Allied Vision Technologies*, Germany) equipped with an infrared-pass filter (e.g. RG715, *Olympus Corporation*, Japan).
   (c) a glass plate as a stand for the animal and the drum.
   (d) a stimulus computer running the open source Python library Vision Egg (Straw, 2008)**.**
   (e) an LCD projector (e.g. PLV-Z3000, *Sanyo*, Japan) (*see* **Note 2**).
   (f) a wide-angle conversion lens (e.g. HD-4500PRO, *Raynox*, Japan).
   (g) a mirror.
   (h) a control computer running custom-made software based on NI LabView 2009 and NI-Vision Development Module 2009 (*National Instruments,* USA).
   (i) a cluster of infrared-emitting diodes ($\lambda_{peak}$ = 940 nm) (e.g. BL0106-15-28, *Kingbright*, Taiwan) shielded by a piece of wax paper in a 35 mm Petri dish.
   (j) 35 mm Petri dish containing the larva embedded in 3% methylcellulose and aligned to lay dorsal side up.
   (k) a transparent plastic drum containing a white blotting paper on its internal wall.

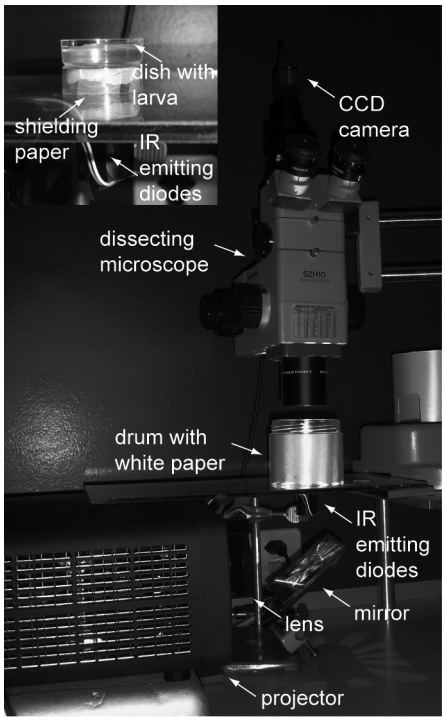


***Figure 2.1: Setup for the measurement of the OKR in larvae.***
*The computer-generated stimulus pattern is projected via a wide-angle conversion lens to a mirror placed below the larva. The stimulus is reflected in the mirror and directed onto a drum surrounding the larva. A cluster of 15 infrared-emitting diodes illuminates the larva from below and is shielded by a piece of wax paper in a 35 mm Petri dish (see inset on the left). An infrared-sensitive CCD camera on the top of a dissecting microscope records the movement of the eyes.*

6. OKR setup for adult fish: (a) to (i) are identical to the setup for larvae. Additionally, the setup for adult fish is comprised of:

   (j) a custom-made glass chamber (W x H x L = 12 mm x 12 mm x 65 mm) (Fig. 2.2) containing the fish restrained by two pieces of sponge and two plastic half pipes. Two inlets attached to both sides of the chamber allow for fish water inflow. A third tube attached at the end of the chamber allows for water outflow back to the supply tank.

   (k) a support stand.

   (l) a peristaltic pump (e.g. SR25, 65 rpm, 24V DC, novoprene tube N 4.8 mm x 1.6 mm, *Gardner Denver Thomas*, USA).

   (m) a 24V power supply for the pump (e.g. FSP 2405, *Voltcraft*, Germany).

   (n) an USB-Relais to switch ON/OFF the pump (e.g. USBREL8, *Quancom Informationssysteme GmbH,* Germany.

   (o) a water bath equipped with an aquarium heater (e.g. 50 W, *Jäger*, Germany).

   (p) an air pump (e.g. R301, *Rena*, USA).

   (q) a white plastic drum (d = 12.5 cm; e.g. cut from a chemical drum) with three small openings at the bottom edge for the tubes of the flow-through chamber.

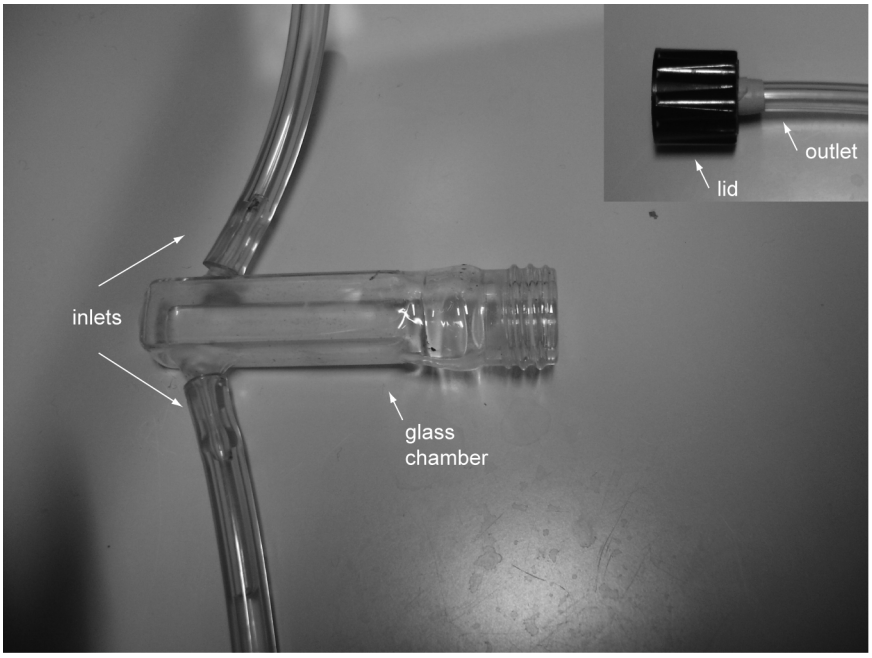


***Figure 2.2: Custom-made flow-through chamber to restrain the fish.***
*The fish is restrained as described in methods. Fish water - maintained at 28°C in a water bath and oxygenated by an air pump (not shown) - flows at max 40ml/min on the gills through two inlets attached to both sides of the chamber. The flow rate is generated by a peristaltic pump (not shown). The water effuses back to the supply tank via a third tube attached on the lid of the chamber.*

### 2.3.3 Equipment for manual OKR measurements

(Fig. 2.3)

1. Dissecting microscope (e.g. SV8, *Zeiss*, Germany).

2. Light source with light guides (e.g. KL 750, *Leica*, Germany).

3. 35 mm Petri dish containing the larva embedded in 3% methylcellulose and aligned to lay dorsal side up.

4. Turntable (turning can be manually or by a motorized drive).

5. Paper with stripes of the desired color and width. The paper has to fit in the turntable.

6. Serum pipette.

7. Dissecting needle.

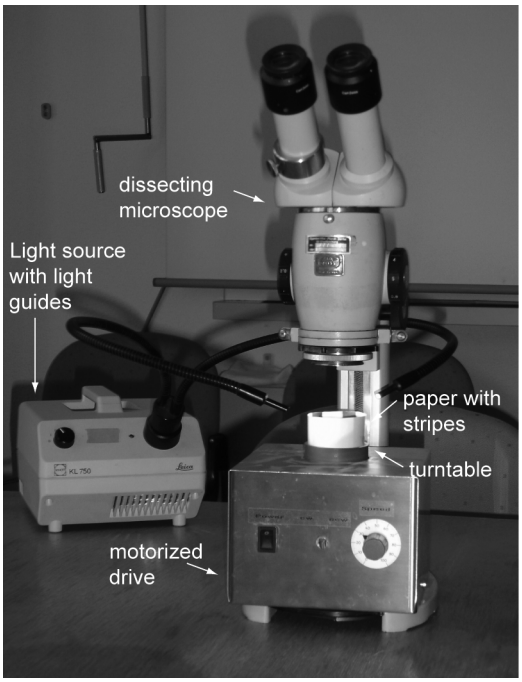


***Figure 2.3: Setup for manual measurement of the OKR in larvae.***
*The larva is placed on a turntable inside of a paper with a striped pattern. Rotation of the drum is driven by a motorized drive. The larva is illuminated from above by a light source with light guides. The eye movement is observed through the dissecting microscope.*

## 2.4 Methods

### 2.4.1 Recording of the OKR in larvae

Protocols for fish breeding can be found online in the Zebrafish book (http://zfin.org/zf_info/zfbook/zfbk.html) or in *Zebrafish: A practical approach* (Nüsslein-Volhard and Dahm, 2002).

#### 2.4.1.1 *Embedding the larva* (*see* **Note 3**)

1. Pour pre-warmed (28°C) 3% methylcellulose solution in a 35-mm Petri dish. Be careful not to produce air bubbles (*see* **Note 4**).
2. Suck a larva with a serum pipette and put it on the methylcellulose together with as little E3 medium as possible. To achieve this, we tap the side of the pipette so that the larva swims to the bottom. Suck off any remaining E3 medium around the larva in order to avoid dilution of the methylcellulose solution.
3. Embed the larva dorsal up in the center of the dish. To orient the larva use a dissecting needle (*see* **Note 4**).
4. Allow the larva to get used to the methylcellulose for about 10 minutes before starting recording.

#### 2.4.1.2 *Starting the setup*

1. Start up the whole setup:

   (a) Switch on both the stimulus and the control computer.

(b) Plug in the infrared LED-cluster.

(c) Switch on the projector.

2. Write the Configuration File containing the stimulus parameters (*see* **Notes 5-7**).

3. Stimulus computer: Start the stimulus program and wait for a message-box. Press “Bind port and listen for connections”.

4. Control Computer: Start the OKR program. Press “New set up larvae”. The OKR user interface will appear on the screen (Fig. 2.4).


***Figure 2.4: OKR user interface for eye movement measurement in larvae.***
*Recording controls are on the top. A real time image of the larva is displayed on the left. Tracking and eye velocity data are shown in the centre: The angle and the velocity of the right and left eye are displayed, the velocity of the rotating pattern is shown with a white line. On the bottom left are the particle detection parameters. On the right is the control of frame rate. Letters (a) to (p) refer to the steps described in the main text.*

#### 2.4.1.3 *Recording eye movement*

1. Choose the data folder where you want to save your data (*see* Fig. 2.4, (a)). Then press “Current folder”.

2. Place the larva under the dissecting microscope and center it in the visual field of the camera (b). The larva should be oriented in the same direction as the light beam. On the screen the larva is seen as in Figure 2.4 (*see* **Note 8**). Choose the highest possible magnification. Pay attention that the eyes are visible on the screen. When the larva is in focus, place the plastic drum around the animal.

3. The software recognizes the dark pigmented eyes based on the pixel intensity. Check if the eyes are recognized well (c), adjust the “threshold offset” (d) if necessary (e.g if body pigmentation spots are close to the eye).

4. Choose between a binocular stimulation (field of view = 360 deg), a monocular stimulation of the right eye and a monocular stimulation of the left eye (e). In the case of a monocular stimulation, the field of view can be regulated (between 0 deg and 180 deg) (f).

5. Choose the frame rate at which the images from the camera are processed by the software (g). We use 5 frames/s for screening of mutants and 25 frames/s for quantitative analysis of the OKR behavior itself. This frame rate has to be lower than the frame rate of the camera (h). Change the opening time of the camera shutter if necessary (i). Lowering the opening time reduces image brightness but increases the frame rate (h).

6. Load the Configuration File (j).

7. Press the "Go"-button (k) to start the experiment (*see* **Notes 9-10**). The experiment can be aborted by pressing "Go" again. If "Go" is pressed without having loaded a Configuration File, the stimulus will run with the parameters shown in (l). These parameters (colors, contrast, spatial frequency and angular velocity) can be changed here. However, without a Configuration File the eye position over time will not be recorded.

8. When the end of the Configuration File is reached, a window appears (Fig. 2.5). Here, the parameters to filter saccades and smooth the velocity curves - saccade threshold, saccaround and running average - can be set (a) (*see* **Note 11**). The velocity curve of each eye after smoothing is shown in (b) and the velocity averaged over the same stimulus conditions is indicated in (c). Enter subject information (fish number, genotype, experiment and, optionally, any comments) (d). Save the results (e).

9. After the first run as well as after having changed the Configuration File, a window pops up with the request to enter the name for a results-file or to choose an already existing one. Enter a name or choose an existing file. As long as the Configuration File is not changed, the following recordings will be saved in the same results-file. The results-file contains values for the average slow phase velocity for each fish and for each measured conditions. For each fish recorded, an additional tab-file containing the raw data is automatically saved. Each line represents a frame. Columns A and B contain values for the angular eye position of the right and the left eye respectively. Columns C and D contain values for the eye velocity in deg/s of the right and the left eye respectively. The further columns contain information about the stimulus parameters.

10. Continue with point 4 to measure the same larva with a new paradigm. Go back to point 2 to measure a different larva.

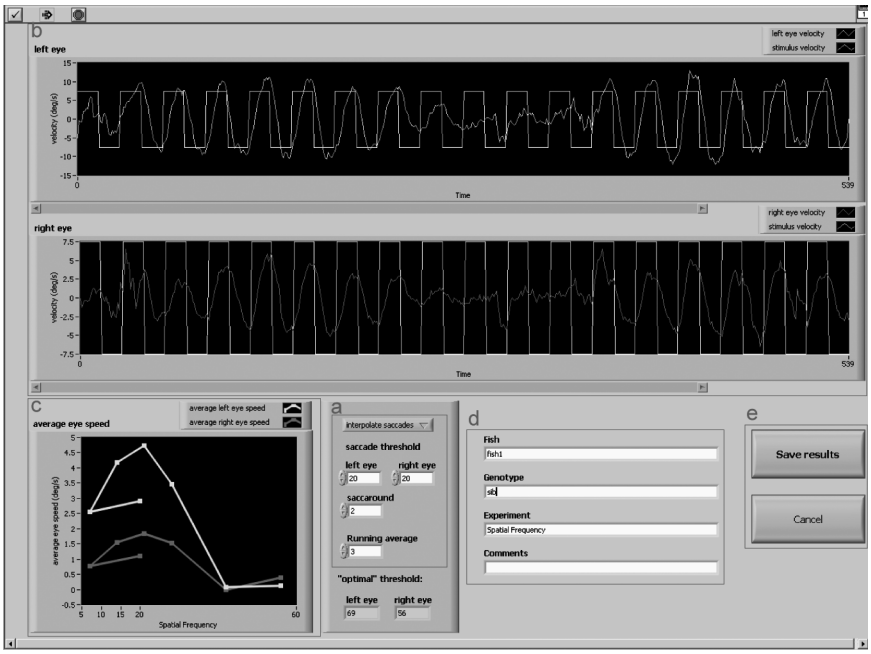


***Figure 2.5: User interface for smoothing and saving the data.***
*On the bottom right the parameters to filter saccades and smoothen the velocity curves can be set. The effect of these changes is seen on the velocity curves on the top and on the velocity averaged over the same stimulus conditions (bottom left). Letters (a) to (e) refer to the steps described in the main text.*

#### 2.4.1.4 *Recording a movie*

All the frames imaged by the camera during stimulus presentation can be recorded and visualized later on.

1. Before starting the stimulus, press the button "Record" (*see* Fig. 2.4, (m)).
2. Enter the name under which the movie has to be saved. Movies are automatically saved in AVI-format.
3. Activate "annotate movie" (n) if it is wished that the current stimulus properties are written in the lower right corner of each frame.
4. Start the stimulus as described above.
5. Press "Record" (m) again to stop recording of the movie.

#### 2.4.1.5 *Shutting down the setup*

1. Press "Quit Stimulus" and "Exit" (*see* Fig. 2.4, (o)).
2. Shut down both computers.
3. Unplug the IR LED-Cluster.
4. Switch off the projector.

## 2.4.2 Recording of the OKR in adult fish

### 2.4.2.1 *Starting the setup*

Point 1. is identical as for the setup for larvae (*see* **2.4.1.2**).

2. Write the Configuration File containing the stimulus parameters (*see* **Note 12**).

3. Stimulus computer: Start the stimulus program and wait for a message-box. Press “Bind port and listen for connections”.

4. Control Computer: Start the OKR program. Press “New set up adults”. The OKR user interface will appear on the screen (Fig. 2.6).

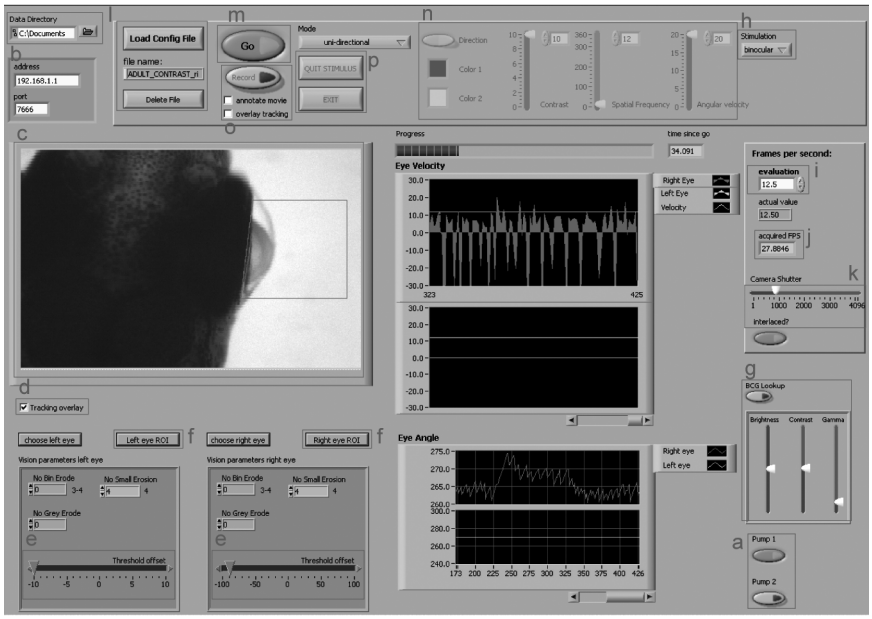


***Figure 2.6: OKR user interface for eye movement measurement in adult.***
*Recording controls are on the top. A real time image of the fish including particle detection is displayed on the left. On the bottom left are the particle detection parameters. Tracking and eye velocity data are shown in the centre. On the right is the control of frame rate. Letters (a) to (p) refer to the steps described in the main text.*

### 2.4.2.2 *Restraining the fish*

1. Warm up fish water in the supply tank using a water bad set at 28°C. Oxygenate the fish water with an air pump.

2. Turn the flow-through chamber to a vertical position (front end down) and fill it with fish water by switching the pump on on the user interface (*see* Fig. 2.6, (a)) until the water level reaches the upper rim.

3. Briefly anesthetize the fish in 300 mg/l MS-222 (*see* **Note 13**).

4. Prepare a half plastic pipe and insert a humid piece of sponge.

5. As soon as the fish stops swimming, gently lay the body on the piece of sponge, leaving the head incl. the gills free (Fig. 2.7*A*).

6. Cover with a second humid piece of sponge (Fig. 2.7*B*) and stabilize the sponges with a second half plastic pipe (Fig. 2.7*C*). Again, pay attention to leave the head and the gills free (*see* **Note 14**).

7. Fit everything into the flow-through chamber which is fixed on a support stand. The fish has to look toward the bottom of the chamber (Fig. 2.7*D*). Use a thin wooden stick to push the fish together with the pieces of sponge and plastic half pipes down until the gills are on the height of the water inlets. Take care no air bubbles are present in the front end of the chamber, i.e. around the head of the fish.

8. Close the lid of the flow-through chamber with the water outlet attached.

9. Switch on the peristaltic pump.

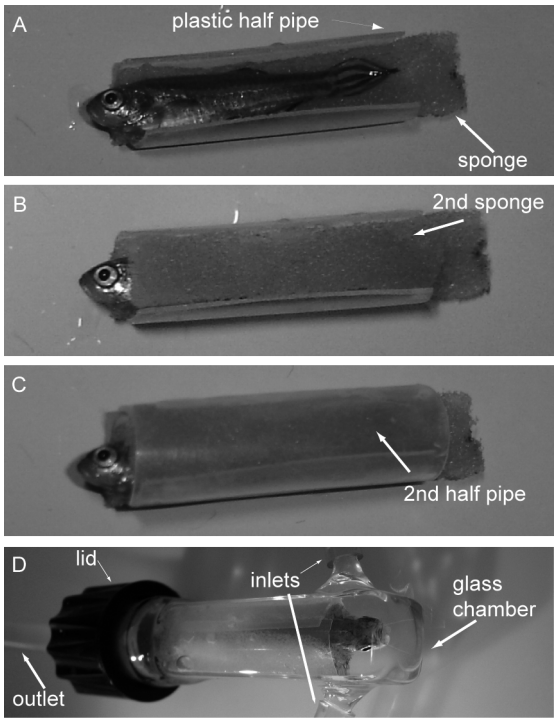


***Figure 2.7: Steps for restraining an adult fish.***
***A,*** *The anesthetized fish is laid on a humid piece of sponge, which had been inserted into a plastic half pipe.* ***B,*** *The fish is covered with a second humid piece of sponge.* ***C,*** *Everything is covered with the second half of the plastic pipe.* ***D,*** *The restrained fish is inserted into the glass chamber that had been connected to the two inlets and filled with fish water. The head of the fish looks to the bottom of the chamber. The chamber is then closed with the lid, which is attached to the outlet.*

#### 2.4.2.3 *Recording eye movements*

The setup for the adult is similar to the larval one.

1. Choose the data folder where you want to save your data (*see* Fig. 2.6, (b)). Then press "Current folder".

2. Turn the flow-through chamber containing the fish into horizontal position, place it under the dissecting microscope and center it in the visual field of the camera (c) (*see* **Note 15**). The fish should be oriented in the same direction as the light beam. Choose an appropriate magnification (the eye to be recorded from should be as large as possible to still fit into the image) (*see* **Note 16**). Place the plastic drum around the fish such that the three tubes of the chamber can exit the drum through its openings.

3. In the setup for adults the particle detection is directly overlaid on the live image (c) if "Tracking overlay" is activated (d). Select a ROI around the lens of the eye to be recorded from by pressing "Right eye ROI" or "Left eye ROI", respectively (f). Check if the rim of the eye is recognized well (c) and adjust the "threshold offset" for the eye to be recorded (e).

4. Contrast, brightness and gamma of the image can be adjusted after having activated the button "BCG Lookup" (g).

5. We usually stimulate adult fish binocularly (field of view = 360 deg). However, it is possible to choose a monocular stimulation of the right eye and a monocular stimulation of the left eye (h). In the case of a monocular stimulation, the field of view can be regulated as in larval experiments.

6. Choose the frame rate at which the images from the camera are processed by the software (i). We typically use 12.5 frames/s. This frame rate has to be lower than the frame rate of the camera (j). Change the opening time of the camera shutter if necessary (k).

7. Load the desired Configuration File (l).

8. Press the "Go"-button (m) to start the experiment. The experiment can be aborted by pressing "Go" again (*see* **Notes 17-19**) If "Go" is pressed without a Configuration File loaded, the stimulus will run with the parameters shown in (n) as in the setup for larvae.

9. When the end of the Configuration File is reached, the data can be filtered and saved as in the setup for larvae (Fig. 2.8 and *see* **Note 20**).

10. The same fish can be measured again with a new paradigm. Fish easily survive for 30 min in the chamber without consequences on their health.

11. After successful measurement, turn the chamber back to a vertical position, switch off the pump and remove the fish together with the sponge and plastic half pipes using forceps. Release the fish into a tank with fish water. Fill the chamber with fish water again by switching the pump on until the water level reaches the upper rim. Continue with *2.4.2.2* point 3 to measure the next fish.

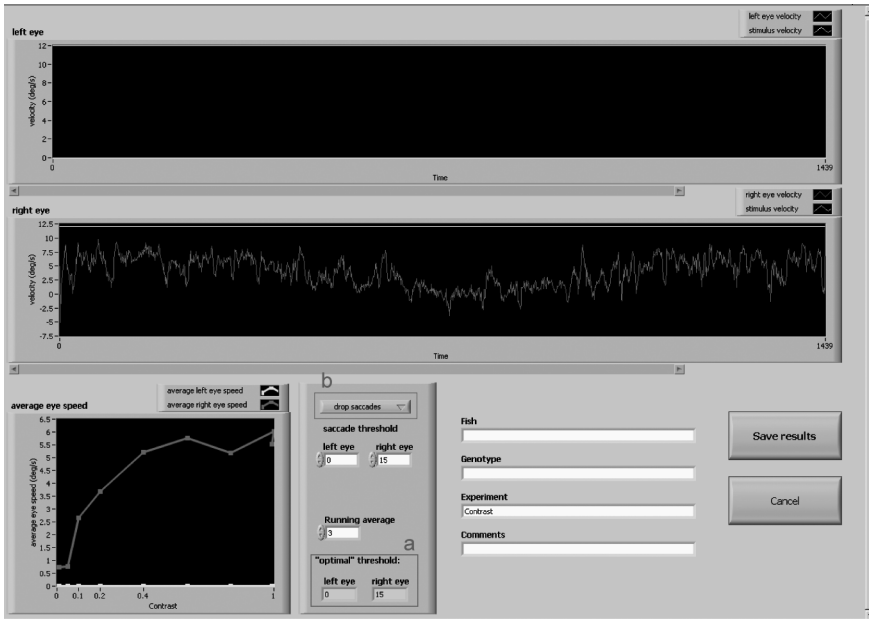


***Figure 2.8: User interface for smoothing and saving the data in the adult fish.***
*On the bottom right the parameters to filter saccades and smoothen the velocity curves can be set. The effect of these changes is seen on the velocity curves on the top and on the velocity averaged over the same stimulus conditions (bottom left). Letters (a) and (b) refer to the steps described in the main text.*

#### 2.4.2.4 *Recording a movie*

A movie of the live image can be recorded as with larvae (*see* Fig. 2.6, (o)). Activate "overlay tracking" to overlay the eye tracking on each frame.

#### 2.4.2.5 *Shutting down the setup*

1. Switch off the peristaltic pump.
2. Remove the fish from the chamber and put it back to its tank.
3. Shut down the aquarium heater, the power supply of the pumps, and the air pump.
4. Press "Quit Stimulus" and "Exit" (*see* Fig. 2.6, (p)).
5. Shut down both computers.
6. Unplug the IR LED-Cluster.
7. Switch off the projector.

### 2.4.3 Quantification of eye movement

Here, we describe the quantification method currently most used in our laboratory. This method is well suited for screening of vision defects. A more precise method for investigation of the OKR itself has been recently developed in our laboratory (Huang et al., 2006) (*see* **Note 21**). However, since investigation of the OKR itself is probably not the aim of most readers, we do not go through the details at this place.

#### 2.4.3.1 *Plotting the average eye velocity over an experimental condition*

We usually plot the average slow phase eye velocity over an experimental condition, e.g. varying contrast. For this, we use the automatically generated results-file which contains the average slow phase velocity for each condition and for each subject. This value has been calculated after filtering and smoothing of the raw data. Data analysis can be performed with any statistics software.

1. Open the results-file with the statistical program of preference.
2. Plot a line graph with the varying condition on the x-axis and the average eye velocity on the y-axis. If different groups need to be compared (e.g. different genotypes or different treatments), plot them as different series in one graph.

### 2.4.4 Manual OKR measurement

#### 2.4.4.1 *Embedding the larva*

Larvae are embedded in 3% methylcellulose as described for OKR recording (*see* **2.4.1.1**).

#### 2.4.4.2 *Measuring of the OKR*

1. Insert the striped pattern of choice in the turntable to form a drum.
2. Place the larva inside the drum.
3. Switch on the light source.
4. Rotate the drum and watch at eye movements through the microscope.
5. Score the direction of slow phase movements (with the drum or reverse to the drum movement). Count the number of saccades per given time interval as a read out of performance (*see* **Note 22**).

## 2.5 Notes

1. Methylcellulose is difficult to solubilize. When methylcellulose is added to hot stirring water, a cloudy dispersion is formed. This takes 1 to 2 minutes. Afterwards, the dispersion has to be poured very quickly into Falcon tubes to avoid sedimentation of the methylcellulose on the bottom of the beaker. This would give rise to aliquots of different concentrations. The Falcon tubes need to rotate as soon as they are at 4°C because the methylcellulose starts to solubilize quickly at this temperature. The day after, the solution has to be centrifugated till all air bubbles disappear. We recommend to keep the solution at 4°C for long term storage. However, the methylcellulose has to be warmed up to 28°C before use. This is the protocol used currently in our laboratory and is based on Brockerhoff et al. (Brockerhoff, 2006). However, other protocols exist and may work as well (e.g (Nüsslein-Volhard and Dahm, 2002)).

2. Resolution of the projector should be as high as possible (preferably use a HD-projector) to enable presentation of narrow stripes necessary to determine spatial resolution. In addition, the projector should have a high contrast ratio and a deep black level.

3. We embed our larvae in a 3% methylcellulose solution in order to restrain body movement with only minimal effect on eye movements. Zebrafish larvae survive in methylcellulose since this is a non-toxic viscous medium that allows oxygenation through the skin. Alternatively, the body of the larva can be embedded in low melting agarose with the head and gills exposed to water as described by Beck et al. (Beck et al., 2004). However, this method is more time consuming.
   Dishes containing methylcellulose can be reused several times, as long as the quality is intact (air bubbles should not be present, the solution should not be diluted or too sticky). In order to recycle them, dishes can be stored at 28°C in a humified chamber for later use.

4. Avoid production of air bubbles at any time point by gently pouring the methylcellulose solution into the dish and by gently positioning the larva inside the solution.

5. To write a Configuration File, open an empty excel datasheet. Each column represents one parameter, each line one sequence. A new sequence needs to be started as soon as one parameter changes. Enter the parameters as described below and save the file as a tab-file (*see* Fig. 2.9 for an example):

   (a) Column A: Write "Contrast" in the first line. For sine-wave grating choose values between 0 and 1. If you want sharp stripes with sharp borders, choose 10. Write a new line for each new sequence.

   (b) Column B: Write "Spatial Frequency" in the first line. The Spatial Frequency (SF) is given in cycles/360 deg and determines how many pattern of two different stripes are displayed in 360 deg (e.g. a value of 1 means that 2 stripes with two different colors are shown). Choose the desired value for each sequence. To determine the visual acuity of a larva, we normally run sequences with values between 7 and 56.

   (c) Column C: Write "angular velocity" in the first line. This parameter determines the angular velocity of the stimulus and is given in deg/s. Choose the desired value for each sequence. To determine temporal resolution , we typically run sequences with values between 5 and 30.

   (d) Column D-F: Always in the first line, write "color1 red" in column D, "color1 green" in column E and "color1 blue" in column F. Choose values between 0 and 1. Each value specifies the intensity of the respective color-channel. For grey stripes choose the same value for all channels, whereby the value has to be higher than 0 and smaller than 1. We routinely use a value of 0.6. For completely white stripes use a value of 1 for all channels.

   (e) Column G-I: Analog to column D-F but for color 2. For black stripes choose the value 0 for all channels. For pure red set green and blue to 0 and red to 1.

   (f) Column J: Write "nr Cycles" in the first line. Choose the number of cycles needed for each sequence. A value of 2 means that the stimulus will change the direction of rotation once during the specific sequence.

(g) Column K: Write "Cycle duration" in the first line. It defines the duration of each cycle in seconds. Choose the value wanted for each sequence.

| | A | B | C | D | E | F | G | H | I | J | K |
|---|---|---|---|---|---|---|---|---|---|---|---|
| 1 | Contrast | Spatial Frequency | angular velocity | Color1 red | Color1 green | Color1 blue | Color2 red | Color2 green | Color2 blue | No. Cycles | Cycle duration |
| 2 | 0.7 | 20 | 7.5 | 0.6 | 0.6 | 0.6 | 0 | 0 | 0 | 3 | 3 |
| 3 | 0.7 | 7 | 7.5 | 0.6 | 0.6 | 0.6 | 0 | 0 | 0 | 3 | 3 |
| 4 | 0.7 | 14 | 7.5 | 0.6 | 0.6 | 0.6 | 0 | 0 | 0 | 3 | 3 |
| 5 | 0.7 | 21 | 7.5 | 0.6 | 0.6 | 0.6 | 0 | 0 | 0 | 3 | 3 |
| 6 | 0.7 | 28 | 7.5 | 0.6 | 0.6 | 0.6 | 0 | 0 | 0 | 3 | 3 |
| 7 | 0.7 | 42 | 7.5 | 0.6 | 0.6 | 0.6 | 0 | 0 | 0 | 3 | 3 |
| 8 | 0.7 | 56 | 7.5 | 0.6 | 0.6 | 0.6 | 0 | 0 | 0 | 3 | 3 |
| 9 | 0.7 | 42 | 7.5 | 0.6 | 0.6 | 0.6 | 0 | 0 | 0 | 3 | 3 |
| 10 | 0.7 | 28 | 7.5 | 0.6 | 0.6 | 0.6 | 0 | 0 | 0 | 3 | 3 |
| 11 | 0.7 | 21 | 7.5 | 0.6 | 0.6 | 0.6 | 0 | 0 | 0 | 3 | 3 |
| 12 | 0.7 | 14 | 7.5 | 0.6 | 0.6 | 0.6 | 0 | 0 | 0 | 3 | 3 |
| 13 | 0.7 | 7 | 7.5 | 0.6 | 0.6 | 0.6 | 0 | 0 | 0 | 3 | 3 |

***Figure 2.9: Example of Configuration File.***
*In this example Spatial Frequency (SF) is changed in each sequence, contrast and angular velocity are constant. The first line represents the calibration sequence (see **Note 7**).*

6. We normally change only one parameter in each Configuration File. E.g. we measure the contrast sensitivity and therefore vary the contrast value but leave all other parameters constant.
   In the case of contrast, we start with the highest contrast, we reduce it stepwise and increase it again. Note that the contrast values from 0 to 1 are relative with 1 being the maximal contrast chosen. The real contrast has to be determined by measuring the luminance from the drum with a photometer.
   In the case of SF and angular velocity, we start with the lowest value, we enhance it stepwise and reduce it again.

7. At the beginning of recording, the eyes are pre-stimulated with a standard stimulus (typically contrast = 0.99, SF = 20 cycles/360 deg and angular velocity = 7.5 deg/s for larvae). This avoids artifacts from starting the experiment. This pre-stimulation is written as the first sequence in the Configuration File and should last typically for 9 s. Data from this sequence will be deleted before analysis.

8. Sometimes the larva is not immobilized properly. In this case it may help to wait for longer till starting the recordings. The larva will eventually calm. A drift of the larval position over time could be due to movement of the viscous solution because of handling. Also in this case the drift should reduce over time. It also helps to use light-adapted larvae if this is compatible with the experiment as light adapted larvae tend to be calmer. If the larva is still moving, please check the following:

   (a) Make sure that the larva is embedded dorsal side up.

   (b) Check the texture of the methylcellulose solution. If it is too diluted, try with a new solution.

   (c) If the mutation/treatment analyzed causes a higher motor activity, it may be necessary to increase the methylcellulose concentration.

9. If the eye movement is low or absent check the following:

   (a) Make sure that the larva is still alive by checking its blood flow.

(b) Make sure that the stimulus is running properly. If the stimulus shut down unexpectedly, close the software and the python program and restart both (first the python program and then the OKR software).

(c) Make sure that the projector lamp is working properly and not getting weaker. Measure the luminance from the drum during stimulus presentation using a photometer. We recommend to do this on a regular basis, at least every six months, in order to assure that contrast and brightness stay constant over time.

(d) Look for light sources in the room that could interfere. Maintain the room as dark as possible.

(e) Check the quality of the methylcellulose solution.

(f) Make sure that the larva is embedded dorsal side up.

(g) Measure a healthy and untreated wild-type larva as a control. If this larva shows a normal OKR and you have checked all points (a) until (f), you may have found a larva with impaired OKR. Congratulation!

10. Sometimes eye movement does not seem to be matched to movement of the stimulus (*see* Fig. 2.4, (p)). If this happens, make sure that the stimulus runs stably. Check for irregularities in stimulus pattern velocity and check for any deviance from the parameters determined in the Configuration File. If deviances are present, restart the python file and then the OKR software.

11. The eye velocity is determined from the eye position over time. We usually consider the eye velocity during the slow phase of the OKR (SPV) as a read out for OKR performance. In order to calculate the SPV, we need to filter out the saccades (fast resetting movements in the opposite direction than the stimulus) and to smooth the curve. We usually do this with the help of an empirically tested formula (Haug et al., 2010): If eye velocity ($v$) in a certain frame ($f$) exceeds a determined saccade threshold (default: 20 deg/s), eye velocity of this frame as well as of a defined amount of preceding frames (saccaround) is replaced with the eye velocity of the frame preceding the saccaround. Analogously, the eye velocity of the defined amount of following frames is replaced by the value one frame after the saccaround. By a frame rate of 5 frames/s, we usually set the saccaround to 2 (($vf...f$-2) is set to $v(f$-3) and ($vf+1...f$+2) is set to $v(f$+3)). The velocity curve is further smoothen by a running average. At a frame rate of 5 frames/s, we usually set a running average of 7 frames ($v(f) = (\Sigma\ v(f$-3...$f$+3))/7). It is also possible to drop the saccades without saccaround. This can be defined in (a) on the top (*see* Fig. 2.5). *See* **2.4.3** and **Note 21** for more details on data analysis.

12. Write the Configuration File following the guidelines for experiments with larvae (*see* **Notes 5-7**). For recordings in adult fish, we typically stimulate binocularly and in one direction only. Therefore, each sequence consists of only one cycle. The length of the sequences can be set as preferred. We usually record with sequences lasting for 9 s. As for recordings in larvae, eyes are pre-stimulated with a standard stimulus typically lasting 9 s with contrast = 0.99, SF = 36 cycles/360 deg and angular velocity = 12 deg/s. This pre-stimulation is not considered in data analysis.

To determine the visual acuity of an adult fish, we usually run sequences with SF values between 18 and 180 cycles/360 deg. To determine the temporal resolution, we usually run sequences with angular velocity values between 5 and 55 deg/s.

13. Always use a freshly prepared solution of MS-222, since tricaine is light-sensitive and quickly loses its activity, and toxic by-products may be formed.

14. In case fish strongly vary in size, use different pieces of sponge with different sizes, or add additional small pieces for smaller fish.

15. Before initiating an experiment, leave the fish in the flow-through chamber for 1-2 min with running water supply in order to let it recover from anaesthesia and calm down.

16. Since temporal-to-nasal eye velocity has been shown to be much higher and more stable (Mueller and Neuhauss, 2010), we usually evaluate only the eye stimulated in temporal-to-nasal direction. This way we can also control the position of that eye more precisely.

17. If eye movements are jerky and not correlated to visual stimulation, stop presentation of gratings and wait for 30 s. Re-start the stimulation with optimal parameters, i.e. high contrast (1 or higher), medium spatial frequency (ca. 36 cycles/360 deg) and high angular velocity (ca. 20 deg/sec). Repeat this until eye movements are stable and well correlated to visual stimulation.

18. If the fish does not show any eye movements at all, make sure the pump is running. Oxygenation may be insufficient if the gills are covered by the sponge. In this case, immediately release the fish and let it recover in a tank with fresh fish water. Turn the chamber back to a vertical position, switch off the pump and remove the fish together with the sponge and plastic half pipes using forceps.

19. If the fish manages to disengage itself from the restraining system, shut down the pump, turn the chamber back to a vertical position, open the lid, remove sponge and plastic half pipes using forceps, position a tank with fish water below the chamber and remove the fish by turning the chamber by 180 deg.

20. In contrast to the method used for larvae, the threshold for saccade filtering is not fixed but an ideal threshold is searched for each eye in an iterative process. The ideal threshold is the one that results in the highest sum of average eye velocities and it is displayed below the smoothing settings (*see* Fig. 2.8, (a)). Moreover, saccades are usually dropped and saccaround is not performed. Nevertheless, it is possible to use the saccaround method. To define the method of choice, press (b). The curve is smoothened by a running average as in recordings of larvae. At a frame rate of 12.5 frames/s, we typically use a running average of 7 (*see* **Note 11** for details about the smoothing algorithm).

21. In our laboratory, different processing methods have been applied in the past depending on the research question (Rinner et al., 2005; Huang et al., 2006; Haug et al., 2010; Mueller and Neuhauss, 2010). Here, we describe in detail the method of choice for a rapid screening of vision defects. However, for a quantitative analysis of the OKR behavior itself - e.g. for analysis of the eye movement waveform - a higher frame rate is needed and the method described here is not precise enough. For this kind of quantitative analysis, we refer to our work on the mutant *belladonna* (Huang et al., 2006). A fraction of the homozygous *belladonna*

larvae displays a reversed OKR and spontaneous eye oscillations in the absence of a moving stimulus. In order to quantitatively analyze those eye movements, a more precise quantification software was developed using the R statistical computing language. Briefly, the eye movement was recorded with a frame rate of 12.5 frames/s (nowadays we record with 25 frames/s). The eye position trace was smoothen with a Gaussian smoothing kernel. Slow phase segments were determined by setting acceleration thresholds. The slow phase velocity was defined by taking the maximum eye velocity across all slow phase segments within a condition.

22. If the eye movement is low or absent check the following:

    (a) Make sure that the larva is still alive by checking its blood flow.

    (b) Check the light intensity from the light source and try to vary it.

    (c) Look for light sources in the room that could interfere. Maintain the room as dark as possible.

    (d) Check the quality of the methylcellulose solution.

    (e) Make sure that the larva is embedded dorsal side up and calm.

    (f) Make sure that the drum is rotating smoothly.

    (g) Measure a healthy and untreated wild-type larva as a control. If this larva shows a normal OKR and you have checked all points (a) till (f), you may have found a larva with impaired OKR.

## 2.6 References

Beck JC, Gilland E, Tank DW, Baker R (2004) Quantifying the ontogeny of optokinetic and vestibuloocular behaviors in zebrafish, medaka, and goldfish. J Neurophysiol 92:3546–3561.

Bergmann F, Chaimovitz M, Gutman J, Zelig S (1963) Optokinetic Nystagmus and Its Interaction with Central Nystagmus. J Physiol 168:318–331.

Brockerhoff SE (2006) Measuring the optokinetic response of zebrafish larvae. Nat Protoc 1:2448–2451.

Brockerhoff SE, Hurley JB, Janssen-Bienhold U, Neuhauss SC, Driever W, Dowling JE (1995) A behavioral screen for isolating zebrafish mutants with visual system defects. Proc Natl Acad Sci USA 92:10545–10549.

Carvalho PS, Noltie DB, Tillitt DE (2002) Ontogenetic improvement of visual function in the medaka oryzias latipes based on an optomotor testing system for larval and adult fish. Animal Behaviour 64:1–10.

Clark DT (1981) Visual Responses in the Developing Zebrafish (Brachydanio rerio). PhD Thesis. University of Oregon.

Easter SS (1972) Pursuit eye movements in goldfish (Carassius auratus). Vision Res 12:673–688.

Easter, SS Jr, Nicola GN (1997) The development of eye movements in the zebrafish (Danio rerio). Dev Psychobiol 31:267–276.

Haug MF, Biehlmaier O, Mueller KP, Neuhauss SC (2010) Visual acuity in larval zebrafish. behavior and histology. Front Zool 7:8.

Henderson JW, Crosby EC (1952) An experimental study of optokinetic responses. AMA Arch Ophthalmol 47:43–54.

Huang YY, Neuhauss SC (2008) The optokinetic response in zebrafish and its applications. Front Biosci 13:1899–1916.

Huang YY, Rinner O, Hedinger P, Liu SC, Neuhauss SC (2006) Oculomotor instabilities in zebrafish mutant belladonna. a behavioral model for congenital nystagmus caused by axonal misrouting. J Neurosci 26:9873–9880.

Maurer CM, Huang YY, Neuhauss SC (2011) Application of zebrafish oculomotor behavior to model human disorders. Rev Neurosci 22:5–16.

Mitchiner JC, Pinto LH, Vanable, J. W., Jr. (1976) Visually evoked eye movements in the mouse (Mus musculus). Vision Res 16:1169–1171.

Mueller KP, Neuhauss SC (2010) Quantitative measurements of the optokinetic response in adult fish. J Neurosci Methods 186:29–34.

Nüsslein-Volhard C, Dahm R (2002) Zebrafish. New York: Oxford University Press.

Rinner O, Rick JM, Neuhauss SC (2005) Contrast sensitivity, spatial and temporal tuning of the larval zebrafish optokinetic response. Invest Ophthalmol Vis Sci 46:137–142.

Roeser T, Baier H (2003) Visuomotor behaviors in larval zebrafish after GFP-guided laser ablation of the optic tectum. J Neurosci 23:3726–3734.

Straw AD (2008) Vision egg. an open-source library for realtime visual stimulus generation. Front Neuroinformatics 2:4.

Zou SQ, Yin W, Zhang MJ, Hu CR, Huang YB, Hu B (2010) Using the optokinetic response to study visual function of zebrafish. J Vis Exp 36.

# Chapter 3

## Comparison of Infantile Nystagmus Syndrome in Zebrafish Mutant *belladonna* and Humans

**Melody Ying-Yu Huang[1δ], Chieng-Cheng Chen[1*], Sabina P. Huber-Reggi[2*], Stephan C. F. Neuhauss[2], Dominik Straumann[1]**

[1]Department of Neurology, University Hospital Zurich, Zurich, Switzerland

[2]Institute of Molecular Life Sciences, University of Zurich, Zurich, Switzerland

* these authors contributed equally to this work

δ corresponding author

**Adaptation from an article published in** *Annals of the New York Academy of Sciences* **1233:** 285-291 (2011).

**Acknowledgments**

The authors would like to thank Patrik Hedinger for the helping with the figure and helpful comments on the manuscript. This work was supported by grants from the Zurich Center for Integrative Human Physiology (ZIHP) and Swiss National Science Foundation (SNF) 31003A-118069.

**Personal contribution**

Recording and screening of zebrafish data, editing the manuscript for integration in this thesis.

## 3.1 Abstract

Infantile nystagmus syndrome (INS; formerly called congenital nystagmus) is an ocular motor disorder characterized by several typical nystagmus waveforms. To date, restrictions inherent to human research and the absence of a handy animal model have impeded efforts to identify the underlying mechanism of INS. Displaying INS-like spontaneous eye oscillations, zebrafish *belladonna* (*bel*) mutants may provide new insights into the mystery of INS. In this study, we demonstrate that these spontaneous eye oscillations match the diagnostic waveforms of INS. As a result, zebrafish *bel* mutants can be used as an animal model for the study of a possible triggering mechanism in INS.

## 3.2 Introduction

Infantile nystagmus syndrome (INS; formerly called congenital nystagmus) is a disorder characterized by involuntary conjugate, predominantly horizontal oscillations of both eyes, present at birth or shortly after (Gresty et al., 1984; CEMASWorkingGroup, 2001; Noorden and Campos, 2002; Maybodi, 2003). Prevalence estimates range from 0.1% to 0.6% in the general population (Forssman and Ringner, 1971; Abadi and Bjerre, 2002; Sarvananthan et al., 2009). INS is associated with substantial visual impairments (Halmagyi et al., 1980; Dickinson and Abadi, 1985; Bedell and Loshin, 1991) that adversely affect occupational and social functioning (Pilling et al., 2005). To date, the pathological mechanism of INS is poorly understood (Abadi, 2002; Dell'Osso, 2006). It has been difficult to gain access to the mechanisms that underlie INS for a number of reasons: the inherent limitations of human research, such as restriction to predominantly noninvasive methods, and the absence of a suitable animal model. In order to work around this problem, INS researchers have mostly relied on a top-down approach using mathematical models (Optican and Zee, 1984; Harris, 1995; Broomhead et al., 2000; Jacobs and Dell'Osso, 2004; Dell'Osso, 2006). Such models are based on the presumed pathology in the ocular motor neurocircuitry that causes INS. If the model readout shows a high correlation with the real-world INS data, it is considered to provide evidence that the pathology incorporated in the model may also be present in INS patients. As plausible as such a conclusion may appear, caution is warranted for two reasons. First, even a high statistical correlation does not prove causation. Second, theoretically, an infinite number of models can be created that fit the real-world INS data sufficiently well. Consequently, it is impossible to determine which of the existing INS models reflects the true pathology based on a system modeling approach alone.

Displaying ocular motor instabilities that resemble INS in humans, zebrafish (a teleost) *belladonna* (*bel*) mutant may be a promising new animal model for INS, possibly paving the way for new insights into the etiology of INS (Rick et al., 2000; Huang et al., 2006). In a screen for mutants with misprojections of the optic nerve, about 45% of the homozygous zebrafish *bel* mutants were found to be achiasmatic (Baier et al., 1996; Karlstrom et al., 1996), a condition caused by a recessive mutation in the zebrafish *lhx2* homolog, a Lim domain homeobox transcription factor (Seth et al., 2006). The study of *lhx2* in zebrafish *bel* mutants revealed that *lhx2* is required for forebrain patterning and midline axon guidance (Seth et al., 2006). The face validity of zebrafish *bel* mutants as a model of human INS goes beyond INS-like spontaneous eye movements: They show other symptoms common to INS in humans such as a reversed optokinetic response (OKR) (Halmagyi et al., 1980; Rick et al., 2000; Huang et al., 2006) and problems in visual motor functioning, observable as looping (swimming in circles) (Guerraz et al., 2000; Huang et al., 2009).

For zebrafish *bel* mutant to earn the label “animal model for INS,” we have to show that the ocular motor instabilities classify as INS. With this goal in mind, we inspected ocular motor data and identified the INS waveform types. We were also interested in how similar the ocular motor instabilities of human INS and zebrafish are. For that purpose, we compared the waveform types and parameters of zebrafish *bel* mutants with those we recorded in human INS patients.

## 3.3 Materials and Methods

### 3.3.1 Zebrafish *bel* mutants

The zebrafish *bel* (*bel*$^{tv42}$) mutant line was maintained and bred as previously described (Mullins et al., 1994). Outcrossed sibling pairs were set up to identify heterozygous carriers. Clutches of these identification crosses and crosses of already identified carriers were used for the eye movement recording. Embryos were raised at 28°C in E3 medium (5 mM NaCl, 0.17 mM KCl, 0.33 mM $CaCl_2$, and 0.33 mM $MgSO_4$) (Haffter et al., 1996) and staged according to development in days postfertilization (dpf). Larvae at 4–5 dpf were anesthetized with 3-aminobenzoic acid ethyl esther methane sulfonate (MS-222, Sigma-Aldrich) to sort the homozygous mutants according to their eye pigmentation phenotype (Karlstrom et al., 1996). The spontaneous eye oscillations were measured in 5–6 dpf larvae. Larvae were embedded dorsal up in the center of a 35 mm diameter Petri dish containing 3% viscous methylcellulose to prevent body movement while only minimally constricting eye movements (Rinner et al., 2005; Huang et al., 2006). The stimulus consisted of a binocularly presented still, vertical black and white sine grating (contrast = 80%, spatial frequency = 0.056 or 0.033 cycles/degree) that was computer generated by an open-source library for real-time visual stimulus generation (Straw, 2008) and projected via a wide-angle conversion lens (HD-4500PRO, Raynox) and a mirror onto a paper drum by a LCD projector (PLV-Z3000, Sanyo) (Mueller and Neuhauss, 2010). The angular eye position was extracted with a custom-developed software package based on LabView 2009 and NI Vision development module 2009 (National Instruments) from each frame recorded by an infrared-sensitive CCD camera (Guppy F-038B NIR, Allied Vision Technologies; frame rate = 25 Hz) (Rinner et al., 2005; Huang et al., 2006). To reduce noise, we smoothed the eye position data with a Gaussian filter (*bt* = 0.2; *n* = 8; *o* = 2). The data were screened for waveforms types based on dell'Osso and Daroff (Dell'Osso and Daroff, 1975).

### 3.3.2 INS patients

INS patients were recruited via the Department of Ophthalmology and/or Department of Neurology of the University Hospital Zurich (*n* = 2). The visual stimulus (1280 × 1025 pixels, 60 Hz) was generated by a custom-made MATLAB (Mathworks, Natick, MA) software package and cast onto a white screen (width = 168 cm, height = 130 cm) mounted 80 cm above the ground 100 cm away from the participant using a projector (VPL-PX30, Sony). The stimulus consisted of a still, vertical black and white sine grating of varied spatial frequency (contrast = 100%), covering the visual field 80° horizontally and 66° vertically. The eye movements were recorded using a video-oculography (VOG) device (goggles, EyeSeeCam) at a frame rate of 220 Hz. The image data captured by the VOG device were simultaneously analyzed by a computer in order to obtain the angular eye position for each frame. To reduce noise, we smoothed the eye position data with a Gaussian filter (*bt* = 0.2; *n* = 8; *o* = 2).

## 3.4 Results

We classified the waveform types based on Dell'Osso and Daroff (Dell'Osso and Daroff, 1975). When presented with a still grating of varying spatial frequency, zebrafish *bel* mutants displayed all the major

waveform characteristics typical to INS (Fig. 3.1). In contrast to human INS, zebrafish *bel* mutants showed no spontaneous oscillations of the eyes in the dark except for some centrifugal saccades followed by a slow drift back to the center (data not shown). Zebrafish oscillations displayed a higher amplitude and lower frequency than oscillations in human patients. Despite this, the size-wise matched waveform cycles in the left column of the figure give an idea of just how similar the nystagmus waveforms in zebrafish and humans are.

### 3.4.1 Pendular nystagmus

Pure pendular nystagmus (P) was rarely seen as dominant waveform in recordings of larval *bel* mutants. Both the amplitude and the frequency were often small compared to those of other nystagmus waveforms. Also in our recording from INS patients, the frequency, but not the amplitude of P, was smaller than that in other waveforms (Fig. 3.1*A*). Zebrafish *bel* mutants sometimes produce waveforms that resemble pendular nystagmus with foveating saccades (PFS) in humans. Because zebrafish lack a fovea (Lyall, 1957), technically, these breaking saccades cannot be called foveating saccades, but instead, may serve a similar purpose by shifting the eye back to a more central and effective position (Fig. 3.1*B*).

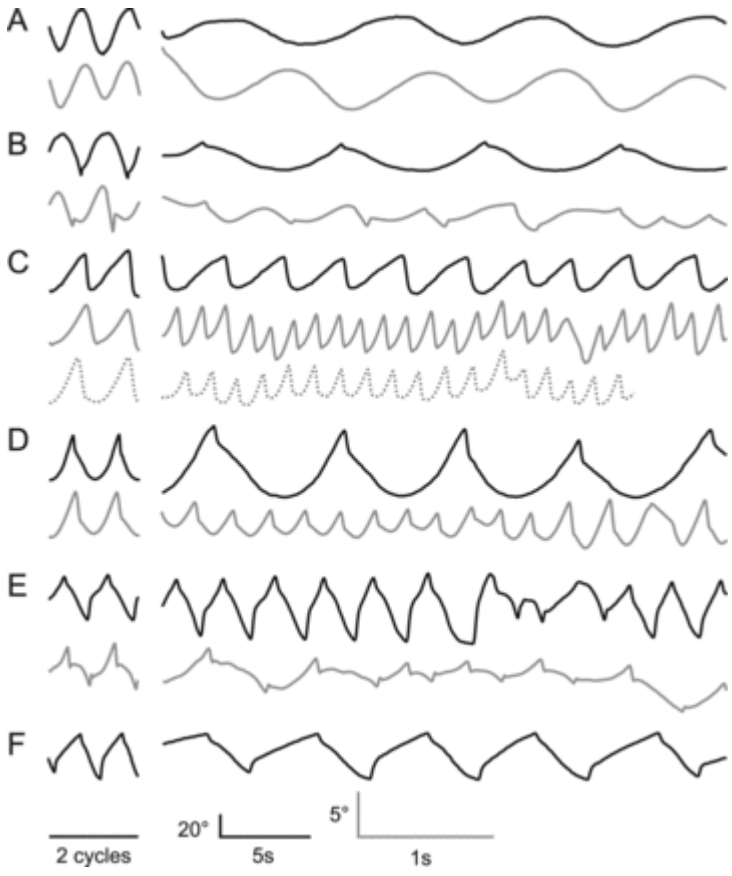


***Figure 3.1: Representative examples of INS waveforms in zebrafish bel mutants (black) and humans (gray).***
*In the left column, two typical cycles of each waveform are shown, scaled to match amplitude and frequency. The right column contains typical traces of the different waveform types. The human INS traces were scaled by a factor (amplitude = 7.5, frequency [time] = 8.0) in order to facilitate comparison. Spatial frequency indicated in parentheses.* ***A****, pure pendular nystagmus (bel = 0.056 cycles/ degree, human = 0.8 cycles/degree).* ***B,*** *pendular nystagmus with "foveating" saccades (bel = 0.033 cycles/degree, human = 0.8 cycles/degree).* ***C,*** *pure unidirectional jerk nystagmus (bel = 0.056 cycles/degree, human = 0.05 cycles/ degree). Unidirectional jerk nystagmus with extended foveation in human (0.05 cycles/degree) (dotted gray).* ***D,*** *pseudo-cycloid unidirectional jerk nystagmus (bel = 0.056 cycles/degree, human = 0.8 cycles/degree).* ***E,*** *pseudo-pendular bidirectional jerk nystagmus (bel = 0.056 cycles/degree, human = 0.6 cycles/degree).* ***F,*** *triangular bidirectional jerk nystagmus (bel = 0.056 cycles/degree, no human data available).*

### 3.4.2 Unidirectional jerk nystagmus

Many zebrafish *bel* mutants had a period in which they showed a unidirectional jerk nystagmus (J). We also provide a sample of unidirectional jerk nystagmus with extended foveation (JEF) in humans (Fig. 3.1*C*). Zebrafish *bel* mutants sometimes display similar waveforms (data not shown), but it is difficult to distinguish them from pseudocycloid unidirectional jerk nystagmus (PC), which also occurs in a number of zebrafish (Fig. 3.1*D*).

### 3.4.3 Bidirectional jerk nystagmus

Pseudo-pendular (PP) and triangular (T) bidirectional jerk nystagmus were common waveform types in our recordings of zebrafish *bel* mutants (Fig. 3.1*E*). Amplitude and frequency varied a lot between recordings. We only report a T in zebrafish because the eye position readings of the two patients did not contain T (Fig. 3.1*F*). Nevertheless, T has been previously reported in INS patients (Dell'Osso and Daroff, 1975).

## 3.5 Discussion

Recently, we reported on zebrafish *bel* mutant that displays misrouting of optic nerve fibers to the ipsilateral brain hemisphere and two abnormal ocular motor behaviors, reversed OKR and spontaneous eye oscillations (Rick et al., 2000; Huang et al., 2006). If the ocular motor instabilities qualify as INS, we can use zebrafish *bel* mutants as a model organism to study possible mechanisms underlying INS. The Committee for the Classification of Eye Movement Abnormalities and Strabismus (CEMAS) defined the following criteria for the diagnosis of INS: “Infantile onset, ocular motor recordings show diagnostic (accelerating) slow phases” (CEMASWorkingGroup, 2001). In accordance with the criterion of infantile onset, spontaneous eye oscillations are already present at the very early larval stage (before 5 dpf) (Huang et al., 2006). Here, we showed representative eye position traces of spontaneous oscillations (*see* Fig. 3.1). They include all the features typical for INS: Accelerating slow phases and many of the characteristic waveforms (Abadi and Dickinson, 1986; Dell'Osso and Daroff, 1975; Yee et al., 1976). In contrast to human INS, zebrafish showed no spontaneous nystagmus and little other ocular motor activity in the dark (data not shown). This difference could be explained by adaptive mechanisms in humans, possibly including the pursuit system (which is not present in fish). With the ocular motor instabilities diagnosed as INS, zebrafish *bel* mutants can be used as a model organism for studying INS.

A zebrafish-based animal model for INS has numerous advantages over the achiasmatic Belgian sheepdog (Williams et al., 1994; Hogan and Williams, 1995; Dell'Osso et al., 1998) and other potential animal models for INS such as albino rats (Lund et al., 1974; Sirkin et al., 1985). Zebrafish larvae are small, easy to raise, inexpensive to maintain, and multiply in large numbers (>100 eggs per pair per week) (Streisinger et al., 1981). Furthermore, the development of the zebrafish visual system is extremely rapid with the OKR and the associated structures being fully functional and experimentally testable at 5 dpf (Easter and Nicola, 1996, 1997; Neuhauss, 2003; Huang and Neuhauss, 2008). In contrast to a rodent model, the cone-dominant retina of zebrafish (Nawrocki et al., 1985) makes it possible to elucidate the role of color vision in INS. As afoveate animal (Lyall, 1957), zebrafish lacks a smooth pursuit system, allowing the study of INS in the absence of smooth pursuit. The downside of this is that the possible contribution of the smooth pursuit system to INS cannot be directly

investigated in zebrafish. Being lateral-eyed, zebrafish have optic nerve fiber projections that map completely to the contralateral side of the brain. In some zebrafish *bel* mutants, these projections map perfectly opposite, allowing the study of the role of a perfectly reversed visual pathway condition in INS. Finally and most importantly, the future potential of this animal model lies in the small larval brain with only a limited number of stereotypic neuronal projections, which will be exceptionally advantageous for studying the information processing involved in INS and in the central nervous system in general as soon as such technologies become available.

## 3.6 References

Abadi RV (2002) Mechanisms underlying nystagmus. J R Soc Med 95:231–234.

Abadi RV, Bjerre A (2002) Motor and sensory characteristics of infantile nystagmus. Br J Ophthalmol 86:1152–1160.

Abadi RV, Dickinson CM (1986) Waveform characteristics in congenital nystagmus. Doc Ophthalmol 64:153–167.

Baier H, Klostermann S, Trowe T, Karlstrom RO, Nusslein-Volhard C, Bonhoeffer F (1996) Genetic dissection of the retinotectal projection. Development 123:415–425.

Bedell HE, Loshin DS (1991) Interrelations between measures of visual acuity and parameters of eye movement in congenital nystagmus. Invest Ophthalmol Vis Sci 32:416–421.

Broomhead DS, Clement RA, Muldoon MR, Whittle JP, Scallan C, Abadi RV (2000) Modelling of congenital nystagmus waveforms produced by saccadic system abnormalities. Biol Cybern 82:391–399.

CEMASWorkingGroup (2001) The National Eye Institute Publications.

Dell'Osso LF (2006) Biologically relevant models of infantile nystagmus syndrome. the requirement for behavioral ocular motor system models. Semin Ophthalmol 21:71–77.

Dell'Osso LF, Daroff RB (1975) Congenital nystagmus waveforms and foveation strategy. Doc Ophthalmol 39:155–182.

Dell'Osso LF, Williams RW, Jacobs JB, Erchul DM (1998) The congenital and see-saw nystagmus in the prototypical achiasma of canines. Comparison to the human achiasmatic prototype. Vision Res 38:1629–1641.

Dickinson CM, Abadi RV (1985) The influence of nystagmoid oscillation on contrast sensitivity in normal observers. Vision Res 25:1089–1096.

Easter, S. S., Jr., Nicola GN (1996) The development of vision in the zebrafish (Danio rerio). Dev Biol 180:646–663.

Easter, S. S., Jr., Nicola GN (1997) The development of eye movements in the zebrafish (Danio rerio). Dev Psychobiol 31:267–276.

Forssman B, Ringner B (1971) Prevalence and inheritance of congenital nystagmus in a Swedish population. Ann Hum Genet 35:139–147.

Gresty M, Page N, Barratt H (1984) The differential diagnosis of congenital nystagmus. J Neurol Neurosurg Psychiatry 47:936–942.

Guerraz M, Shallo-Hoffmann J, Yarrow K, Thilo KV, Bronstein AM, Gresty MA (2000) Visual control of postural orientation and equilibrium in congenital nystagmus. Invest Ophthalmol Vis Sci 41:3798–3804.

Haffter P, Granato M, Brand M, Mullins MC, Hammerschmidt M, Kane DA, Odenthal J, van Eeden, F. J., Jiang YJ, Heisenberg CP, Kelsh RN, Furutani-Seiki M, Vogelsang E, Beuchle D, Schach U, Fabian C, Nusslein-Volhard C (1996) The identification of genes with unique and essential functions in the development of the zebrafish, Danio rerio. Development 123:1–36.

Halmagyi GM, Gresty MA, Leech J (1980) Reversed optokinetic nystagmus (OKN). mechanism and clinical significance. Ann Neurol 7:429–435.

Harris CM (1995) Problems in modelling congenital nystagmus. towards a new model. Stud. Vis. Inf. Process. 6:239–253.

Hogan D, Williams RW (1995) Analysis of the retinas and optic nerves of achiasmatic Belgian sheepdogs. J Comp Neurol 352:367–380.

Huang YY, Neuhauss SC (2008) The optokinetic response in zebrafish and its applications. Front Biosci 13:1899–1916.

Huang YY, Rinner O, Hedinger P, Liu SC, Neuhauss SC (2006) Oculomotor instabilities in zebrafish mutant belladonna. a behavioral model for congenital nystagmus caused by axonal misrouting. J Neurosci 26:9873–9880.

Huang YY, Tschopp M, Neuhauss SC (2009) Illusionary self-motion perception in zebrafish. PLoS One 4:e6550.

Jacobs JB, Dell'Osso LF (2004) Congenital nystagmus. hypotheses for its genesis and complex waveforms within a behavioral ocular motor system model. J Vis 4:604–625.

Karlstrom RO, Trowe T, Klostermann S, Baier H, Brand M, Crawford AD, Grunewald B, Haffter P, Hoffmann H, Meyer SU, Muller BK, Richter S, van Eeden, F. J., Nusslein-Volhard C, Bonhoeffer F (1996) Zebrafish mutations affecting retinotectal axon pathfinding. Development 123:427–438.

Lund RD, Lund JS, Wise RP (1974) The organization of the retinal projection to the dorsal lateral geniculate nucleus in pigmented and albino rats. J Comp Neurol 158:383–403.

Lyall AH (1957) Cone Arrangements in Teleost Retinae. Quarterly Journal of Microscopical Science s3-98:189–201.

Maybodi M (2003) Infantile-onset nystagmus. Curr Opin Ophthalmol 14:276–285.

Mueller KP, Neuhauss SC (2010) Quantitative measurements of the optokinetic response in adult fish. J Neurosci Methods 186:29–34.

Mullins MC, Hammerschmidt M, Haffter P, Nusslein-Volhard C (1994) Large-scale mutagenesis in the zebrafish. in search of genes controlling development in a vertebrate. Curr Biol 4:189–202.

Nawrocki L, BreMiller R, Streisinger G, Kaplan M (1985) Larval and adult visual pigments of the zebrafish, Brachydanio rerio. Vision Res 25:1569–1576.

Neuhauss SC (2003) Behavioral genetic approaches to visual system development and function in zebrafish. J Neurobiol 54:148–160.

Noorden G, Campos EC (2002). In: Binocular Vision and Ocular Motility, pp 508–533. Mosby St. Louis.

Optican LM, Zee DS (1984) A hypothetical explanation of congenital nystagmus. Biol Cybern 50:119–134.

Pilling RF, Thompson JR, Gottlob I (2005) Social and visual function in nystagmus. Br J Ophthalmol 89:1278–1281.

Rick JM, Horschke I, Neuhauss SC (2000) Optokinetic behavior is reversed in achiasmatic mutant zebrafish larvae. Curr Biol 10:595–598.

Rinner O, Rick JM, Neuhauss SC (2005) Contrast sensitivity, spatial and temporal tuning of the larval zebrafish optokinetic response. Invest Ophthalmol Vis Sci 46:137–142.

Sarvananthan N, Surendran M, Roberts EO, Jain S, Thomas S, Shah N, Proudlock FA, Thompson JR, McLean RJ, Degg C, Woodruff G, Gottlob I (2009) The prevalence of nystagmus. the Leicestershire nystagmus survey. Invest Ophthalmol Vis Sci 50:5201–5206.

Seth A, Culverwell J, Walkowicz M, Toro S, Rick JM, Neuhauss SC, Varga ZM, Karlstrom RO (2006) belladonna/(Ihx2) is required for neural patterning and midline axon guidance in the zebrafish forebrain. Development 133:725–735.

Shallo-Hoffmann J, Apkarian P (1993) Visual evoked response asymmetry only in the albino member of a family with congenital nystagmus. Invest Ophthalmol Vis Sci 34:682–689.

Sirkin DW, Hess BJ, Precht W (1985) Optokinetic nystagmus in albino rats depends on stimulus pattern. Exp Brain Res 61:218–221.

Straw AD (2008) Vision egg. an open-source library for realtime visual stimulus generation. Front Neuroinform 2:4.

Streisinger G, Walker C, Dower N, Knauber D, Singer F (1981) Production of clones of homozygous diploid zebra fish (Brachydanio rerio). Nature 291:293–296.

Williams RW, Hogan D, Garraghty PE (1994) Target recognition and visual maps in the thalamus of achiasmatic dogs. Nature 367:637–639.

Yee RD, Wong EK, Baloh RW, Honrubia V (1976) A study of congenital nystagmus. waveforms. Neurology 26:326–333.

# Chapter 4

# Severity of Infantile Nystagmus Syndrome-Like Ocular Motor Phenotype is Linked to the Extent of the Underlying Optic Nerve Projection Defect in Zebrafish *belladonna* Mutant

**Sabina Huber-Reggi[1,4], Chien-Cheng Chen[2,4], Lea Grimm[1], Dominik Straumann[2,3], Stephan C. F. Neuhauss[1,3,δ], Melody Ying-Yu Huang[2,δ]**

[1]Institute of Molecular Life Sciences, University of Zurich, Zurich, Switzerland

[2]Department of Neurology, University Hospital Zurich, Zurich, Switzerland

[3]Center for Integrative Human Physiology, University of Zurich, Zurich, Switzerland

[4]PhD Program in Integrative Molecular Medicine, Life Science Graduate School, Zurich, Switzerland

[δ] corresponding authors

**Article published in** *Journal of Neuroscience*, **32:** 18079-18086 (2012).

**Acknowledgments**

This work was supported by the Zurich Center for Integrative Human Physiology and by the Swiss National Foundation (Grants PMPDP3 139754 and 31003A-118069). We would like to thank Dr. Christian Grimm and Dr. Maarten Frens for fruitful discussion, Dr. Matthias Gesemann for critical reading of this manuscript, and Fabian Huber for help with writing of the analysis software. We thank Kara Dannenhauer for excellent fish care. Imaging was performed with equipment maintained by the Center for Microscopy and Image Analysis, University of Zurich.

**Personal contribution**

Design of experiments together with SN, MH, and DS. Performing of the experiments and data analysis (ERG and OMR together with LG), preparation of all figures, writing of the manuscript. Eye movements were analyzed with a software written by CCC.

## 4.1 Abstract

Infantile nystagmus syndrome (INS), formerly known as congenital nystagmus, is an ocular motor disorder in humans characterized by spontaneous eye oscillations (SOs) and, in several cases, reversed optokinetic response (OKR). Its etiology and pathomechanism is largely unknown, but misrouting of the optic nerve has been observed in some patients. Likewise, optic nerve misrouting, a reversed OKR and SOs with INS-like waveforms are observed in zebrafish *belladonna* (*bel*) mutants. We aimed to investigate whether and how misrouting of the optic nerve correlates with the ocular motor behaviors in *bel* larvae.

OKR and SOs were quantified and subsequently the optic nerve fibers were stained with fluorescent lipophilic dyes. Eye velocity during OKR was reduced in larvae with few misprojecting optic nerve fibers and reversed in larvae with a substantial fraction of misprojecting fibers. All larvae with reversed OKR also displayed SOs. A stronger reversed OKR correlated with more frequent SOs. Since we did not find a correlation between additional retinal defects and ocular motor behavior, we suggest that axon misrouting is in fact origin of INS in the zebrafish animal model. Depending on the ratio between misprojecting ipsilateral and correctly projecting contralateral fibers, the negative feedback loop normally regulating OKR can turn into a positive loop, resulting in an increase in retinal slip. Our data not only give new insights into the etiology of INS but may also be of interest for studies on how the brain deals with and adapts to conflicting inputs.

## 4.2 Introduction

Infantile nystagmus syndrome (INS) is a congenital ocular motor disorder characterized by involuntary conjugate, predominantly horizontal oscillations of the eyes, present at birth or shortly after (Gresty et al., 1984; Maybodi, 2003). Prevalence is ~2 per 1000 individuals (Sarvananthan et al., 2009). Visual performance is often impaired affecting occupational and social functioning (Pilling et al., 2005; McLean et al., 2012).

INS is often associated with visuosensory abnormalities affecting the cornea, lens, retina or optic nerve, such as aniridia, fovea hypoplasia, and misprojections of optic nerve fibers (e.g., in albinism), but can also be idiopathic (Khanna and Dell'Osso, 2006). Because of the broad range of accompanying symptoms, it has been difficult to define the etiology of INS. Most likely different mechanisms can lead to eye oscillations. The lack of a suitable animal model forced researchers to depend on system modeling, leading to varying hypotheses (Abadi, 2002): INS may be a result of a defect in the internal gain calibration of one of the ocular motor subsystems (Harris, 1995; Broomhead et al., 2000; Jacobs and Dell'Osso, 2004) or a consequence of abnormal positive feedback loops caused by neuronal miswiring (Optican and Zee, 1984; Tusa et al., 1992). Recently, mutations in the gene encoding FERM domain-containing 7 protein (*FRMD7*) have been related to idiopathic forms of INS (Tarpey et al., 2006; Watkins et al., 2012). FRMD7 is involved in neuronal outgrowth and development, suggesting a role in neuronal network formation (Betts-Henderson et al., 2010).

Recently, we showed that the zebrafish mutant *belladonna* (*bel*) may be a suitable animal model for INS in the presence of optic nerve fiber misprojections (Huang et al., 2006, 2011). In *bel* homozygous larvae, a variable fraction of retinal ganglion cell (RGC) axons (optic nerve fibers) misroute in the optic chiasm and project to the wrong brain hemisphere. In wild type (wt) larvae, all optic nerve fibers project contralaterally forming a crossed optic chiasm. In some *bel* larvae, all axons misproject ipsilaterally leading to achiasmia. Those larvae display a reversed optokinetic response (OKR) (i.e., the eyes move opposite to the visual stimulus) (Neuhauss et al., 1999; Rick et al., 2000), as observed in some human patients (for example, see Halmagyi et al., 1980). In later studies we observed in larvae with a reversed OKR spontaneous eye oscillations (SOs) (Huang et al., 2006) displaying all the major waveforms typical of INS (Huang et al., 2011). Because of the coexistence of achiasmia and reversed OKR, we formulated the hypothesis that axonal misrouting in achiasmatic larvae results in a positive visuo-ocular motor feedback loop, which increases the velocity of a moving visual stimulus on the retina (called retinal slip), thus leading to the observed ocular motor instability in stable visual surround (Rick et al., 2000; Huang et al., 2006). Patients often show misprojection of a portion of optic nerve fibers (Jeffery, 1997) and display complex OKRs (Collewijn et al., 1985). We speculate that the proportions of correct and incorrect optic nerve fiber projections could be a key factor in determining the ocular motor phenotype in each individual. In this study we quantify for the first time the correlation between extent of optic nerve misprojection and different ocular motor phenotypes in *bel* mutants.

## 4.3 Material and Methods

### 4.3.1 Fish maintenance and breeding

Fish were maintained and bred as previously described (Mullins et al., 1994). Embryos were raised at 28°C in E3 medium (5 mM NaCl, 0.17 mM KCl, 0.33 mM $CaCl_2$, and 0.33 mM $MgSO_4$) and staged according to development in days postfertilization (dpf). *bel* (*bel*$_{tv42}$) homozygous larvae were obtained from mating of identified heterozygous carriers. Larvae at 4 dpf were anesthetized with 200 mg/L 3-aminobenzoic acid ethyl esther methane sulfonate (MS-222; Sigma-Aldrich) and sorted according to eye pigmentation phenotype. *albino* larvae were obtained from mating of homozygous adult fish.

### 4.3.2 OKR and SOs stimulation

The OKR, a compensatory ocular motor reflex evoked by a moving visual environment, was elicited in a similar way as described previously (Rinner et al., 2005; Huang et al., 2006). Briefly, larvae were embedded dorsal-up in the center of a 35 mm diameter Petri dish containing prewarmed (28°C) 3% methylcellulose to constrain whole-body movement without significantly affecting eye movement. Using an LCD projector (PLV-Z3000; Sanyo), a computer generated visual stimulus was projected via a wide-angle conversion lens and a mirror to the internal walls of a paper drum (diameter = 9 cm), mounted on a transparent glass plate. The embedded larva was placed in the center of the drum and was illuminated from below with infrared emitting diodes ($\lambda_{peak}$ = 940 nm, BL0106–15-28; Kingbright). If not indicated otherwise, only one eye of the larva was stimulated via restriction of the visual field to the stimulated eye. OKR was elicited with a computer-generated (Straw, 2008) black and white sine-wave grating pattern with 85% contrast (maximum illumination 400 lux), a spatial frequency of 20 cycles/360° and an angular velocity of 7.5 deg/s. Stimulation lasted for 180 s whereby the direction of the moving grating changed every 60 s. The first 60 s, during which OKR is building up, were not used for analysis. For SOs stimulation, one eye was exposed during 5 min with black and white stationary gratings with the same contrast and spatial frequency as described above.

### 4.3.3 Eye movement recording and analysis

During visual stimulation, binocular eye movements were recorded by an infrared-sensitive CCD camera (Guppy F-038B NIR; Allied Vision Technologies). Frames were processed simultaneously by custom-developed software based on Lab- View 2009 and NI Vision Development Module 2009 (National Instruments) with a sample rate of 25 samples/s. Data were analyzed by custom-developed software written in MATLAB (MathWorks). Eye position traces were smoothed using a Gaussian filter with cutoff frequency of 2.28 or 2.56 Hz. OKR during unidirectional visual stimulation is characterized by a nystagmus consisting of compensatory slow phases, normally in the direction of the stimulus, and fast phases, or saccades, in the opposite direction bringing the eyes back to a more central position. To distinguish fast phases and slow phases, the eye position traces were split in segments spanning from one change in velocity direction to the next. Subsequently, an eye acceleration threshold was set (18°/s$^2$). Segments with accelerations lower than this threshold were considered as slow phases. Erroneously classified slow phases were discarded by visual inspection. Slow phases were used for OKR

velocity calculation. The OKR velocity was defined as the slow-phase velocity (SPV), computed by averaging the median eye velocity across all slow phases in one measurement. SPVs in the same direction as the stimulus were given positive velocity values; SPVs in the opposite direction were given negative velocity values. Analysis was restricted to the eye with the higher absolute velocity.

### 4.3.4 Optomotor response stimulation

Optomotor response (OMR), a reflexive swimming behavior in the direction of perceived motion, was measured in a similar way as published previously (Neuhauss et al., 1999; Roeser and Baier, 2003). Briefly, 7 dpf larvae were individually transferred into 25 cm long and 1 cm wide transparent Plexiglas tanks on an upward-facing monitor. The sidewalls of the tanks were obscured with a matt black adhesive film to avoid reflection of the stimulus. Fish were placed in the middle of the tank and a computer-generated (Straw, 2008) moving sine-wave black and white grating pattern (98% contrast with maximum illumination of 90 lux, spatial frequency of 4 cycles/1280 pixel (screen size), temporal frequency of 2 Hz) was presented twice for 45 s with an interstimulus interval of 20 s. Fish position over time was recorded by a video camera (HDR-CX130E; Sony). The distance from the starting position to the final position was measured and normalized to the maximal value possible (length of the tank/2). This gave a score between 0 and 1. Larvae resting at the starting position or swimming in the opposite direction were given a score of 0. Fish underwent 10 trials with alternating direction of movement. The scores were averaged for all the trials resulting in the optomotor index (OMI).

### 4.3.5 Electroretinogram

Electroretinograms (ERGs) were recorded as described previously (Makhankov et al., 2004). Briefly, larvae were dark adapted for 30 min. For recording, a reference electrode was placed on a sponge soaked with E3 medium. The larva was placed dorsal-up on a moist paper covering the reference electrode. The recording electrode with a tip diameter of 20 µm was filled with E3 and placed on the cornea of the larva. Light stimuli of 100 ms with interstimulus intervals of 10 s were applied. The light stimulus intensity was 700 lux.

### 4.3.6 Anterograde labeling of the optic nerve fibers

To label optic nerve fibers, larvae were fixed in 4 % paraformaldehyde in PBS overnight. For lipophilic dye injection, the fish were embedded dorsal-up in 1.5 % low melting agarose (Nu Sieve GTG Agarose; Lonza) in PBS on a glass slide. Solutions (1 % in chloroform) of DiO (Invitrogen) and DiI (Invitrogen) were pressure injected (40 psi, 20–30 ms pulse time) with a pneumatic Pico Pump (PV820; World Precision Instruments) between lens and retina using glass capillaries. Microscopy *z*-stacks images were obtained using a Leica SP5 confocal laser scanning microscope (Leica Microsystems). Signal intensities were measured using ImageJ (MacBiophotonics).

### 4.3.7 Statistical analysis

Statistical analysis and graph generation were performed with SPSS Statistics 19 (IBM).

## 4.4 Results

The *bel* mutant was first identified in a large-scale screening of mutations affecting optic nerve fiber pathfinding (Karlstrom et al., 1996). It carries a recessive mutation in the zebrafish *lhx2* homolog, a Lim domain homeobox transcription factor involved in neural development, including midline axon guidance and eye morphogenesis (Seth et al., 2006). *bel* mutants show variable morphological eye defects, optic nerve fiber misprojections, and an abnormal pigmentation near the lens, which causes the pupil to appear enlarged (Karlstrom et al., 1996; Seth et al., 2006).

### 4.4.1 The optic nerve projection and optokinetic phenotypes in *bel* mutants

In wt larvae, all optic nerve fibers project contralaterally forming a completely crossed optic chiasm. In *bel* mutants, the extent of the optic nerve misrouting phenotype is highly variable even within one clutch of eggs. Some *bel* larvae have contralateral projections like seen in wt (Fig. 4.1*A*). The remaining *bel* larvae display abnormal pathfinding of the optic nerve fibers at the chiasm. Among them, some larvae display a bilateral projection with a subpart of axons growing ipsilaterally (Fig. 4.1*B*), whereas others are achiasmatic, with a completely ipsilateral projection (Fig. 4.1*C*) (Rick et al., 2000).

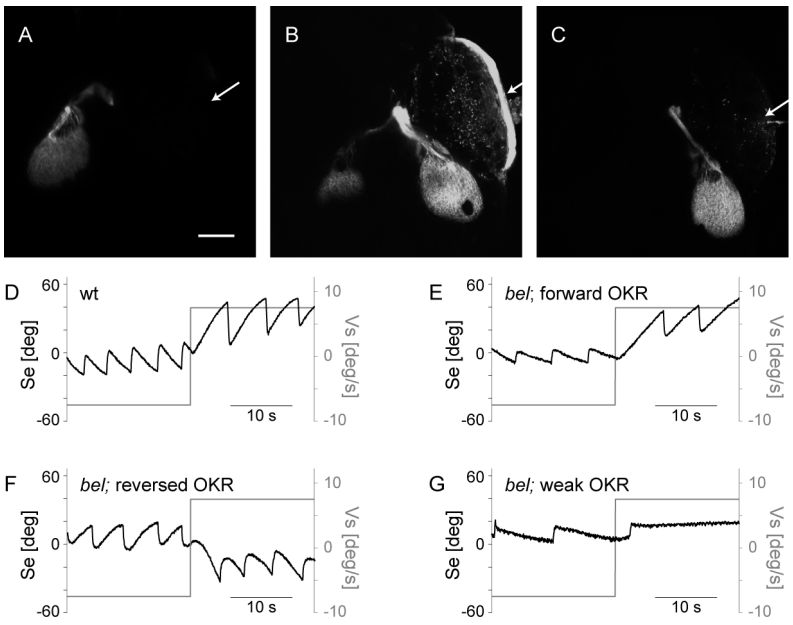


***Figure 4.1: Phenotypes of bel mutant larvae.***
***A–C****, Maximum intensity projections of z-stacks showing projection of optic nerve fibers in bel mutant larvae. The RGC axons were labeled by injecting the green lipophilic tracer dye DiO in the right eye and the red lipophilic tracer dye DiI in the left eye. Here the projection from the right eye is shown. Anterior is up. Scale bar, 100 µm. Arrow points to side of injection. The wt larvae as well as some bel larvae have a complete contralateral projection (**A**). In some bel larvae a variable fraction of axons misprojects ipsilaterally leading to a bilateral projection (**B**). Finally, some bel larvae are achiasmatic having a complete ipsilateral projection (**C**). **D–G**, OKR sample traces of eye position (Se) during stimulation with horizontal moving gratings (Vs). Some bel larvae show a properly directed OKR (**E**). Other larvae show a reversal of the OKR (**F**). Finally, some larvae show a weaker OKR with strongly reduced eye velocity and unclear direction (**G**).*

Larvae with contralateral projections show an OKR that is slightly reduced compared with wt but properly directed (forward OKR) (Fig. 4.1*D-E*). Larvae with achiasmatic projections show a reversal of the OKR (Fig. 4.1*F*) (Rick et al., 2000). Here, we additionally found some homozygous *bel* larvae with a clearly weaker (in some cases nearly abolished) OKR in terms of magnitude of eye velocity compared with other *bel* larvae (Fig. 4.1*G*). The magnitude of eye velocity refers to the absolute velocity of slow phases, i.e., the velocity independent of the direction. A weak OKR is often associated with alterations in the retina in both humans and zebrafish (Brockerhoff et al., 1995; Neuhauss et al., 1999; Shin et al., 2006; Wester et al., 2007). Thus, the weak OKR

observed in some *bel* larvae could be caused by morphological defects in the *bel* eye. On the other hand, it is conceivable that a weak OKR is the consequence of partial misrouting of the optic nerve. Misrouting of a fraction of optic nerve fibers could reduce OKR performance by introducing erroneously interpreted signals in the ocular motor system.

### 4.4.2 Larvae with a bilateral optic nerve projection display a weak OKR

To investigate whether a weaker OKR in terms of magnitude of eye velocity, as observed in a subset of *bel* larvae (*see* Fig. 4.1*G*), is linked to a particular form of optic nerve misrouting, we measured the OKR behavior using a monocular stimulation paradigm and subsequently stained with lipophilic tracer dyes the optic nerve fibers arising from the stimulated eye. Larvae were grouped according to their optic nerve projection phenotype (contralateral, bilateral, or ipsilateral projection) and the OKR SPV was compared among phenotypes (Fig. 4.2). As expected from previous reports (Neuhauss et al., 1999; Rick et al., 2000), larvae with a contralateral projection displayed a forward OKR with a slightly reduced velocity, while achiasmatic larvae displayed a reversed OKR. Interestingly, larvae with bilateral projections displayed a significantly weaker OKR compared with the other groups, i.e., a lower magnitude of eye velocity (Dunnett's T3 multiple comparison, $p < 0.001$).

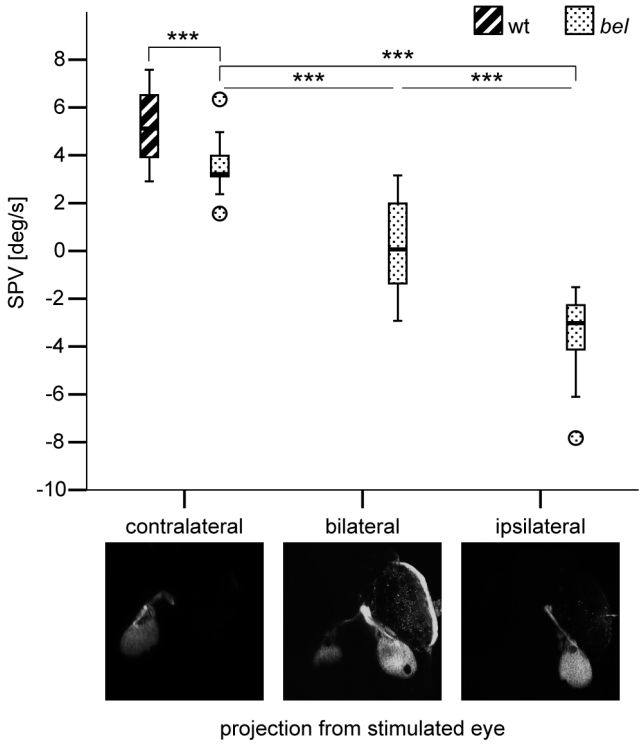


***Figure 4.2: OKR behavior in larvae with different optic nerve fiber projection phenotypes.***
*Box-and-whisker plot of the SPV during monocular OKR stimulation with moving gratings (7.5 deg/s) in wt (n = 17) and in bel larvae with different projection phenotypes (n = 17 in each group). A negative SPV value represents reversal of the OKR direction. The ends of the whiskers represent the lowest data point within 1.5 interquartile range of the lower quartile and the highest data point within 1.5 interquartile range of the upper quartile. Circles represent outliers. A one-way ANOVA showed that the OKR behavior differed significantly among groups of bel larvae with different projection phenotypes ($F_{(2,48)} = 81.007$, $p < 0.001$). Post hoc analysis using the Dunnett's T3 multiple-comparison criterion for significance indicated that the average SPV was significantly closer to 0 in bel larvae with bilateral projections (M = 0.22, SD = 1.95) than in both bel larvae with contralateral (M = 3.56, SD = 1.13) and ipsilateral (M = 49, SD = 1.66) projections. ***p < 0.001.*

### 4.4.3 The amount of misprojection correlates with the OKR SPV

Since the SPV in larvae with bilateral projections showed a high within-group variability (*see* Fig. 4.2), we asked whether the SPV correlates with the fraction of misprojecting axons. Therefore, the extent of misprojection from the stimulated eye was estimated in each larva by signal intensity quantification on both brain hemispheres and was correlated to the SPV (Fig. 4.3*A*). The extent of misprojection exhibited a strong negative correlation with SPV ($R^2$ = 0.75; $F_{(1,19)}$ = 56.95; $p$ < 0.001), which was maximal and positive in larvae with no misprojection, reduced in larvae with few misprojecting optic nerve fibers, and negative in larvae with a substantial fraction of misprojecting fibers (Fig. 4.3*B*).

In most larvae the amount of misprojection from the two eyes was comparable. In rare cases misprojection was different between the two eyes (Table 4.1). In these larvae we compared the correlation between the fraction of misprojecting fibers and SPV separately for each eye being stimulated. Within the same subject, the SPV correlated with the projection phenotype of the stimulated eye. This was particularly evident for one specimen (larva 4 in Table 4.1) in which the projection from the right eye was contralateral and the projection from the left eye was ipsilateral. Thus axons from both eyes projected to the same brain hemisphere. Stimulation of the right eye led to a positive SPV (+ 3.07 deg/s), stimulation of the left eye led to nearly the same absolute value, but negative (- 3.08 deg/s) (Table 4.1).

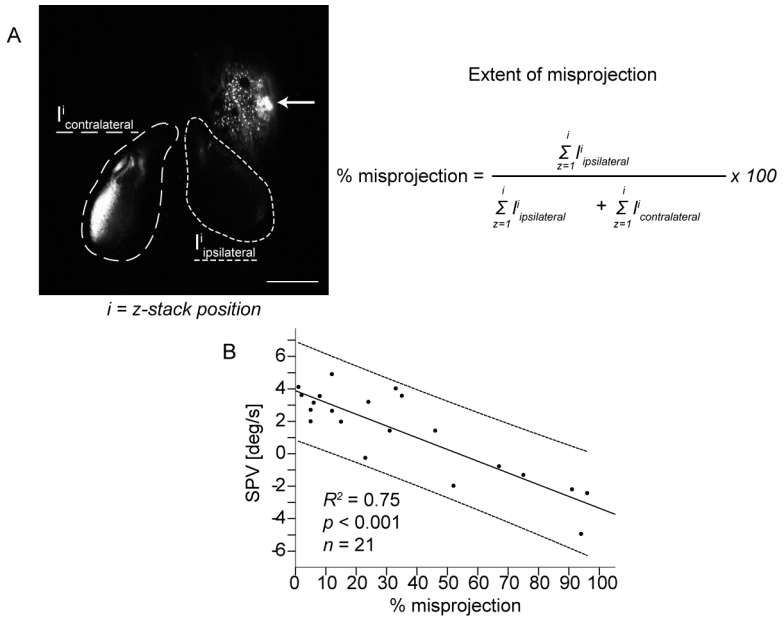


***Figure 4.3: Correlation between the extent of optic nerve fiber misprojection and SPV during monocular OKR stimulation with moving gratings (7.5 deg/s).***

***A**, Estimation of the extent of misprojection (percentage misprojection) after background subtraction: integrated signal intensity of the contralaterally projecting axons ($I_{contralateral}$, area marked with long dashes); integrated signal intensity of the ipsilaterally projecting axons ($I_{ipsilateral}$, area marked with short dashes); and i = z-stack position. Scale bar, 100 µm. Arrow points to the injection side. **B**, Extent of misprojection exhibited a negative correlation with the SPV ($R^2$ = 0.75; $F_{(1,19)}$ = 56.95; p < 0.001). Line of best fit and individual 95% confidence interval are shown.*

***Table 4.1: SPV in larvae with different optic nerve fibers projection phenotypes from the two eyes***

| | St.eye | % mispr. | SPV [deg/s] |
|---|---|---|---|
| Larva nr 1 | Right | 91 | -2.19 |
| | Left | 100 | -3.40 |
| Larva nr 2 | Right | 67 | -0.77 |
| | Left | 94 | -3.49 |
| Larva nr 3 | Right | 75 | -1.30 |
| | Left | 0 | 1.14 |
| Larva nr 4 | Right | 0 | 3.07 |
| | Left | 100 | -3.08 |

*St. eye, Stimulated eye; % mispr., percentage of misprojecting axons from stimulated eye; SPV, slow-phase velocity.*

### 4.4.4 Correlation between OKR velocity and SOs

INS patients show SOs of the eyes despite absent movement of the visual surround (Gresty et al., 1984). We previously reported about SOs in the presence of stationary gratings in a subset of *bel* larvae with a reversed OKR and presumed achiasmia (Huang et al., 2006). Here, we correlate the SOs with a quantitative extent of optic nerve fiber misprojection.

OKR in wt larvae ceases with the termination of motion of the visual surround and subsequently only saccades and small eye drifts are observed (Fig. 4.4*A*). In larvae with SOs the eyes keep moving under stationary structured background with eye position traces displaying characteristic nystagmus waveforms that can easily be distinguished from the OKR (Fig. 4.4*B*) (Huang et al., 2011). We hypothesized that both reversed OKR and SOs may be caused by optic nerve fiber misrouting. To compare the OKR phenotype with the occurrence of SOs, we first quantified the OKR SPV during stimulation with a monocular paradigm and subsequently we quantified the occurrence of SOs during fixation of a stationary background. Figure 4.4*C* shows the correlation between the duration of SOs and SPV and between the duration of SOs and the projection phenotype of optic nerve fibers. The wt larvae and *bel* larvae with a contralateral projection never displayed SOs. We did not observe SOs in larvae with a forward OKR, either. In contrast, both larvae with bilateral and completely ipsilateral projections displayed SOs if their OKR was reversed. The duration of SOs positively correlated with the velocity of the reversed OKR ($R^2 = 0.52$; $F_{(1,23)} = 22.56$; $p < 0.001$).

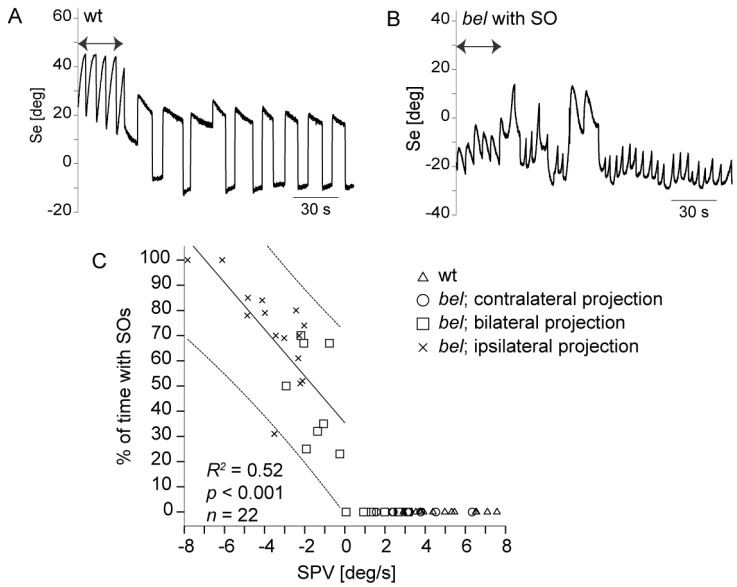


***Figure 4.4: Correlation between velocity of the reversed OKR and occurrence of SOs.***
***A-B,*** *Sample traces of eye position (Se) during stimulation with moving (7.5 deg/s) and horizontal stationary gratings. Arrows indicate a unidirectionally moving grating. The wt larva only showed saccades and slow eye drifts during presentation of stationary gratings (**A**). Under identical conditions, bel larvae with a reversal of the OKR displayed SOs without motion stimulus (**B**).* ***C,*** *Correlation between SPV during monocular OKR stimulation with moving gratings (7.5 deg/s) and occurrence of SOs. SOs were elicited during 5min by stationary black and white gratings presented to the same eye that was optokinetically stimulated. Finally, the optic nerve fibers from the stimulated eye were stained (see Materials and Methods). The duration of SOs showed a positive linear correlation with the reversed OKR ($R^2 = 0.52$; $F_{(1,21)} = 22.56$, $p < 0.001$). Line of best fit and individual 95% confidence interval are shown. Line of best fit was only defined for SPV < 0, since larvae with SPV > 0 never displayed SOs.*

### 4.4.5 Additional visual defects in *bel* mutants do not correlate with the ocular motor behavior

Although our data show a very strong correlation between the fraction of misprojecting optic nerve fibers and the ocular motor behavior, they cannot rule out a role of retinal defects in the ocular motor phenotype. Subtle morphological changes - a pigmentation defect and an acellular aggregate near the lens, disorganization of Mueller glial cells - have been observed in the *bel* eye (Seth et al., 2006). Like the optic nerve projection defect, those changes are highly variable. With the correlation studies outlined above we cannot exclude the possibility that the more severe ocular motor phenotype seen in larvae with more misprojecting axons is eventually due to a more severe general eye phenotype. Thus, larvae with more misprojecting axons could as well have more severe morphological defects in the eye. The retinal cell disorganization in *bel* larvae has been histologically described (Seth et al., 2006). However, there is no established method for quantification of the extent of those defects. Nevertheless, if the observed morphological changes in the eye played a role, we would expect additional aspects of visual performance to be affected and we would see a correlation between them and the ocular motor behavior.

Morphological changes of the Mueller glial cells affecting OKR are likely reflected in the electrical activity in the retina (Miller and Dowling, 1970). Therefore, an OKR phenotype caused by disorganization of Mueller glial cells is expected to result in an altered overall electrical activity of the retina as measured by the ERG. The ERG output of dark-adapted larvae consists of a small a-wave reflecting photoreceptor activation and a larger b-wave

reflecting ON bipolar cell activation (Fig. 4.5*A*). Here, we measured the ERG and quantified the b-wave amplitude in *bel* larvae to find out if there is any functional defect affecting the ON pathway, which is known to be involved in the OKR (Emran et al., 2007). To exclude any correlation between putative functional defects in the outer retina and ocular motor instabilities, we first quantified the OKR SPV of each larva during monocular OKR stimulation and subsequently recorded the ERG from the stimulated eye. Larvae were classified according to the SPV and the b-wave amplitude was compared between groups. The b-wave amplitude was significantly reduced in *bel* mutants compared with wt (one-way ANOVA, $F_{(5,73)} = 5.64$; $p < 0.001$). However, we did not find any difference between *bel* larvae with different SPV (Tukey-HSD, $p > 0.05$) (Fig. 4.5*B*).

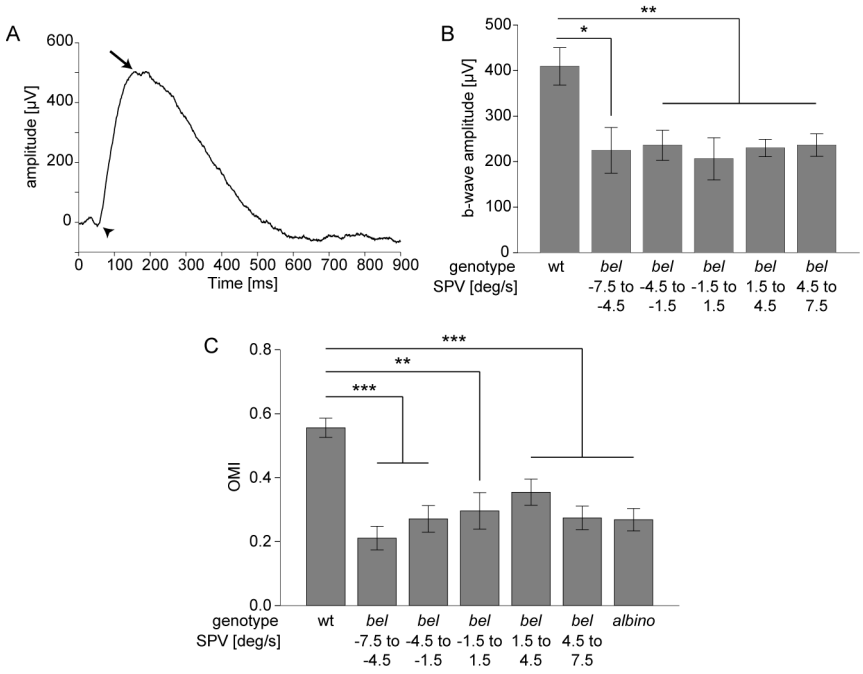


***Figure 4.5: General visual properties of bel larvae.***

***A*-*B***, *Electroretinography.* ***A***, *A typical ERG trace of a wt larva is shown. A stimulus of 700 lux was used. Arrowhead points to the a-wave; arrow points to the b-wave.* ***B***, *Graph showing b-wave average amplitudes (µV) (means of n ≥ 8 ± SEM) of wt and bel with different OKR phenotypes. A one-way ANOVA showed significant differences among groups ($F_{(5,73)} = 5.64$, $p < 0.001$). The mean b-wave amplitude of wt larvae differed significantly from all categories of bel larvae. The mean b-wave amplitude did not differ significantly between bel larvae with different OKR phenotypes (Tukey-HSD, $p > 0.05$). *$p < 0.05$; **$p < 0.01$.* ***C***, *OMR. Larvae were placed in tanks with a transparent bottom and were presented with gratings projected from below and moving from one end of the tank to the other. The magnitude of OMR was expressed as the OMI, the ratio between distance swum and length of the tank (see Materials and Methods). Graph shows OMI (means of n_10_SEM) of wt, of bel with different OKR phenotypes during binocular stimulation, and of albino mutants. A one-way ANOVA showed significant differences among groups ($F_{(6,114)} = 10.75$, $p < 0.001$). The mean OMI of wt larvae differed significantly from all categories of bel larvae and from albino mutants. The mean OMI did not significantly differ between bel larvae with different OKR phenotypes or between bel and albino larvae (Tukey-HSD, $p > 0.05$). **$p < 0.01$; ***$p < 0.001$.*

These results indicate that, although morphological eye defects in *bel* mutants do functionally affect the ON pathway, they equally change the retinal electrical activity among *bel* groups with different ocular motor phenotypes.

Morphological defects in the retina could affect visual acuity and motion vision (Neuhauss et al., 1999; Muto et al., 2005). However, they would affect general motion-dependent vision pathways and not only the OKR. To test whether the OKR abnormalities observed are specific to horizontal motion and thus caused by optic nerve fibers misrouting or whether general motion perception pathways are impaired, we performed an OMR assay. The OMR is a reflexive swimming behavior in the same direction as the perceived motion in the surround and is an indicator for the ability to correctly detect forward motion (Neuhauss et al., 1999; Muto et al., 2005). Of each larva we first measured the SPV during binocular optokinetic stimulation. Then we quantified the OMR (see Materials and Methods) and subsequently stained the retinofugal projections. The wt larvae displayed an average OMI (distance swum/length of the tank) of 0.56 ($M$ = 0.56, $SD$ = 0.17). The magnitude of the response was significantly reduced in *bel* larvae (one-way ANOVA, $F_{(6,114)} = 10.75$; $p < 0.001$), and was comparable to the magnitude in *albino* mutants (Fig. 4.5*C*). *albino* mutants have defects in the retinal pigment epithelium without major visual impairments (Neuhauss et al., 1999). When a whole clutch of *albino* larvae was placed inside a tank and the OMR performance of the clutch was analyzed (measured as the percentage of larvae being at the end of the tank after the trial), only a slight reduction in performance was observed compared with wt (data not shown). These results suggest a slight deficiency in perceiving and processing forward motion in *bel* mutants. Nevertheless, we did not detect any difference in the OMR magnitude between *bel* larvae with different SPV during OKR (Tukey-HSD, $p > 0.05$) (Fig. 4.5*C*) or different optic nerve projection phenotypes (data not shown), indicating that the general deficit in motion vision does not correlate with the ocular motor abnormalities.

Together, our data indicate that the observed morphological defects in the retina are not related to the INS-like phenotype.

## 4.5 Discussion

Several studies in humans have described an association of reversed OKR and/or SOs with abnormal decussation of optic nerve fibers in the optic chiasm (St John et al., 1984; Collewijn et al., 1985; McCarty et al., 1992). Often, misrouted axons are mixed in with correctly projecting ones (Jeffery, 1997). Possibly because of this, the OKR is not always reversed but can also be weak or nearly normal (Collewijn et al., 1985). In our study we show for the first time in *bel* mutants a wide range of forward and reversed OKR with different velocities (*see* Fig. 4.1) and an effect on the ocular motor phenotype when a few optic nerve fibers are misrouted. To understand this effect, we performed an in-depth correlation study between the extent of optic nerve misprojection and the ocular motor phenotype. Our data not only give new insights into the pathomechanisms underlying INS in patients with optic nerve fiber misprojections but are also an example of how interference with feedback loops in the nervous system affects behavior and on how the brain adapts to conflicting neuronal signals.

### 4.5.1 OKR velocity and direction correlate with the fraction of misprojecting optic nerve fibers

We show that the OKR efficiency is directly correlated with the extent of optic nerve misrouting with a reduction of the OKR SPV in larvae with few misprojecting fibers and a reversal in larvae with a substantial amount of misprojecting fibers (*see* Fig. 4.3). We show a direct correlation between optic nerve misrouting and OKR phenotype even in larvae in which the projection phenotype is different between the two eyes (*see* Table 1). These results further support our previously formulated hypothesis that misprojecting optic nerve axons lead to direction inverted interpretation of an information about horizontal whole field motion (Rick et al., 2000). In wt zebrafish a moving visual input triggers movement of the eyes in the same direction via the contralaterally located OKR integration network (OIN; Fig. 4.6*A*). This negative feedback loop reduces retinal slip. In achiasmatic larvae the visual input signal is fed to the ipsilaterally located OIN and is therefore interpreted as originating from the opposite eye. A stimulation of the left eye with horizontal clockwise rotating gratings triggers a temporal to nasal movement of the eyes. Since the information is interpreted as originating from the right eye in an achiasmatic larva, temporal to nasal corresponds to counterclockwise rotation so that the eyes will move in the opposite direction (Fig. 4.6*E*). This generates a positive feedback loop in the optokinetic system, which further increases retinal slip. In larvae with a bilateral projection, misrouting of a fraction of optic nerve fibers leads to a conflict between correctly and erroneously interpreted signals. Few misprojecting axons might insert some erroneous signals in an otherwise normal OKR, thus just leading to a reduction of the SPV (Fig. 4.6*B*). When around half of the axons are misprojecting, the conflict between correct and erroneous signals is the highest leading to a disappearance of the OKR (Fig. 4.6*C*). Finally, when a majority of axons project to the wrong brain hemisphere, this misinterpreted information prevails, leading to a reversal of the OKR (Fig. 4.6*D*).

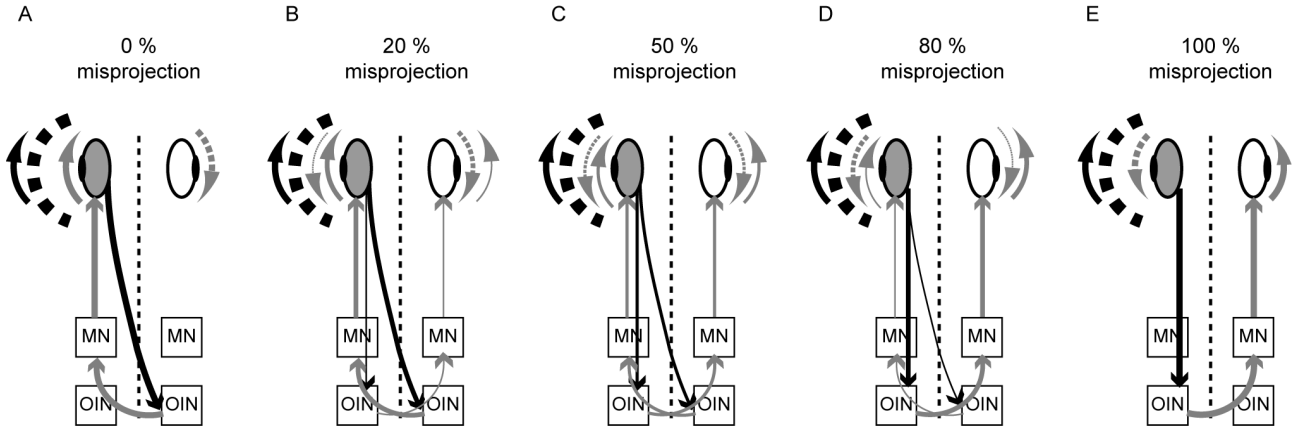


***Figure 4.6: Model of OKR feedback loop in bel larvae with different amounts of misprojection.***
***A,*** *In the absence of misprojecting fibers, the clockwise rotating visual stimulus (black and white) is perceived by the stimulated eye (gray) and the information is transferred across the midline (dashed line) to the yet unknown contralaterally located OIN. The OIN sends the signal again across the midline to the motor nuclei (MN) of the stimulated eye, leading to a compensatory eye movement in the direction of the stimulus (gray arrow around the eye). The other eye is driven in the same direction (dashed arrow).* ***B–E,*** *With an increasing amount of misprojection, more signal is sent to the ipsilateral OIN, leading to transmission of the information to the wrong eye (see Discussion). The size of the arrows represents the amount of information flow in each direction.*

Previous studies have shown that pretectal nuclei rather than the tectum, which is the main arborization field of RGCs, are involved in the zebrafish OKR circuit (Roeser and Baier, 2003). As a consequence, we expect only a small subset of RGCs to be involved in the OKR. Since we stained the complete optic nerve, the correlation between OKR phenotype and extent of misprojection in the general RGC population is surprisingly strong. This can be explained by the fact that terminals of misprojecting axons are found at different arborization locations and topographic arborization of RGC axons is maintained in *bel* mutants (Karlstrom et al., 1996). Thus misprojecting axons can originate from everywhere in the retina and the amount of misprojection in the whole population reflects quite well the amount of misprojection within the subclass of RGCs involved in the OKR circuit.

### 4.5.2 Extent of the OKR reversal correlates with the occurrence of spontaneous oscillations

We could demonstrate that SOs only occur in larvae with a reversed OKR and that the overall duration of oscillations during fixations correlates positively with the reversed SPV. This correlation is highly significant ($p < 0.001$) but rather low ($R^2 = 0.52$). This can easily be explained by the fact that, once oscillations stop, a random spontaneous saccade is most likely needed to start oscillations again.

In zebrafish optic nerve fibers pathfinding and arborization are completed before visual experience and development of the eye movements (Burrill and Easter, 1994; Easter and Nicola, 1996), This is also true for misprojecting axons of the optic nerve fibers in *bel* mutants (Seth et al., 2006). Thus, SOs cannot be the primary cause that leads to adaptation of the visual system. In contrast, the relationships observed agree with the idea of a feedback loop that has become positive because of the miswired optokinetic nerve fibers, thus leading to the inability to stabilize retinal slip. Misrouting of a small fraction of axons leads to a weaker OKR but not to SOs. Interestingly, the observation of a weak OKR in the absence of SOs has been made also in obligate carriers of the *FRMD7* mutation in what can be seen as a subclinical manifestation of idiopathic INS (Thomas et al., 2008).

It has been suggested that the reversal of the OKR is an illusion due to the superimposition of SOs (Yee et al., 1980). We can exclude this in *bel* mutants because in most cases the OKR had its own characteristics with decelerating slow phases synchronized with the direction of stimulation, either being in the same direction or being inverted (*see* Fig. 4.1). We only rarely observed superimposition of OKR and SOs. Those few larvae were excluded from analysis.

### 4.5.3 Additional visual defects in *bel* mutants do not correlate with the ocular behavior

INS in humans has not only been associated to optic nerve misrouting but also to abnormalities in the retina (Khanna and Dell'Osso, 2006). Subtle retinal defects - a pigmentation defect and an acellular aggregate near the lens, disorganization of Mueller glial cells - are also observed in *bel* mutants (Seth et al., 2006). Comparison between the extent of the pigmentation defect and the ocular motor phenotype did not provide evidence for such a relationship (data not shown). However, a possible correlation and causal relationship between defects in the retina and ocular motor abnormalities cannot be excluded a priori. We previously reported on a slight reduction of eye velocity during OKR in *bel* larvae with a forward OKR (Huang et al., 2006). Here, we found a significant reduction of the ERG b-wave amplitude, indicative of functional defects in the ON pathway, and a significant

impairment of general motion pathways (*see* Fig. 4.5). Thus morphological eye defects affect vision in *bel* larvae, but do not lead to blindness, as indicated by the residual ERG b-wave and by a normal increase in reflexive body movement as a reaction to changes in illumination (data not shown). This is also true for *bel* larvae with an abolished OKR. Moreover, general visual impairment is present homogenously in all *bel* larvae, regardless of the ocular motor phenotype. Therefore, we can assume that INS-like findings in zebrafish are caused by the optic nerve fibers misrouting.

### 4.5.4 Significance for the debate on the etiology of INS in humans

The mechanisms underlying INS are still under debate. Approaches using mathematical models support possibilities that range from an essentially motor defect (Harris, 1995; Broomhead et al., 2000; Jacobs and Dell'Osso, 2004) to a clearly sensory driven pathology (Optican and Zee, 1984; Tusa et al., 1992). Another hypothesis states that INS is a developmental disorder triggered by any event that disturbs either calibration of visual feedback loops (Tusa et al., 2002; Harris and Berry, 2006a, b; Dell'Osso, 2006) or regulation of innervations during early development (Berg et al., 2012). Here, we show that INS in zebrafish has a sensory origin, being triggered by optic nerve fiber misrouting. The association of INS with visual pathway abnormalities in a subset of human patients (e.g., in albinism) suggests that optic nerve misrouting may indeed trigger the pathology in a similar way in those patients. However, the observation of SOs only in larvae with an OKR reversal is in contrast with reports in albino humans and, most recently, in hypopigmented mice (Collewijn et al., 1985; Traber et al., 2012). Interestingly, in the hypopigmented mouse model the OKR became reversed if the visual stimulation was restricted to the temporal retina only, where most misrouting occurs (Traber et al., 2012). This suggests that a reversal of the OKR could also be elicited in subjects with only a limited fraction of axons misprojecting if only that very part of the retina is stimulated from where those misrouted axons originate. In contrast, a full-field stimulation of the OKR in a laboratory setting, as is now routinely performed, stimulates all optic nerve fibers. Together, our data combined with findings in other models suggest that, during early development, optokinetic stimulation of retinal regions from where misrouting axons originate increases retinal slip and triggers SOs. Adaptive calibration of the efferent ocular motor system later during development may lead to maintenance of SOs - although at reduced amplitude - when few misrouting axons are stimulated or even in darkness, thus in the absence of vision.

### 4.5.5 Conclusion

Our study provides detailed insights on how optic nerve misrouting influences ocular motor stability in the zebrafish INS model. The use of larval zebrafish enables us to study the triggering mechanisms without the complication of further adaptive mechanisms during the ocular motor system development. We suggest that abnormal decussation of retinofugal fibers at the optic chiasm might be the origin of INS in a substantial number of patients, although not in all as eye oscillations also occur in patients that do not show abnormal decussation. Nevertheless, as visual pathway abnormalities are not routinely investigated in INS patients and are difficult to quantify, they are most likely underdiagnosed.

## 4.6 References


Abadi RV (2002) Mechanisms underlying nystagmus. J R Soc Med 95:231-234.

Berg KT, Hunter DG, Bothun ED, Antunes-Foschini R, McLoon LK (2012) Extraocular muscles in patients with infantile nystagmus: adaptations at the effector level. Arch Ophthalmol 130:343-349.

Betts-Henderson J, Bartesaghi S, Crosier M, Lindsay S, Chen HL, Salomoni P, Gottlob I, Nicotera P (2010) The nystagmus-associated FRMD7 gene regulates neuronal outgrowth and development. Hum Mol Genet 19:342-351.

Brockerhoff SE, Hurley JB, Janssen-Bienhold U, Neuhauss SC, Driever W, Dowling JE (1995) A behavioral screen for isolating zebrafish mutants with visual system defects. Proc Natl Acad Sci U S A 92:10545-10549.

Broomhead DS, Clement RA, Muldoon MR, Whittle JP, Scallan C, Abadi RV (2000) Modelling of congenital nystagmus waveforms produced by saccadic system abnormalities. Biol Cybern 82:391-399.

Burrill JD, Easter SS, Jr. (1994) Development of the retinofugal projections in the embryonic and larval zebrafish (*Brachydanio rerio*). J Comp Neurol 346:583-600.

Collewijn H, Apkarian P, Spekreijse H (1985) The oculomotor behaviour of human albinos. Brain 108 ( Pt 1):1-28.

Dell'Osso LF (2006) Biologically relevant models of infantile nystagmus syndrome: the requirement for behavioral ocular motor system models. Semin Ophthalmol 21:71-77.

Easter SS, Jr., Nicola GN (1996) The development of vision in the zebrafish (Danio rerio). Dev Biol 180:646-663.

Emran F, Rihel J, Adolph AR, Wong KY, Kraves S, Dowling JE (2007) OFF ganglion cells cannot drive the optokinetic reflex in zebrafish. Proc Natl Acad Sci U S A 104:19126-19131.

Gresty M, Page N, Barratt H (1984) The differential diagnosis of congenital nystagmus. J Neurol Neurosurg Psychiatry 47:936-942.

Halmagyi GM, Gresty MA, Leech J (1980) Reversed optokinetic nystagmus (OKN): mechanism and clinical significance. Ann Neurol 7:429-435.

Harris C, Berry D (2006a) A developmental model of infantile nystagmus. Semin Ophthalmol 21:63-69.

Harris CM (1995) Problems in modelling congenital nystagmus: Towards a new model. In: Eye Movement Research: Processes, Mechanisms and Applications (Findlay JM, Walker R, Kentridge RW, eds), pp 239-253. Amsterdam: Elsevier.

Harris CM, Berry D (2006b) A distal model of congenital nystagmus as nonlinear adaptive oscillations. Nonlinear Dynamics 44:367-380.

Huang MY, Chen CC, Huber-Reggi SP, Neuhauss SC, Straumann D (2011) Comparison of infantile nystagmus syndrome in achiasmatic zebrafish and humans. Ann N Y Acad Sci 1233:285-291.

Huang YY, Rinner O, Hedinger P, Liu SC, Neuhauss SC (2006) Oculomotor instabilities in zebrafish mutant belladonna: a behavioral model for congenital nystagmus caused by axonal misrouting. J Neurosci 26:9873-9880.

Jacobs JB, Dell'Osso LF (2004) Congenital nystagmus: hypotheses for its genesis and complex waveforms within a behavioral ocular motor system model. J Vis 4:604-625.

Jeffery G (1997) The albino retina: an abnormality that provides insight into normal retinal development. Trends Neurosci 20:165-169.

Karlstrom RO, Trowe T, Klostermann S, Baier H, Brand M, Crawford AD, Grunewald B, Haffter P, Hoffmann H, Meyer SU, Muller BK, Richter S, van Eeden FJ, Nusslein-Volhard C, Bonhoeffer F (1996) Zebrafish mutations affecting retinotectal axon pathfinding. Development 123:427-438.

Khanna S, Dell'Osso LF (2006) The diagnosis and treatment of infantile nystagmus syndrome (INS). ScientificWorldJournal 6:1385-1397.

Makhankov YV, Rinner O, Neuhauss SC (2004) An inexpensive device for non-invasive electroretinography in small aquatic vertebrates. J Neurosci Methods 135:205-210.

Maybodi M (2003) Infantile-onset nystagmus. Curr Opin Ophthalmol 14:276-285.

McCarty JW, Demer JL, Hovis LA, Nuwer MR (1992) Ocular motility anomalies in developmental misdirection of the optic chiasm. Am J Ophthalmol 113:86-95.

McLean RJ, Windridge KC, Gottlob I (2012) Living with nystagmus: a qualitative study. Br J Ophthalmol 96: 981-986.

Miller RF, Dowling JE (1970) Intracellular responses of the Muller (glial) cells of mudpuppy retina: their relation to b-wave of the electroretinogram. J Neurophysiol 33:323-341.

Mullins MC, Hammerschmidt M, Haffter P, Nusslein-Volhard C (1994) Large-scale mutagenesis in the zebrafish: in search of genes controlling development in a vertebrate. Curr Biol 4:189-202.

Muto A, Orger MB, Wehman AM, Smear MC, Kay JN, Page-McCaw PS, Gahtan E, Xiao T, Nevin LM, Gosse NJ, Staub W, Finger-Baier K, Baier H (2005) Forward genetic analysis of visual behavior in zebrafish. PLoS Genet 1:e66.

Neuhauss SC, Biehlmaier O, Seeliger MW, Das T, Kohler K, Harris WA, Baier H (1999) Genetic disorders of vision revealed by a behavioral screen of 400 essential loci in zebrafish. J Neurosci 19:8603-8615.

Optican LM, Zee DS (1984) A hypothetical explanation of congenital nystagmus. Biol Cybern 50:119-134.

Pilling RF, Thompson JR, Gottlob I (2005) Social and visual function in nystagmus. Br J Ophthalmol 89:1278-1281.

Rick JM, Horschke I, Neuhauss SC (2000) Optokinetic behavior is reversed in achiasmatic mutant zebrafish larvae. Curr Biol 10:595-598.

Rinner O, Rick JM, Neuhauss SC (2005) Contrast sensitivity, spatial and temporal tuning of the larval zebrafish optokinetic response. Invest Ophthalmol Vis Sci 46:137-142.

Roeser T, Baier H (2003) Visuomotor behaviors in larval zebrafish after GFP-guided laser ablation of the optic tectum. J Neurosci 23:3726-3734.

Sarvananthan N, Surendran M, Roberts EO, Jain S, Thomas S, Shah N, Proudlock FA, Thompson JR, McLean RJ, Degg C, Woodruff G, Gottlob I (2009) The prevalence of nystagmus: the Leicestershire nystagmus survey. Invest Ophthalmol Vis Sci 50:5201-5206.

Seth A, Culverwell J, Walkowicz M, Toro S, Rick JM, Neuhauss SC, Varga ZM, Karlstrom RO (2006) belladonna/(Ihx2) is required for neural patterning and midline axon guidance in the zebrafish forebrain. Development 133:725-735.

Shin YJ, Park KH, Hwang JM, Wee WR, Lee JH, Lee IB (2006) Objective measurement of visual acuity by optokinetic response determination in patients with ocular diseases. Am J Ophthalmol 141:327-332.

St John R, Fisk JD, Timney B, Goodale MA (1984) Eye movements of human albinos. Am J Optom Physiol Opt 61:377-385.

Straw AD (2008) Vision egg: an open-source library for realtime visual stimulus generation. Front Neuroinformatics 2:4.

Tarpey P et al. (2006) Mutations in FRMD7, a newly identified member of the FERM family, cause X-linked idiopathic congenital nystagmus. Nat Genet 38:1242-1244.

Thomas S, Proudlock FA, Sarvananthan N, Roberts EO, Awan M, McLean R, Surendran M, Kumar AS, Farooq SJ, Degg C, Gale RP, Reinecke RD, Woodruff G, Langmann A, Lindner S, Jain S, Tarpey P, Raymond FL, Gottlob I (2008) Phenotypical characteristics of idiopathic infantile nystagmus with and without mutations in FRMD7. Brain 131:1259-1267.

Traber GL, Chen CC, Huang YY, Spoor M, Roos J, Frens MA, Straumann D, Grimm C (2012) Albino Mice as an Animal Model for Infantile Nystagmus Syndrome. Invest Ophthalmol Vis Sci.

Tusa RJ, Zee DS, Hain TC, Simonsz HJ (1992) Voluntary control of congenital nystagmus. Clinical Vision Science 7:195-210.

Tusa RJ, Mustari MJ, Das VE, Boothe RG (2002) Animal models for visual deprivation-induced strabismus and nystagmus. Ann N Y Acad Sci 956:346-360.

Watkins RJ, Thomas MG, Talbot CJ, Gottlob I, Shackleton S (2012) The Role of FRMD7 in Idiopathic Infantile Nystagmus. J Ophthalmol 2012:460956.

Wester ST, Rizzo JF, 3rd, Balkwill MD, Wall C, 3rd (2007) Optokinetic nystagmus as a measure of visual function in severely visually impaired patients. Invest Ophthalmol Vis Sci 48:4542-4548.

Yee RD, Baloh RW, Honrubia V (1980) Study of congenital nystagmus: optokinetic nystagmus. Br J Ophthalmol 64:926-932.

# Chapter 5

# Individual Zebrafish Larvae with Infantile Nystagmus Syndrome Display Multiple Nystagmus Waveforms, which Are Influenced by Viewing Conditions

**Sabina Huber-Reggi[1,4], Kaspar P. Mueller[1], Dominik Straumann[2,3], Melody Ying-Yu Huang[2,3], Stephan C. F. Neuhauss[1,3,δ]**

[1]Institute of Molecular Life Sciences, University of Zurich, Zurich, Switzerland
[2]Department of Neurology, University Hospital Zurich, Zurich, Switzerland
[3]Center for Integrative Human Physiology, University of Zurich, Zurich, Switzerland
[4]PhD Program in Integrative Molecular Medicine, Life Science Graduate School, Zurich, Switzerland
[δ] corresponding author

**Article submitted for publication to** *Investigative Ophthalmology & Visual Sciences*

**Funding**

This work was supported by the Zurich Center for Integrative Human Physiology, by the EU Framework 7 (ZF_HEALTH) and the Swiss National Foundation (grants PMPDP3 139754, 31003A-133125, and 31003A-135598)

**Acknowledgments**

The authors thank Drs. Christian Grimm, Maarten Frens, and Chris Bockisch for fruitful discussion, Dr. Matthias Gesemann for critical reading of the manuscript, and Kara Dannenhauer for excellent fish care.

**Personal contribution**

Performing of all the experiments and data analysis, preparation of all figures, writing of the manuscript. Movies of eye movements were recorded with an unpublished software written by KM.

## 5.1 Abstract

Purpose: Infantile nystagmus syndrome (INS) is characterized by involuntary eye oscillations that can assume different waveforms. Previous attempts to uncover reasons for the presence of several nystagmus waveforms have not led to a general consensus in the community. Recently, we characterized the zebrafish mutant *belladonna* (*bel*), in which INS-like ocular motor abnormalities are caused by misprojection of a variable fraction of optic nerve fibers. Here, we study the intrinsic and extrinsic factors influencing the occurrence of different waveforms in *bel*.

Methods: Eye movements of *bel* larvae were recorded in the presence of a stationary grating pattern. Waveforms of spontaneous oscillations were grouped in three categories: "pendular", "unidirectional jerk", and "bidirectional jerk" and the occurrence of each category was compared among individual larvae. Moreover, the effects of the characteristics of a preceding optokinetic response (OKR), of the field of view and of the eye orbital position were analyzed.

Results: The different waveform categories co-occurred in most individuals. We found waveforms being influenced by the characteristics of a preceding OKR and by the field of view. Moreover, we found in a subset of individuals a significant correlation between orbital position and initiation of a specific waveform either due to pendular nystagmus occurring in a more eccentric orbital position or due to differences among jerk oscillations regarding beating direction of the first saccade or waveform amplitude.

Conclusions: Our data suggest that waveform categories in *bel* larvae do not reflect the severity of the morphological phenotype but rather are influenced by viewing conditions.

## 5.2 Introduction

Infantile nystagmus syndrome (INS), present at birth or shortly after, is a congenital ocular motor disorder characterized by involuntary conjugate, predominantly horizontal oscillations of the eyes (Gresty et al., 1984; Maybodi, 2003) which can have a severe effect on occupational and social functioning (Pilling et al., 2005; McLean et al., 2012). The prevalence is approximately 2 per 1000 individuals (Sarvananthan et al., 2009). Eye oscillations can display pendular or jerk waveforms. Pendular nystagmus is a sinusoidal oscillation, jerk nystagmus is characterized by accelerating slow drifts and fast resetting phases (saccades). Although INS can be idiopathic, it is often associated with visuo-sensory abnormalities such as fovea hypoplasia, misprojecting optic nerve fibers, and aniridia (Khanna and Dell'Osso, 2006). Attempts to cluster INS according to the underlying condition and the eye oscillation characteristics in patients have led to contradictory conclusions (Abadi and Dickinson, 1986; Hertle and Dell'Osso, 1999; Abadi and Bjerre, 2002; Thomas et al., 2008; Kumar et al., 2011), mainly due to the variety of concomitant conditions. Mathematical models, developed to generate common waveforms, may be able to simulate recorded data of human eye movements, but they do not necessarily signify biological relevance. Therefore, a study of the occurrence and characteristics of nystagmus waveforms in an animal model with a well defined underlying morphological phenotype is needed.

Recently, we introduced the zebrafish mutant *belladonna* (*bel*) as an animal model for INS (Huang et al., 2006; Huang et al., 2011). In *bel* homozygous larvae, a variable fraction of optic nerve fibers are misrouted in the optic chiasm and project to the wrong brain hemisphere, a condition caused by mutations in *lhx2*, a Lim domain homeobox transcription factor (Karlstrom et al., 1996; Neuhauss et al., 1999; Rick et al., 2000; Seth et al., 2006). Depending on the percentage of misprojecting fibers, *bel* larvae display INS-like ocular motor instabilities, such as a reversed optokinetic response (OKR) and - in the presence of a structured background - spontaneous eye oscillations with the same diagnostic waveforms reported in humans (Dell'Osso and Daroff, 1975; CEMASWorkingGroup, 2001; Huang et al., 2011; Huber-Reggi et al., 2012). Here, we investigate whether the occurrence of different waveforms varies among *bel* individuals, thus reflecting different morphological conditions (i.e. optic nerve projection phenotypes). Moreover, we investigate how viewing conditions affect waveform characteristics.

## 5.3 Material and Methods

All experiments were performed in accordance with the animal welfare guidelines of the Federal Veterinary Office of Switzerland. Experiments adhered to the ARVO Statement for the Use of Animals in Ophthalmic and Vision Research.

### 5.3.1 Fish maintenance and breeding

Fish were maintained and bred as previously described (Mullins et al., 1994). Embryos were raised at 28°C in E3 medium (5 mM NaCl, 0.17 mM KCl, 0.33 mM $CaCl_2$, 0.33 mM $MgSO_4$) and staged according to development in days post-fertilization (dpf). *bel* ($bel_{tv42}$) homozygous larvae were obtained from mating of identified heterozygous carriers. Larvae at 4 dpf were anesthetized with 200 mg/l 3-aminobenzoic acid ethyl esther

methane sulfonate (MS-222, Sigma-Aldrich) and sorted according to eye pigmentation phenotype (Karlstrom et al., 1996).

### 5.3.2 Eye movement recording and analysis

Larval eye movements were elicited as described previously (Huber-Reggi et al., 2012; Huber-Reggi et al., 2013). The presented stimulus was a computer-generated (Straw, 2008) black and white sine-wave grating pattern (contrast 85 % and maximum illumination 400 lux, spatial frequency 20 cycles/360 deg). Spontaneous oscillations occurred in the presence of a stimulating stationary pattern (in complete darkness *bel* larvae do not show eye oscillations (Huang et al., 2006)), OKR was elicited by a rotating pattern (angular velocity 7.5 deg/s). Depending on the experiment, the pattern was presented binocularly or monocularly. Monocular presentation was achieved by restriction of the visual field to one eye.

Binocular eye movements were recorded by an infrared-sensitive CCD camera (Guppy F-038B NIR, Allied Vision Technologies). Frames were processed by a custom-developed tracking software based on LabView 2011 and NI Vision Development Module 2011 (National Instruments) with a frame rate of 25 frames/s. The software recognizes the eyes based on pixel intensity, extracts the angular position relative to the stimulation/recorded picture and calculates the velocity. Eye position and eye velocity traces were both used for the characterization of nystagmus waveforms. The relative frequency of a specific waveform (% of period with spontaneous oscillations) was computed by dividing the total time of oscillations with this waveform by the total time of all oscillations during the recorded period. Since nystagmus was always conjugate, only the data from the right eye were used in the analysis. For analysis of orbital position relative to the larval body, movie frames were analyzed with the angle tool of ImageJ (Abramoff et al., 2004). Orbital position was defined by the angle between a transversal line caudal to the eyes and a line that goes through the lens of the stimulated eye (*see* Fig. 5.4*A*). Both lines were drawn manually. Body movements were detected by visual inspection. If such a movement occurred, the transversal line was manually repositioned according to the position of body pigmentation.

### 5.3.3 Statistical analysis

Statistical analysis and graph generation were performed with SPSS Statistics 19 (IBM). Influence of stimulus condition on the occurrence of each waveform was analyzed using paired t-tests after transformation of percentage data using the formula $\sin^{-1}\sqrt{x}$, where x is the experimental data expressed as percentage. Since orbital position data were not normally distributed (Kolmogorov-Smirnov test), the relationship between orbital position and nystagmus waveform was analyzed in each larva using non parametric tests, i.e. Mann-Whitney U Test or Kruskal-Wallis Test (*see* Fig. 5.4). In the case of multiple comparison, the level of significance was adjusted for multiple testing by means of a Bonferroni correction.

## 5.4 Results

### 5.4.1 Categorization of nystagmus waveforms

Nystagmus in *bel* mutants matches the diagnostic waveforms of INS described by Dell'Osso and Daroff (Dell'Osso and Daroff, 1975; Huang et al., 2011). For quantification of waveforms occurrence, we grouped them into 3 main categories - pendular nystagmus, unidirectional jerk and bidirectional jerk - depending on the presence and direction of intercalated saccades (Fig. 5.1*A*). Pendular nystagmus is a sinusoidal oscillation without saccades. The absence of saccades is verified by examining the eye velocity trace. Unidirectional jerk consists of cycles of accelerating slow phases in one direction and breaking saccades in the opposite direction. Bidirectional jerk consists of cycles in alternating direction of slow phases and saccades. Saccades are seen as spikes in the eye velocity trace either always in the same direction (unidirectional jerk) or in alternating direction (bidirectional jerk).

### 5.4.2 Co-occurrence of multiple waveform categories in single larvae

To investigate whether individual larvae show single or multiple waveform categories, we quantified the occurrence of waveform categories during eye movement recordings in individual larvae with OKR ranging from weakly reversed to strongly reversed (data not shown), which indicates a variable morphological phenotype among them (Huber-Reggi et al., 2012). The presence of predominant waveforms in single larvae would suggest that different waveforms might reflect different morphological phenotypes.

To quantify occurrences and co-occurrences of waveforms in individual larvae, we selected the time points at which oscillations started or at which oscillations of one waveform changed to oscillations of another waveform. We frequently observed changes of waveforms without interruption of the ongoing oscillations (Fig. 5.1*B-C*). If oscillations stopped for a certain period, they reappeared either with an accelerating slow drift of the eyes (Fig. 5.1*D*) or after a saccade (Fig. 5.1*E*).

Waveforms of different categories occurred over time within the same larva and all three waveform categories co-occurred in 16 out of 20 larvae (Fig. 5.2). Hence, classical waveform categories are not useful as predictors of specific morphological phenotypes.

In 5 out of 20 larvae some cycles of unidirectional jerk with decelerating slow phases were observed. Although this waveform is characteristic of Fusion Maldevelopment Nystagmus (FMNS) (formerly known as latent nystagmus), it has been reported to occur for short periods in INS patients as well (CEMASWorkingGroup, 2001).

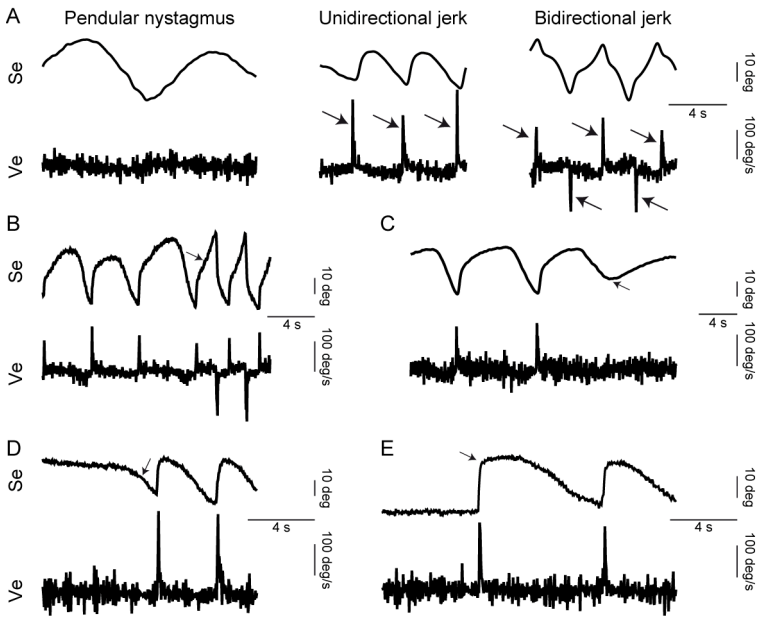


***Figure 5.1: Nystagmus waveforms.***

*Movements of the right eye in the presence of a stationary grating pattern. A higher value on the y-axis indicates a more temporal position.* ***A,*** *Representative eye position traces (Se (deg)) are shown together with corresponding eye velocity traces (Ve (deg/s)). Arrows in the eye velocity trace indicate saccades.* ***B-E,*** *Representative oscillations with waveform change are shown on eye position traces and their corresponding eye velocity traces. Arrows indicate the time point of waveform change. In* ***B,*** *a change from unidirectional jerk to bidirectional jerk is shown: After a saccade, the decelerating eye increases its velocity again before turning to the opposite direction. In* ***C,*** *a change from unidirectional jerk to pendular nystagmus is shown: A saccade is replaced by a slow eye movement. In* ***D*** *and* ***E,*** *a starting unidirectional jerk after a period without oscillations is shown. A period with nystagmus started either with an accelerating eye drift (****D****) or after a spontaneous saccade (****E****).*

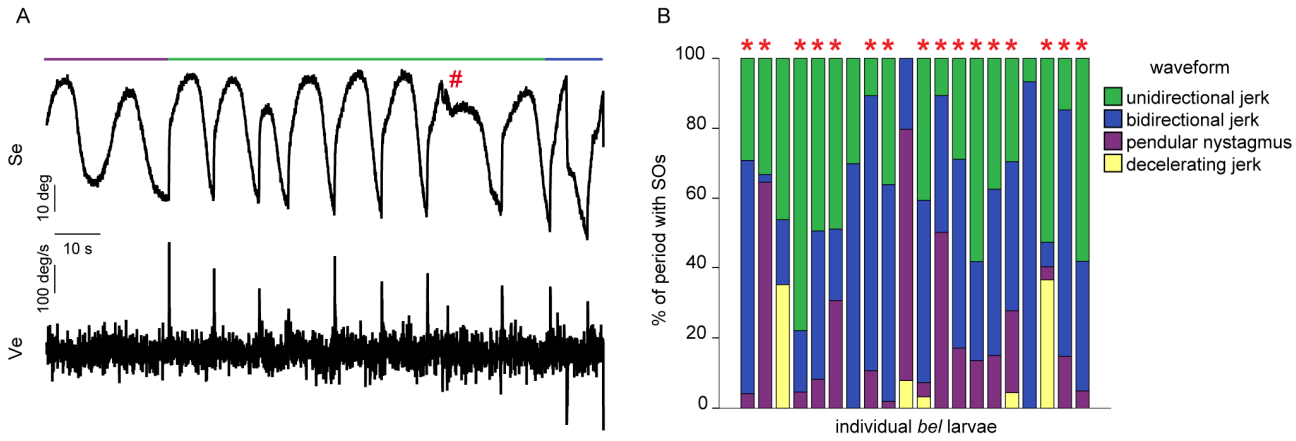


***Figure 5.2: Co-occurring waveforms.***

*A stationary grating pattern was presented to the full field of view of both eyes (binocular stimulation) during 5 minutes. Movements of the right eye were used for analysis.* ***A,*** *Representative segment of an eye position trace (Se (deg)) is shown together with the corresponding eye velocity trace (Ve (deg/s)). The 3 main waveform categories occurred without interruption of the oscillations in this larva. Pendular nystagmus (violet horizontal bar) was followed by unidirectional jerk (green horizontal bar) and by bidirectional jerk (blue horizontal bar). A higher eye position on the y-axis indicates a more temporal position. # indicates a body movement artifact.* ***B,*** *Stacked bar graph showing the occurrence of spontaneous oscillations (SOs) waveforms in individual larvae. Asterisks indicate larvae that displayed all main waveforms within one recording (16 out of 20 larvae). 5 larvae displayed periods of unidirectional jerk with decelerating slow phases.*

### 5.4.3 Influence of viewing conditions on nystagmus waveforms

Next, we asked whether the occurrence of waveform categories is influenced by a preceding optokinetic stimulation. Traces of eye movements during monocular presentation of a stationary grating pattern were analyzed in each larva after a period of a unidirectional or directionally alternating optokinetic response (OKR). Unidirectional OKR, elicited by a unidirectional rotating grating pattern, is characterized by cycles of slow phases and resetting saccades. Directionally alternating OKR, elicited by a rotating grating pattern changing direction every 2 s, is characterized by short slow phases in alternating direction without or with only few saccades. Unidirectional jerk occurred more often following a unidirectional OKR than following a directionally alternating OKR (paired t-test; $t_{15}$ = 2.946; $p$ = 0.01). In contrast, pendular nystagmus occurred more often following a directionally alternating OKR than following a unidirectional OKR (paired t-test; $t_{15}$ = 2.815; $p$ = 0.013). OKR properties did not have a significant effect on bidirectional jerk (paired t-test; $t_{15}$ = 0.453; $p$ > 0.05) (Fig. 5.3*A*).

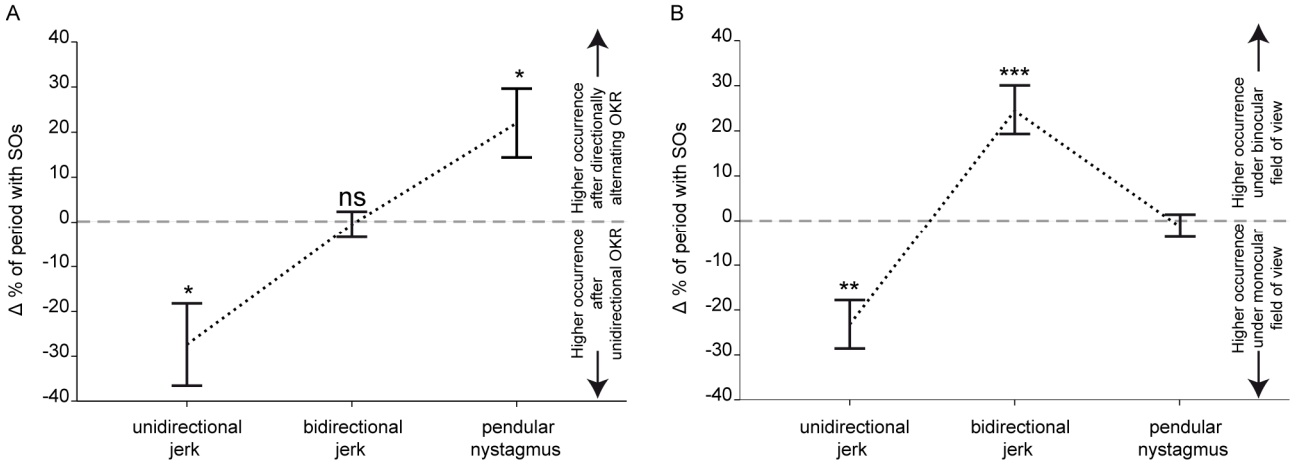


***Figure 5.3: Influence of stimulus conditions on nystagmus waveforms.***

***A, Difference in occurrence of waveform categories after directionally alternating OKR and after unidirectional OKR.*** *A stationary grating pattern was presented to one eye (monocular stimulation) during 1 minute following a period of 1 minute in which OKR was elicited by a moving grating pattern (7.5 deg/s). Movements of the right eye were used for analysis. Spontaneous oscillations (SOs) waveforms were determined within a period starting right after the OKR and ending when the oscillation discontinued. Data were considered if SOs lasted for at least 15 seconds without interruption. For each waveform category, the difference in occurrence (Δ % of period with SOs) after a directionally alternating OKR and after a unidirectional OKR was calculated and plotted (mean ± SEM; n = 16). The horizontal dashed line indicates no difference in occurrence between the two conditions. A negative value indicates a higher occurrence after unidirectional OKR and a positive value indicates a higher occurrence after directionally alternating OKR. * p < 0.05; ns p > 0.05.*

***B, Difference in occurrence of waveform categories under binocular and monocular field of view.***

*A stationary grating pattern was presented during 5 minutes. Movements of the right eye were used for analysis. For each waveform category, the difference in occurrence (Δ % of period with SOs) under binocular and monocular visual field stimulation was calculated and plotted (mean ± SEM; n = 20). The horizontal line indicates no difference in occurrence between the two conditions. A negative value indicates a higher occurrence with a monocular field of view, a positive value indicates a higher occurrence with a binocular field of view. ** p < 0.01; *** p < 0.001; ns p > 0.05.*

To ask whether the field of view influences the occurrence of waveform categories, traces of eye movements were analyzed in each larva during monocular or binocular presentation of a stationary grating pattern. Unidirectional jerk occurred more often with a monocular field of view than with a binocular field of view (paired t-test; $t_{19}$ = 4.168; $p$ = 0.001), while bidirectional jerk occurred more often with a binocular than with a

monocular field of view (paired t-test; $t_{19}$ = 4.236; $p$ < 0.001). Field of view did not have a significant effect on the incidence of pendular nystagmus (paired t-test; $t_{19}$ = 0.574; $p$ > 0.05) (Fig. 5.3*B*).

### 5.4.4 Influence of orbital position on waveform initiation

Since waveform changes are observed under the same stimulus conditions, there must be larval intrinsic factors that change over time and influence the nystagmus waveform. In human patients waveforms are influenced by the eye position (Dell'Osso and Daroff, 1975; Optican and Zee, 1984; Abadi and Dickinson, 1986; Jacobs and Dell'Osso, 2004; Dell'Osso, 2006; Thomas et al., 2008; Kumar et al., 2011). To investigate whether orbital position has an effect on waveforms in *bel* larvae, we recorded eye movements during monocular presentation of a stationary grating pattern and we measured orbital position of the stimulated eye (Fig. 5.4*A*) when a period with a specific waveform started. Because of the high variation among larvae, the statistical significance of the relationship between orbital position and nystagmus waveform was computed separately in each larva using non-parametric tests and larvae were grouped in classes according to the relationship observed. In 7 out of 13 measured larvae we found a significant tendency ($p$ < 0.05) towards a defined orbital position when a period with a specific waveform started. Three different phenotype classes were observed among these 7 larvae. In 3 of these larvae (Class I), pendular nystagmus was observed in eccentric position and jerk nystagmus started after a resetting saccade to a more central position (Fig. 5.4*B*-*C*). In 3 larvae (Class II) unidirectional jerk started after a N-T saccade, short periods of bidirectional jerk - typically one cycle - started after a T-N saccade (Fig. 5.4*D*-*E*). In 1 larva (Class III) bidirectional jerk was of higher amplitude than unidirectional jerk and therefore it covered a bigger orbital range (Fig. 5.4*F*-*G*). In the remaining 6 out of 13 larvae we did not find a significant relationship between orbital position and waveform ($p$ > 0.05). In 4 of these larvae (Class IV) eyes oscillated around the central position and jerk waveforms were of similar amplitude (Fig. 5.4*H*-*I*), in 1 larva we found a not significant tendency toward Class I (Mann-Whitney U Test; $U_{6,7}$ = 11.5; $p$ = 0.174), in another larva a not significant tendency toward Class II (Mann-Whitney U Test; $U_{5,11}$ = 11.0; $p$ = 0.061).

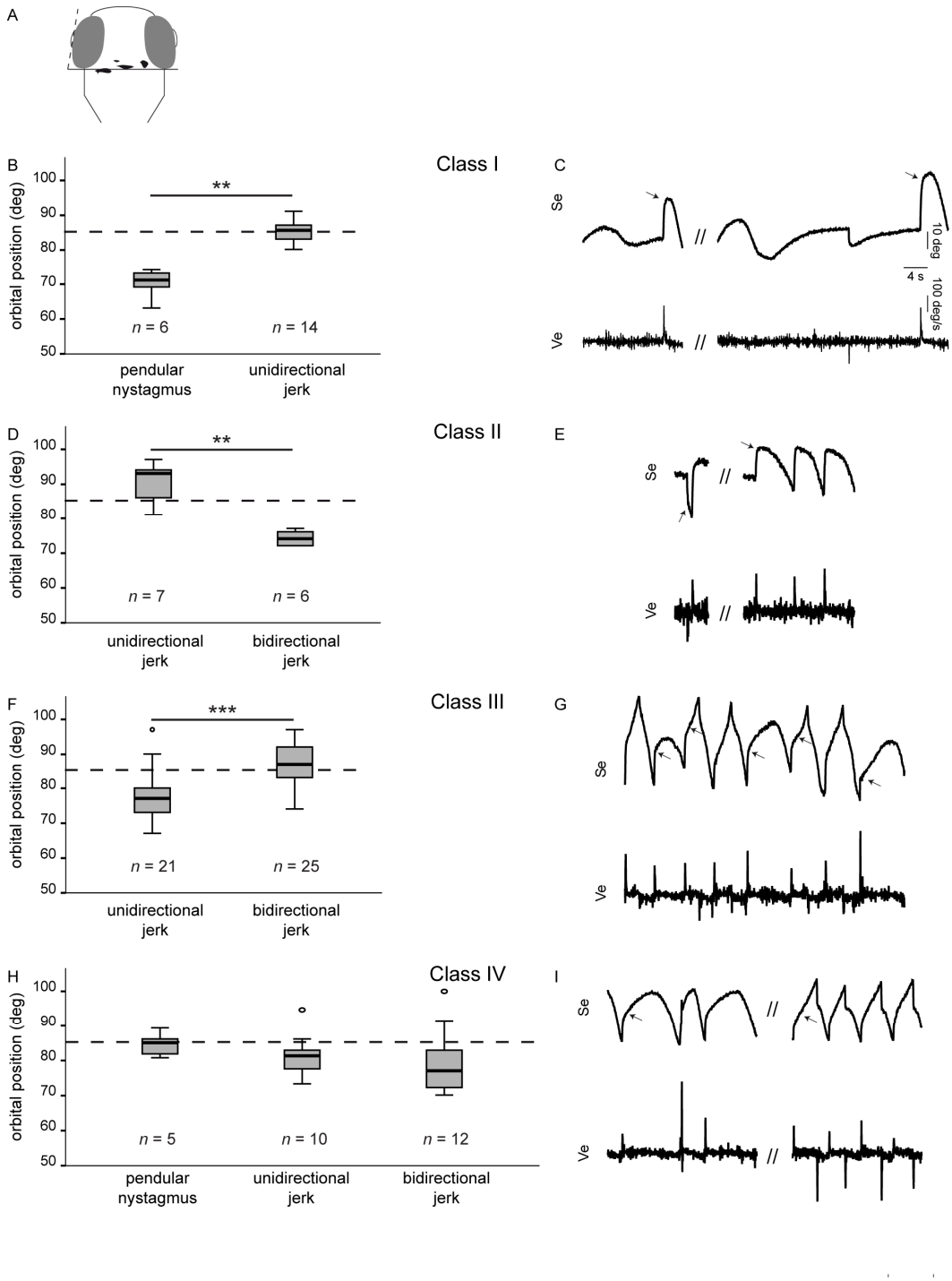


***Figure 5.4: Influence of orbital position on waveform initiation.***
*A stationary grating pattern was presented to one eye during 10 minutes. Orbital position of the stimulated eye was quantified at time points when a period with a specific waveform started. Statistical analysis was performed in each larva separately, whereby a larva was considered for statistical analysis if of at least 2 waveform categories at least 5 periods occurred in one recording. Waveforms occurring for less than 5 periods were not considered. Median orbital position at begin of the oscillation was compared among different waveforms in each recording by means of non-parametric tests (Mann-Whitney U Test or Kruskall-Wallis test).* ***A,*** *Quantification of the orbital position. The angle between a transversal line caudal to the eyes (black horizontal line) and a line going through the lens (dashed line) was quantified with Image J. In the case of a body movement, the transversal line was manually repositioned using the body pigmentation (black spots) as reference points.* ***B - I,*** *Larvae were grouped in 4 classes according to the phenotype observed. For each class, data from a representative larva are shown. On the left, Box-and-whisker plots of the orbital position at begin of periods with each waveform category are shown. Circles represent outliers. Dashed horizontal line represents the central orbital position. A higher value indicates a more temporal position. n = number of*

*periods with a specific waveform category within one recording. ** p < 0.01; *** p < 0.001. On the right, representative segments from the eye position trace (Se (deg)) and the corresponding eye velocity trace (Ve (deg/s)) are shown. A higher value on the y-axis indicates a more temporal position. Arrows indicate the time point of waveform change.* ***B-C,*** *Class I phenotype. Pendular nystagmus is observed on eccentric orbital position, jerk nystagmus starts after a resetting saccade.* ***D-E,*** *Class II phenotype. Unidirectional jerk starts after a N-T saccade, bidirectional jerk after a T-N saccade.* ***F-G,*** *Class III phenotype. Bidirectional jerk cycles are characterized by a higher amplitude.* ***H-I,*** *Class IV phenotype. Orbital position does not influence waveform changes.*

## 5.5 Discussion

Research on the mechanisms underlying eye oscillations in INS has been based for a long time mainly on theoretical considerations and models due to the absence of suitable animal models. Recently, we introduced and characterized two new putative animal models displaying INS-like ocular motor abnormalities: Albino mouse strains and zebrafish *belladonna* (*bel*) mutant (Huang et al., 2006; Huang et al., 2011; Huber-Reggi et al., 2012; Traber et al., 2012). We demonstrated that in the *bel* mutant those abnormalities are caused by an aberrant decussation of retinofugal fibers at the optic chiasm leading to the projection of variable numbers of optic nerve fibers to the wrong brain hemisphere. We could show that additional eye morphological defects do affect visual performance in *bel* larvae but are not related to ocular motor abnormalities (Huber-Reggi et al., 2012). Thus, INS-like behavior in *bel* is explained by a normally negative feedback loop turning into a positive loop, which increases retinal slip (Rick et al., 2000; Huang et al., 2006; Huber-Reggi et al., 2012). In the present study, we described how nystagmus waveforms are influenced by intrinsic and extrinsic factors.

### 5.5.1 Occurrence of nystagmus waveforms in *bel*

In agreement with the concept of a destabilizing positive feedback loop, we observed periods of spontaneous eye oscillations following a reversed OKR, a spontaneous saccade or starting with a spontaneous eye drift of exponential velocity (*see* Fig. 5.1).

Although only one mechanism - misrouting of optic nerve fibers - is at the origin of spontaneous eye oscillations in *bel* mutants (Huber-Reggi et al., 2012), all classical INS waveforms are observed (Huang et al., 2011). Our main aim was to investigate whether waveform categories reflect specific morphological phenotypes, which in *bel* would most likely be the extent of the underlying optic nerve projection phenotype (Huber-Reggi et al., 2012). If this holds true, one would expect to see, depending on the underlying phenotype, a predominant waveform in each individual, what could be used as a diagnostic tool. In contrast, we observed all main waveform categories co-occurring in the same individual in most cases (16 out of 20 larvae) whereby waveform changes were often observed without interruption of the oscillations (*see* Fig. 5.2). These data suggest that different waveforms in *bel* larvae are not linked to the severity of the underlying morphological phenotype and may not be of diagnostic benefit.

Several factors may influence a sudden change in waveform or the relative occurrence of different waveforms. Here, we investigated the role of viewing conditions and observed a strong influence of both the properties of a preceding optokinetic stimulus and the field of view (*see* Fig. 5.3). Pendular nystagmus was more often observed after a directionally alternating OKR than after a unidirectional OKR. In contrast, unidirectional jerk was more often observed after a unidirectional OKR than after a directionally alternating OKR. Both

directionally alternating OKR and pendular nystagmus are characterized by a symmetric oscillation without or with only few saccades. In contrast, unidirectional OKR and unidirectional jerk both consist of cycles of slow phases and resetting saccades. Our data may indicate a possible biasing action of a preceding OKR on the spontaneous oscillation: The ocular motor system might tend to keep the oscillations characteristics when real motion of the visual word is stopped but retinal slip is maintained by the positive feedback loop. We observed an effect of the visual field on the relative incidence of waveform categories. Unidirectional jerk occurred more frequently during monocular presentation of the stationary pattern (monocular field of view), whereas bidirectional jerk occurred more frequently during binocular presentation of the stationary pattern (binocular field of view). A possible explanation might lay in the preferential direction of nystagmus. With a monocular field of view, saccades of the stimulated eye were mostly nasally to temporally (N-T) directed, i.e. a left-beating unidirectional jerk was more often observed if the left eye was stimulated with the stationary pattern and a right-beating unidirectional jerk was more often observed if the right eye was stimulated (data not shown). With a binocular field of view, both eyes were stimulated and they both presented alternately N-T saccades giving rise to bidirectional jerk.

Despite the influence of environmental factors, waveform changes are often observed under the same stimulus conditions. Thus, changes in waveform must be triggered by intrinsic factors that change over time. A possible factor may be orbital position, shown to affect waveform changes in human INS patients (e.g. (Dell'Osso and Daroff, 1975; Abadi and Dickinson, 1986; Thomas et al., 2008; Kumar et al., 2011)). Here, we described a significant correlation between initiation of a specific waveform and orbital position in a subset of larvae (*see* Fig. 5.4). However, the effect of orbital position in *bel* larvae is unclear and highly variable. In contrast to humans, zebrafish larvae are afoveate animals (Lyall, 1957) so that the effect of gaze may be of less importance. Moreover, eye oscillations are of higher amplitude than in humans (Huang et al., 2011), often covering a big range of orbital positions within one cycle.

### 5.5.2 Significance for INS research

The mechanisms behind eye oscillations in INS are poorly understood. For a long time research was based on clinical observations and mathematical modeling. Some models only simulate some waveforms but not others (e.g. (Optican and Zee, 1984; Jacobs and Dell'Osso, 2004)), thus different waveforms may reflect instabilities in different subsystems of the ocular motor system. Other models reproduce all waveforms starting from one mechanism (e.g. (Broomhead et al., 2000; Harris and Berry, 2006)), suggesting that waveforms may be a single entity and occur together in one individual or reflect a different severity of one pathological mechanism. Experimental data can help shed light on which of those different modeled mechanisms really occur in nature.

The data presented here from the zebrafish *bel* mutant provide experimental support for INS waveforms being a single entity caused by reversal of a velocity feedback loop. Such a feedback reversal has been previously suggested (Optican and Zee, 1984) and is also supported by studies in goldfish and amphibians, in which ocular motor instabilities were induced by surgically produced achiasmia (Easter and Schmidt, 1977) or by rotation of the eye balls by 180 deg (Sperry, 1943). Although in the zebrafish *bel* mutant INS is caused by optic nerve fibers misprojections, a reversed feedback loop could also be caused by other aberrant projections, e.g. of afferents from extraocular muscles (Optican and Zee, 1984).

Because all three main waveform categories co-occurred in most larvae, waveforms most likely do not reflect the severity of the morphological phenotype. Rather, they are influenced by the viewing conditions, e.g. - as shown here - properties of the preceding optokinetic stimulus, field of view, and, partially, orbital position. Waveforms changes under unaltered stimulus properties might depend on intrinsic factors such as eye position and eye velocity, regulated by the naturally fluctuating activity of a neural integrator network (Optican and Zee, 1984) and/or by the activity of the saccadic system (Broomhead et al., 2000). Psychological factors, including stress, fatigue, and level of attention have been suggested as further influencing factors in humans (Abadi and Dickinson, 1986; Wiggins et al., 2007).

Here, we only studied the incidence of waveforms in the presence of a positive feedback loop. We did not investigate the possibility that different mechanisms can lead to the same oscillations and we cannot exclude some differences in relative incidence of waveform categories among groups with different background conditions, as described by Kumar et al. (Kumar et al., 2011).

### 5.5.3 Conclusions

We have described an experimental model of INS in which one pathological mechanism leads to all classical waveform categories within one individual. Classical waveforms did not reflect the severity of the disease, suggesting that they are unlikely to provide much diagnostic benefit for evaluation of the severity of the underlying condition. Our findings of a strong influence of viewing conditions on nystagmus waveforms suggest that it may be difficult to compare different studies in which conditions are not identical. Our observation are not only of benefit for clinical INS research but may also help elucidating how changes in ocular motor control systems influence eye movement.

## 5.6 References

Abadi RV, Dickinson CM (1986) Waveform characteristics in congenital nystagmus. Doc Ophthalmol 64:153-167.

Abadi RV, Bjerre A (2002) Motor and sensory characteristics of infantile nystagmus. Br J Ophthalmol 86:1152-1160.

Abramoff MD, Magalhaes PJ, Ram SJ (2004) Image Processing with ImageJ. Biophotonics International 11:36-42.

Broomhead DS, Clement RA, Muldoon MR, Whittle JP, Scallan C, Abadi RV (2000) Modelling of congenital nystagmus waveforms produced by saccadic system abnormalities. Biol Cybern 82:391-399.

CEMASWorkingGroup (2001) A classification of eye movement abnormalities and strabismus (CEMAS). In: The National Eye Institute Publications: National Institutes of Health, National Eye Institute.

Dell'Osso LF (2006) Biologically relevant models of infantile nystagmus syndrome: the requirement for behavioral ocular motor system models. Semin Ophthalmol 21:71-77.

Dell'Osso LF, Daroff RB (1975) Congenital nystagmus waveforms and foveation strategy. Doc Ophthalmol 39:155-182.

Easter SS, Jr., Schmidt JT (1977) Reversed visuomotor behavior mediated by induced ipsilateral retinal projections in goldfish. J Neurophysiol 40:1245-1254.

Gresty M, Page N, Barratt H (1984) The differential diagnosis of congenital nystagmus. J Neurol Neurosurg Psychiatry 47:936-942.

Harris C, Berry D (2006) A developmental model of infantile nystagmus. Semin Ophthalmol 21:63-69.

Hertle RW, Dell'Osso LF (1999) Clinical and ocular motor analysis of congenital nystagmus in infancy. J AAPOS 3:70-79.

Huang MY, Chen CC, Huber-Reggi SP, Neuhauss SC, Straumann D (2011) Comparison of infantile nystagmus syndrome in achiasmatic zebrafish and humans. Ann N Y Acad Sci 1233:285-291.

Huang YY, Rinner O, Hedinger P, Liu SC, Neuhauss SC (2006) Oculomotor instabilities in zebrafish mutant belladonna: a behavioral model for congenital nystagmus caused by axonal misrouting. J Neurosci 26:9873-9880.

Huber-Reggi SP, Mueller KP, Neuhauss SC (2013) Analysis of optokinetic response in zebrafish by computer-based eye tracking. In: Retinal Degeneration (Weber BHF, Langmann T, eds), pp 139-160. New York: Humana Press.

Huber-Reggi SP, Chen CC, Grimm L, Straumann D, Neuhauss SC, Huang MY (2012) Severity of infantile nystagmus syndrome-like ocular motor phenotype is linked to the extent of the underlying optic nerve projection defect in zebrafish belladonna mutant. J Neurosci 32:18079-18086.

Jacobs JB, Dell'Osso LF (2004) Congenital nystagmus: hypotheses for its genesis and complex waveforms within a behavioral ocular motor system model. J Vis 4:604-625.

Karlstrom RO, Trowe T, Klostermann S, Baier H, Brand M, Crawford AD, Grunewald B, Haffter P, Hoffmann H, Meyer SU, Muller BK, Richter S, van Eeden FJ, Nusslein-Volhard C, Bonhoeffer F (1996) Zebrafish mutations affecting retinotectal axon pathfinding. Development 123:427-438.

Khanna S, Dell'Osso LF (2006) The diagnosis and treatment of infantile nystagmus syndrome (INS). ScientificWorldJournal 6:1385-1397.

Kumar A, Gottlob I, McLean RJ, Thomas S, Thomas MG, Proudlock FA (2011) Clinical and oculomotor characteristics of albinism compared to FRMD7 associated infantile nystagmus. Invest Ophthalmol Vis Sci 52:2306-2313.

Lyall AH (1957) Cone Arrangements in Teleost Retinae. Quarterly Journal of Microscopical Science s-3-98:189-201.

Maybodi M (2003) Infantile-onset nystagmus. Curr Opin Ophthalmol 14:276-285.

McLean RJ, Windridge KC, Gottlob I (2012) Living with nystagmus: a qualitative study. Br J Ophthalmol 96:981-986.

Mullins MC, Hammerschmidt M, Haffter P, Nusslein-Volhard C (1994) Large-scale mutagenesis in the zebrafish: in search of genes controlling development in a vertebrate. Curr Biol 4:189-202.

Neuhauss SC, Biehlmaier O, Seeliger MW, Das T, Kohler K, Harris WA, Baier H (1999) Genetic disorders of vision revealed by a behavioral screen of 400 essential loci in zebrafish. J Neurosci 19:8603-8615.

Optican LM, Zee DS (1984) A hypothetical explanation of congenital nystagmus. Biol Cybern 50:119-134.

Pilling RF, Thompson JR, Gottlob I (2005) Social and visual function in nystagmus. Br J Ophthalmol 89:1278-1281.

Rick JM, Horschke I, Neuhauss SC (2000) Optokinetic behavior is reversed in achiasmatic mutant zebrafish larvae. Curr Biol 10:595-598.

Sarvananthan N, Surendran M, Roberts EO, Jain S, Thomas S, Shah N, Proudlock FA, Thompson JR, McLean RJ, Degg C, Woodruff G, Gottlob I (2009) The prevalence of nystagmus: the Leicestershire nystagmus survey. Invest Ophthalmol Vis Sci 50:5201-5206.

Seth A, Culverwell J, Walkowicz M, Toro S, Rick JM, Neuhauss SC, Varga ZM, Karlstrom RO (2006) belladonna/(Ihx2) is required for neural patterning and midline axon guidance in the zebrafish forebrain. Development 133:725-735.

Sperry RW (1943) Effect of 180 degree rotation of the retinal field on visuomotor coordination. J Exp Zool 92:263-279.

Straw AD (2008) Vision egg: an open-source library for realtime visual stimulus generation. Front Neuroinformatics 2:4.

Thomas S, Proudlock FA, Sarvananthan N, Roberts EO, Awan M, McLean R, Surendran M, Kumar AS, Farooq SJ, Degg C, Gale RP, Reinecke RD, Woodruff G, Langmann A, Lindner S, Jain S, Tarpey P, Raymond FL, Gottlob I (2008) Phenotypical characteristics of idiopathic infantile nystagmus with and without mutations in FRMD7. Brain 131:1259-1267.

Traber GL, Chen CC, Huang YY, Spoor M, Roos J, Frens MA, Straumann D, Grimm C (2012) Albino Mice as an Animal Model for Infantile Nystagmus Syndrome. Invest Ophthalmol Vis Sci 53: 5737-5747.

Wiggins D, Woodhouse JM, Margrain TH, Harris CM, Erichsen JT (2007) Infantile nystagmus adapts to visual demand. Invest Ophthalmol Vis Sci 48:2089-2094.

# Chapter 6

## Effect of Asymmetric Fiber Crossing at the Optic Chiasm on Visual-Postural Control in Zebrafish Larvae

**Sabina P. Huber-Reggi[1], J. Torben Halbe[1], Björn M. Kampa[2], Fritjof Helmchen[2], Stephan C. F. Neuhauss[1]**

[1] Institute of Molecular Life Sciences, University of Zurich, Zurich, Switzerland

[2] Department of Neurophysiology, Brain Research Institute, University of Zurich, Zurich, Switzerland

**Report on an ongoing research project**

**Ackowledgments**

We like to thank Dr. Kaspar Müller for help with recording of swimming behavior, Drs Dominik Straumann and Christian Grimm for fruitful discussion. The *mitfa*$^{-/-}$*;Tg(elavl3:GCaMP5)* zebrafish line - developed by Jennifer Li, Drew Robson, Dr. Florian Engert and Dr. Alexander Schier, Harvard University, Boston, USA - was a generous gift of Prof. Emre Yaksi, Flanders Institute for Biotechnology, Leuven, Belgium. We thank Kara Dannenhauer for excellent fish care.

**Personal contribution**

Project idea together with JTH, performing of all the experiments on postural control, implementation of calcium imaging with supervision from BK and FH, preparation of all figures, writing of the manuscript.

## 6.1 Abstract

Postural control in vertebrates is mediated by inputs originating from different sensory systems, including the visual system. In zebrafish larvae, abnormal postural control has been so far associated with vestibular deficits and the influence of visual input on postural balance remains unclear. By using the zebrafish mutant *belladonna* (*bel*), we aim to shed light on visual-postural control. In *bel* a variable fraction of retinofugal fibers fail to cross the midline at the optic chiasm and misproject to the ipsilateral brain hemisphere. Here, we describe in a subset of *bel* mutants postural defects such as swinging or tumbling around the longitudinal body axis that are absent in complete darkness, indicating that they are visually driven. Postural defects occur in larvae with asymmetric innervations of retinofugal fibers to the two retinocipient brain hemispheres. The extent of asymmetric innervations correlates with the extent of postural instabilities. We suggest that asymmetric innervations might lead to a stronger output from one brain hemisphere upon visual stimulation and consequently to an imbalance of motor commands to the muscles during swimming. To test our hypothesis, we plan to study stimulus-evoked responses on the two body sides of *bel* larvae using calcium imaging. Towards this aim, we worked on the implementation of the technique in our laboratory. Imaging of neuronal activity in larvae with postural instabilities would not only help to validate our conceptual model but might also provide the basis for the identification of the circuit involved in visual-postural control in zebrafish.

## 6.2 Introduction

Postural control in vertebrates requires multisensory inputs about body position and movement relative to the external world. Afferent information originating from the visual, vestibular and somatosensory systems is integrated in the central nervous system, which elaborates proper motor commands. The different input systems are likely to be partially redundant since removal of one of them can lead to different clinical outcomes, ranging from loss of balance to no effect due to compensation from the remaining systems (Straube et al., 1990; Massion, 1994; Simoneau et al., 1995; Maurer et al., 2000).

The involved neuronal circuits are poorly understood. An attractive animal model to study them is the larval zebrafish, due to its small size, its transparency, and fast development. In zebrafish larvae inputs coming from the lateral line (a serie of neuromast hair cells along the trunk of the larva detecting water motion (Coombs et al., 1988)) and the vestibular system in the inner ear are integrated for postural control (Nicolson, 2005). At this young age the vestibular system solely relies on the otholits and not on the semicircular canals, most likely because of their small size (Beck et al., 2004). The well developed visual system is likely involved too, but the effect of visual input on postural control is still not understood in zebrafish.

Mutagenesis screenings have led to the isolation of several mutations affecting postural control: Mutant larvae often swim on the side or on the back or display rolling motions following a corkscrew-like path (Granato et al., 1996; Haffter et al., 1996; Trowe et al., 1996; Whitfield et al., 1996; Nicolson et al., 1998). Most mutations have been related to morphological and functional defects of the inner ear or of the lateral line (Granato et al., 1996; Whitfield et al., 1996; Nicolson et al., 1998). Only in two mutants with impaired postural control, *never mind* and *macho*, defects in ordering and topographic mapping of optic nerve fibers in the tectum have been shown (Trowe et al., 1996). However, the presence of additional defects, such as a missing swim bladder and a reduced response to vibrational stimuli, suggests that the relationship between locomotor behavior and defects of the visual system is not direct in these mutants (Trowe et al., 1996; Ribera and Nusslein-Volhard, 1998; Gnuegge et al., 2001; Pineda et al., 2005). Here, we describe to our knowledge for the first time postural instabilities in a mutant zebrafish with specific abnormalities in the visual system. We describe in a subset of homozygous *belladonna* (*bel*) mutants a similar swimming behavior as in mutants with vestibular and/or somatosensory deficits. Larvae show periods of tumbling and rolling over following a corkscrew-path, swinging around the body axis and swimming on the back. Since vestibular and somatosensory deficits have not been detected in *bel*, we formulated the hypothesis that the observed postural instabilities are caused by a visual defect. Indeed, we show here that the behavioral phenotype is rescued in darkness.

The strongest morphological phenotype in *bel* larvae is a failure of a variable fraction of optic nerve fibers to cross the midline at the optic chiasm (*see* Chapters 1 and 4). These fibers misproject to the ipsilateral brain hemisphere (Rick et al., 2000; Huber-Reggi et al., 2012). In this study, we aimed to shed light on visual-postural control by studying the effect of misrouting optic nerve fibers on balance. Although the amount of misprojecting fibers is often comparable between eyes, in some cases the projection phenotype is unequally distributed (Huber-Reggi et al., 2012). In these larvae more fibers are reaching one brain hemisphere than the other giving rise to an asymmetric retinotectal projection. Here, we show that postural instabilities correlate with asymmetry of the optic nerve projection and propose that asymmetric innervations might lead to a stronger stimulus-

evoked output from one brain hemisphere and as a consequence to an imbalance of motor commands. To test this hypothesis, we plan to compare neuronal activity on the two body sides of *bel* larvae using calcium imaging. In the second part of this chapter, I summarize the work done toward implementation of this technique in our laboratory.

## 6.3 Material and Methods

### 6.3.1 Fish maintenance and breeding

Fish were maintained and bred as previously described (Mullins et al., 1994). Embryos were raised at 28°C in E3 medium (5 mM NaCl, 0.17 mM KCl, 0.33 mM $CaCl_2$, 0.33 mM $MgSO_4$) and staged according to development in days post-fertilization (dpf). *bel* ($bel_{tv42}$) homozygous larvae were obtained from mating of identified heterozygous carriers. Larvae at 4 dpf were anesthetized with 200 mg/l 3-aminobenzoic acid ethyl esther methane sulfonate (MS-222, Sigma-Aldrich) and sorted according to eye pigmentation phenotype (Karlstrom et al., 1996). $bel^{+/-}$;$mitfa^{-/-}$ fish were generated by first outcrossing $bel^{+/-}$ and $mitfa^{-/-}$ and by subsequently incrossing the F1 generation. $bel^{+/-}$; $mitfa^{-/-}$; *Tg(elavl3:GCamp5)* fish were obtained by outcrossing $mitfa^{-/-}$;*Tg(elavl3:GCamp5)* and $bel^{+/-}$;$mitfa^{-/-}$ and by subsequent screening for *Gcamp5* expression in the developing brain.

### 6.3.2 Analysis of swimming behavior

Larvae were placed in a 6 cm diameter dish filled with 10 ml E3 medium. The swimming behavior was analyzed during 5 minutes episodes and time spent displaying postural instabilities was quantified. Postural instabilities were defined as tumbling, rolling over and swinging around the body axis during swimming and swimming on the back. Larvae without inflated swim bladder or not swimming were not considered.

For comparison of swimming behavior under light condition and in the dark, larvae were imaged during 6 minutes by an infrared-sensitive CCD camera (Stingray F-046B, Allied Vision Technologies) at a rate of 12 frames per second. The recordings were performed twice, once in the dark and once with a light source coming from above, whereby the order of recordings was changed between larvae. The larva was illuminated from below with an array of 6 infrared (IR)-emitting diodes shielded by an IR-pass filter with cutoff at 1000 nm. Movie recording was controlled by a custom built program based on LabView 2011 and NI Vision development module 2011 (National Instruments). Time spent swimming and time displaying postural instabilities was quantified offline for the last 5 minutes of the recording. The first 60 s were not analyzed to exclude artifacts from changing the light condition.

### 6.3.3 Anterograde labeling of the optic nerve fibers with lipophilic dyes

To label optic nerve fibers, larvae were fixed in 4% paraformaldehyde in PBS overnight. For lipophilic dye injection, the fish were embedded dorsal-up in 1.5% low melting agarose (Nu Sieve GTG Agarose, Lonza) in PBS on a glass slide. Solutions of DiO (Molecular Probes) and DiI (Molecular Probes) (both 1 % in chloroform) were pressure-injected (40 psi, 20-30 ms pulse time) with a pneumatic Pico Pump (PV820, World Precision

Instruments) between lens and retina using glass capillaries. Microscopy z-stacks images were obtained using a Leica HCS LSI confocal microscope (Leica Microsystems). Signal intensities were measured using ImageJ (MacBiophotonics). The extent of projection to each hemisphere and the resulting asymmetry index were quantified as described in Fig. 6.3.

### 6.3.4 Statistical analysis

Statistical analysis and graph generation were performed with SPSS Statistics 19 (IBM). Time spent swimming and postural instabilities under light conditions and in the dark were compared using paired t-tests. Since asymmetry indexes of the optic nerve projection were not normally distributed, the relationship between asymmetry index and postural instabilities was analyzed using non parametric tests, i.e. Mann-Whitney U Test or Spearman correlation.

### 6.3.5 Injection of Calcium-Green dextran at the 4-cells stage

Injections of Calcium-Green™-1 dextran 3000 MW (CGD) (Molecular Probes) were performed as described by Cox and Fetcho (Cox and Fetcho, 1996). Embryos of the zebrafish strain *mitfa*$^{-/-}$ (*nacre*) were collected 20 minutes after fertilization and transferred to a warmed agarose microinjection plate that had been prepared in advance according to (Nüsslein-Volhard and Dahm, 2002). CGD was injected into the yolk or into one cell at the 4-cells-stage using a micromanipulator and a pressure pump (FemtoJet, Eppendorf). Around 5 nl of a 5% CGD solution in 0.2 M KCl was injected. The approximate injection volume was determined by injection of the indicator into oil (Oil 10 s VOLTATEF, VWR Prolabo) and by subsequent quantification of the drop diameter with a scaled eyepiece lens. During injection embryos were kept in Fish Ringer solution (116 mM NaCl, 2.9 mM KCl, 5 mM HEPES, pH 7.2), after injection embryos were raised in E3 medium as described above. For imaging, 5 dpf larvae were embedded in 1.5 low melting agarose (Nu Sieve GTG Agarose, Lonza) and imaged with a fluorescence widefield microscope (BX61, Olympus).

### 6.3.6 Anterograde labeling of optic nerve fibers with Calcium-green dextran

For injection into the eye cup, 4 dpf larvae of the zebrafish strain *mitfa*$^{-/-}$ (*nacre*) were embedded dorsal-up in 1.2 % low melting agarose (Nu Sieve GTG Agarose, Lonza) dissolved in Fish Ringer solution (116 mM NaCl, 2.9 mM KCl, 5 mM HEPES, pH 7.2). A solution of CGD 10000 MW (5 % in Fish Ringer) was pressure-injected (40 psi, 20-40 ms pulse time) with a pneumatic Pico Pump (PV820, World Precision Instruments) between lens and retina using glass capillaries. After injection, larvae were incubated at 28°C in E3 medium for at least 20 h before re-embedding in 1.5 % low-melting agarose in a 35 mm Petri dish for microscopy. Microscopy images were obtained using a fluorescence widefield microscope (BX61, Olympus).

### 6.3.7 Visual stimulation and calcium imaging

Images of CGD or GCaMP5 fluorescence were acquired at 4 Hz using a fluorescence widefield microscope (BX61, Olympus) equipped with a black and white camera F-View II CCD camera, an air 10x objective and a water-immersion 10x objective.

For visual stimulation, movies were projected by a laser pico-projector (ShowWX+, Microvision) onto a miniature screen made of a blotting paper and a coverslip and placed 2 cm away from the larva's eye. The computer-generated stimulus (Straw, 2008) was either a moving black and red sine-wave grating pattern (spatial frequency of 12 cycles/screen width, temporal frequency of 1 Hz), or a moving red bar (10 pixels width, temporal frequency of 1 Hz), or 50 moving red random dots (diameter of 20 pixel, velocity of 20 pixels/s), presented for 1 s with a 8 s interstimulus interval.

Images from 5 to 7 trials were averaged in Image J (MacBiophotonics) and regions of interest (ROI) were selected manually. Baseline fluorescence intensity (F) was quantified by averaging the 10 frames before stimulus onset and was used to calculate the relative changes in fluorescence intensity upon visual stimulation ($\Delta F/F$).

## 6.4 Results and Discussion

### 6.4.1 Postural instabilities in *bel* larvae

Some *bel* homozygous larvae displayed postural instabilities, best described as spinning behaviors such as tumbling, rolling over on a corkscrew-like path and swinging along the longitudinal body axis (Fig. 6.1). Sometimes, larvae were swimming on their side or on the back.

This spinning behavior resembles the swimming path observed in vestibular mutants (e.g. (Whitfield et al., 1996, Nicolson et al., 1998)) and differs from the previously described looping behavior in another subset of homozygous *bel* larvae (Huang et al., 2009). Looping is defined as swimming in circles around an axis centered outside the larval body and occurs in *bel* larvae with ocular motor instabilities. In contrast to the larvae described here, looping larvae are stable on their body axis (Huang et al., 2009).

The observed spinning behavior could be due to so far unknown vestibular deficits in a subset of *bel* larvae or, alternatively, *bel* could be the first described spinning mutant with a visual deficit as the direct cause of postural instability.

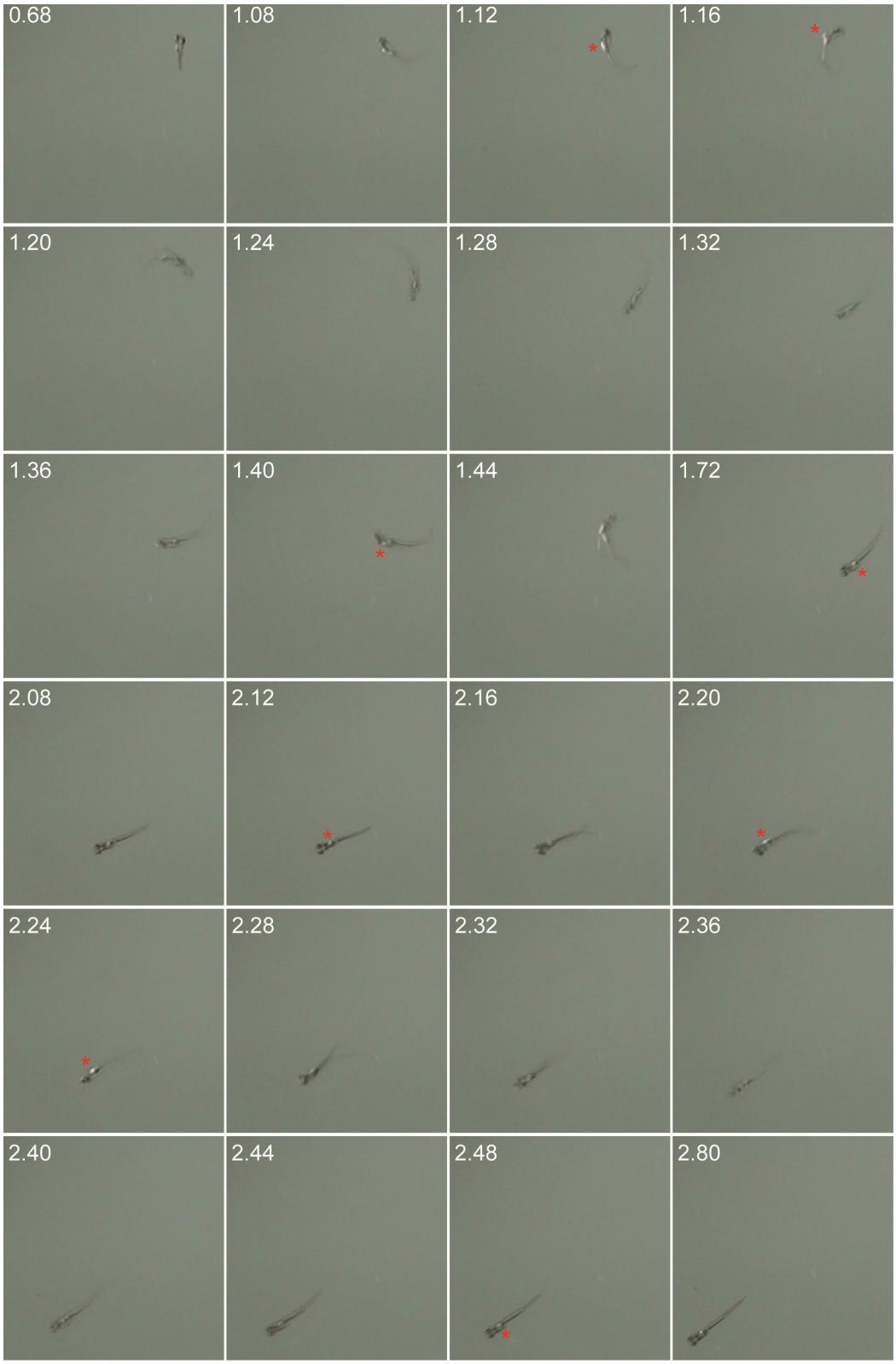


***Figure 6.1: Dorsal view of the spinning behavior of bel larvae.***
*Frame series of a movie from a representative bel larva with postural instabilities. Time is shown in seconds. The position of the swim bladder is marked in some frames by an asterisk. This larva lays on the side at the begin of the movie, then spins on its body side and around an axis centered outside of the body. From time point 1.72 s on, the larva starts tumbling around the longitudinal body axis.*

### 6.4.2 Postural instabilities are visual input dependent

We next asked if postural instabilities are discontinued in darkness, which would support a role of vision in this behavior. We selected individual *bel* larvae with postural instabilities and recorded their swimming behavior under light conditions and in the dark. Postural instabilities were strongly reduced when the light was off (Fig. 6.2*A*). Reduction of postural instabilities was not due to decreased locomotion, since overall swimming activity was not influenced by the illumination conditions (Fig. 6.2*B*). As a control, we quantified swimming behavior of 6 wild-type (wt) larvae under the same conditions and we did not observe postural instabilities. Some remaining postural instabilities were still observed in *bel* larvae in the dark (*see* Fig. 6.2*A*). This can be explained by a small reaction to some remaining light or by body shape alterations due to the constant bended swimming position. Similar anatomical deformations have been reported in mutants with vestibular deficits (Nicolson et al., 1998). The strong reduction of postural instabilities in darkness indicate that postural instabilities in *bel* larvae are visually-driven and that alteration of the body shape is secondary to the behavior.

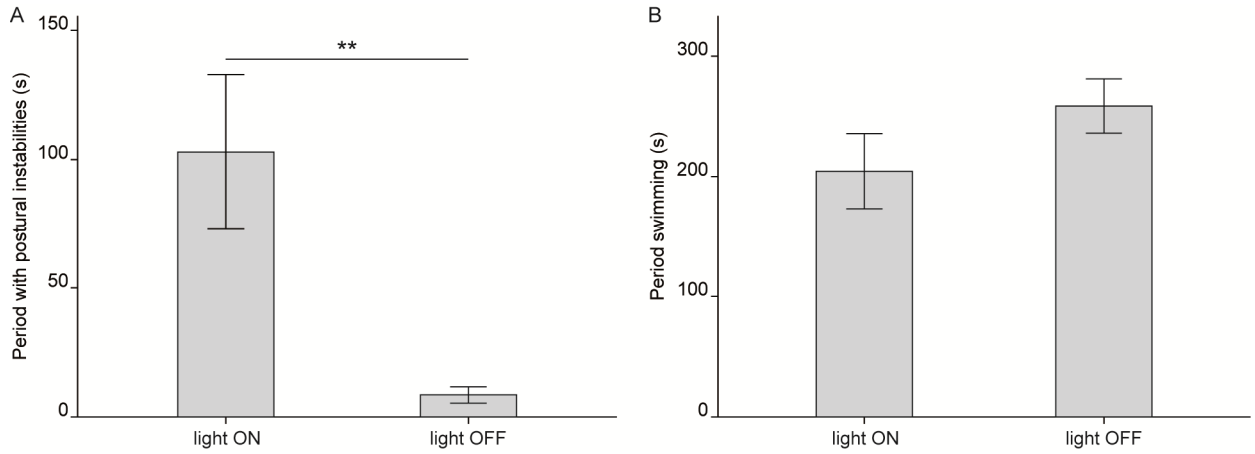


***Figure 6.2: Visual input dependence of postural instabilities.***
*Swimming behavior was recorded with an infrared sensitive camera during 5 minutes for each condition. Infrared-emitting diodes were shielded by an infrared-pass filter with cutoff at 1000 nm. Graphs show means ± SEM of period with postural instabilities (**A**), respectively of period spent swimming (**B**). **A,** quantification of time spent with abnormal swimming behavior by bel larvae with postural instabilities (n = 9) in the presence of a light source and in darkness. ** p = 0.009 (paired t-test). **B,** quantification of time spent swimming (n = 9) in the presence of a light source and in darkness. p = 0.215 (paired t-test).*

### 6.4.3 Postural instabilities correlate with asymmetric innervations of the brain by optic nerve fibers

Beside some subtle eye defects, the strongest morphological phenotype in *bel* larvae is the misprojection of a variable amount of optic nerve fibers to the ipsilateral brain hemisphere, leading to misinterpreted visual input (Huber-Reggi et al., 2012). In wt larvae as well as in some *bel* larvae, all optic nerve fibers project to the contralateral brain hemisphere. In the remaining *bel* larvae fibers of the optic nerve fail to cross the midline at the optic chiasm. Some of these larvae show a complete ipsilateral projection, some others show a bilateral projection with a subpart of axons growing ipsilaterally. In chapter 4, we showed that the amount of misprojecting optic nerve fibers determines the ocular motor phenotype (Huber-Reggi et al., 2012). Analogously, misprojecting optic nerve fibers could influence postural control. To test this hypothesis, we first analyzed

swimming behavior and then stained with lipophilic tracer dyes the optic nerve fibers arising from each eye. Preliminary observations suggested that postural instabilities often occurred in larvae with bilateral projections, in which disparate projection patterns emanate from the two eyes. Fig. 6.3*C* shows a staining from one larva in which fibers from the right eye are projecting correctly, whereas most fibers from the left eye are misprojecting, leading to a higher amount of afferents reaching the left hemisphere. In this case, the projection is asymmetric. In contrast, in wt larvae the same amount of fibers is reaching each hemisphere, thus the projection is symmetric (Fig. 6.3*A*). The same is true in the case of achiasmatic larvae, in which all fibers from both eyes are misprojecting so that the proper amount of afferents is reaching each hemisphere (Fig. 6.3*B*). Based on the preliminary observation of an accumulation of larvae with bilateral projections among those that are affected by postural instabilities, we formulated the hypothesis that postural instabilities may occur in larvae with asymmetric innervations of the two brain hemispheres.

To test our hypothesis, we quantified signal intensity on both brain hemispheres as described in Chapter 4 (Huber-Reggi et al., 2012) and we correlated the extent of asymmetric innervations with the extent of postural instabilities. *bel* larvae with postural instabilities displayed a significantly stronger asymmetry than *bel* larvae with normal posture (Mann-Whitney U Test, $p = 0.003$) (Fig. 6.3*D*). Additionally, we compared larvae displaying some swinging around the longitudinal body axis but otherwise swimming normally with larvae displaying complete tumbling around the longitudinal axis as shown in Fig. 1. The latter showed a significantly stronger asymmetry (Mann-Whitney U Test, $p = 0.003$) (Fig. 6.3*E*). Finally, we compared the period with postural instabilities with the extent of asymmetry in each larva. A Spearman correlation showed that there was a significant positive correlation between them (*Spearman rank correlation* $\rho_{29} = 0.54$; $p = 0.001$) (Fig. 6.3*F*).

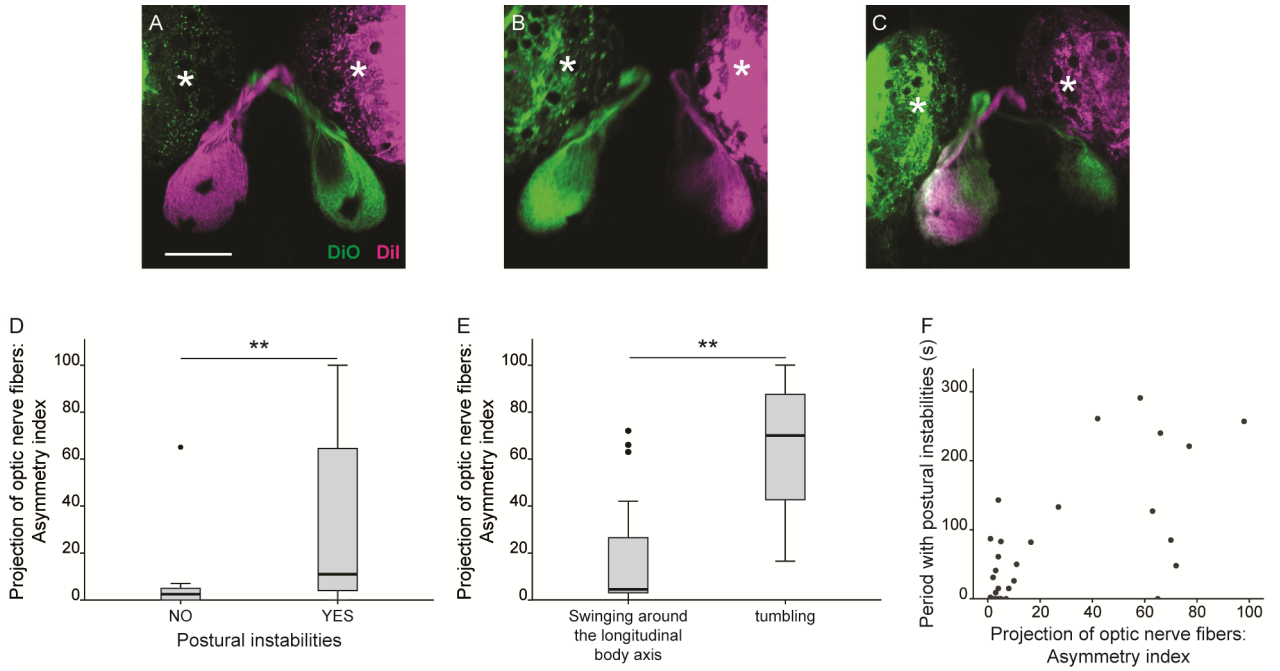


***Figure 6.3. A-C, Maximum intensity projections of confocal z-stacks showing projection of optic nerve fibers in bel larvae.***

*The fibers were labeled by injecting the lipophilic tracer dye DiO (green) in the left eye and the lipophilic tracer dye DiI (magenta) in the right eye. Anterior is up. Scale bar, 100 µm. Asterisks indicate the location of the eyes. wt larvae as well as some bel larvae have complete contralateral projections (**A**). In some bel larvae all fibers project ipsilaterally (**B**). In some bel larvae a variable fraction of fibers project ipsilaterally leading to a bilateral projection. If the fraction of misprojecting fibers originating from the two eyes is different, a higher number of fibers project to the one brain hemisphere and the projection is asymmetric (**C**).*

***D-F, Postural instabilities correlate with asymmetric innervations of the brain by optic nerve fibers.***

*Extent of projection to each hemisphere from each eye was extrapolated by signal intensity quantification and the total amount of fibers in each hemisphere (R and L) was estimated. Asymmetry index = abs ((R-L)/(R+L)). **D**, Box-and-whisker plot of the projection asymmetry in bel larvae with normal swimming behavior (n = 14) and in bel larvae with postural instabilities (n = 23). The ends of the whiskers represent the lowest data point within the 1.5 interquartile range of the lower quartile and the highest data point within 1.5 interquartile range of the upper quartile. Circles represent outliers. ** = p < 0.01 (Mann-Whitney U Test). **E**, Box-and-whisker plot of the projection asymmetry in bel larvae swinging around the longitudinal body axis (n = 16) and in bel larvae additionally displaying periods of complete tumbling around the longitudinal body axis (n = 7). The ends of the whiskers represent the lowest data point within the 1.5 interquartile range of the lower quartile and the highest data point within 1.5 interquartile range of the upper quartile. Circles represent outliers. ** = p < 0.01 (Mann-Whitney U Test). **F**, Extent of periods with postural instabilities correlates with extent of asymmetry. Spearman $\rho_{29} = 0.54$; p = 0.001; n = 31.*

Summarizing, postural instabilities were more severe and occurred more often in larvae with a more asymmetric distribution of retinal afferents in the two brain hemispheres. Based on these observations, we suggest a conceptual model predicting that asymmetric innervations of the two brain hemispheres leads to a stronger visual input to one brain hemisphere. This might lead to a stronger output from this hemisphere and as consequence to an imbalance of motor commands to the muscles during swimming (Fig. 6.4).

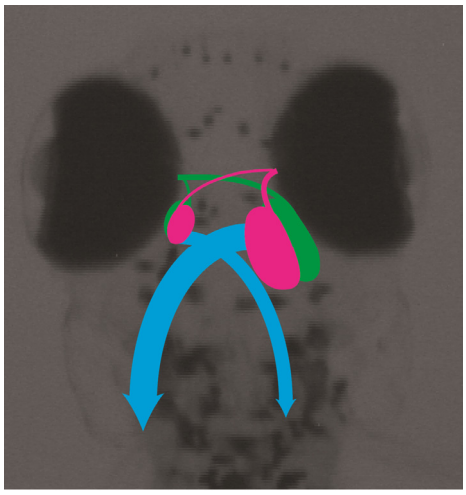

***Figure 6.4: Model of visual-postural control deficits in larvae with asymmetric innervations.***
*More optic nerve fibers (green and magenta) reach one brain hemisphere (in this case the right hemisphere). Because of the higher amount of fibers, more neuronal input reaches the neuronal cells in the right hemisphere upon visual stimulation. As a consequence, a higher activity is generated in these cells leading to a stronger output from the left hemisphere and to an imbalance of motor commands (blue arrows).*

Such an asymmetry in signal input and output could be demonstrated by quantification of stimulus-evoked responses on the two body sides of *bel* larvae using calcium imaging. Towards this aim, we worked at establishing this technique in our laboratory. In the next section of this chapter I summarize the principal steps.

### 6.4.4 Toward a working method for quantification of neuronal activity by calcium imaging

Neuronal activity is coupled with an influx of calcium ions in the cell body and in the presynaptic boutons, thus with an increase in the cytosolic calcium concentration that can be indirectly visualized and quantified by means of calcium indicators. Calcium indicators are synthetic or genetically expressed fluorescent molecules that increase their fluorescence upon binding to calcium ions. Thus, calcium flux can be translated into changes in fluorescence intensity and the neuronal activity can be visualized (Gobel and Helmchen, 2007). Changes in fluorescence intensity are recorded by time-lapse microscopy whereby confocal or multiphoton instruments are preferred if single cell resolution has to be achieved, e.g. to unravel single cells participating in a specific neuronal circuit. However, a widefield approach may be advantageous if broad regions of neuronal activation have to be determined, as performed recently by Muto and colleagues (Muto et al., 2013). During my thesis, I worked on the implementation of a working method for calcium imaging during visual stimulation using a widefield approach and I tested different ways to label neurons. For a better visualization of calcium-dependent fluorescence signal we used the zebrafish strain *mitfa*$^{-/-}$ (*nacre*), which has no melanophores on the body but normal pigmentation in the eyes (Lister et al., 1999). *nacre* larvae display normal behavior and have been used widely for calcium imaging (e.g. (Ahrens et al., 2013; Muto et al., 2013)).

In order to visualize neuronal activity throughout the zebrafish brain a calcium indicator can be injected into one cell of an embryo at the 4-cells-stage leading to a mosaic of labeled and unlabeled cells in the larva. This technique has been described previously by Cox and Fetcho (Cox and Fetcho, 1996) but has not been used extensively afterwards. In our laboratory, injection of embryos following the protocol described in the literature

led either to a too weak fluorescence signal or to general developmental defects such as a curved tail, small eyes and edemas. Moreover, successfully injected larvae displayed a reduced OKR, indicating that behavior was affected (data not shown).

Calcium signals in tectal cells in response to visual stimulation have been successfully detected in zebrafish larvae by bolus-injection of membrane-permeable acetoxylmethyl ester dyes such as Oregon Green BAPTA-1 AM ester in the tectum (e.g. (Niell and Smith, 2005; Ramdya and Engert, 2008)). The dye diffuses through the cell membrane and is trapped in the cytoplasm after cleavage of the ester groups by a cytosolic esterase. We reasoned that calcium signals in the tectal neuropil - reflecting afferent synaptic inputs from the retinal ganglion cells - could be detected by injecting dextran-conjugated calcium indicators (e.g. calcium-green dextran) into the eye cup, as dextran-coupled dyes are taken up by the cells and anterogradely or retrogradely transported along the axons (O'Donovan et al., 1993). Injection of calcium-green dextran 10000 MW into the eye led after around 20 hours of incubation to a homogeneous staining in the contralateral tectum of some larvae without affecting survival and behavior. However, successful staining was achieved only in a small portion of injected larvae and signal intensity was mostly too dim for calcium imaging (data not shown).

An emerging alternative to synthetic dyes are genetically encoded calcium indicators (GECIs). GECIs are calcium-sensitive fluorescence proteins that are expressed homogenously in a subset of cells in transgenic animals by means of specific promoters. Although less sensitive than synthetic indicators, GECIs have many advantages regarding stability and signal reproducibility. Moreover, new GECIs with increasing efficiency and sensitivity are constantly being developed. Here, we tested GCaMP5 (Akerboom et al., 2012) - a new improved version of the single-wavelength GECI GCaMP - expressed under the control of the pan-neuronal *elavl3* promoter (formerly known as *HuC*) (Park et al., 2000) in *nacre* larvae. GCaMP consists of a circularly permuted green fluorescent protein (cpGFP), calmodulin (CaM) and the $Ca^{2+}$/CaM-binding M13 peptide. Binding of calcium ions to CaM induce a conformational change of cpGFP, increasing its fluorescence (Nakai et al., 2001). In Fig. 6.5 representative images of 5 dpf larvae imaged with a HCS LSI confocal microscope (Leica Microsystems) (Fig. 6.5*A*-*B*) and with a widefield fluorescence microscope (BX61, Olympus) (Fig. 6.5*C*-*D*) are shown. Baseline signal is strong and homogeneous with little background.

For calcium imaging we mounted the larva in agarose to restrain body movement. The visual stimulus was generated using the open source Python library Vision Egg (Straw, 2008) and projected via a laser pico-projector on a miniature screen made of a coverslip and a blotting paper (Fig. 6.5*E*). Time-lapse recording of fluorescence signal was performed during visual stimulation. Neuronal responses were measured as the change of mean fluorescence intensity in a manually selected region of interest (*see* Materials and Methods for details). Beside substantial spontaneous (thus visual stimulus independent) activity in the tectal neuropil, neuronal responses evoked by visual stimulation in preliminary recordings were detected in the tectal neuropil (afferent signal from the retina) (Fig. 6.5*F*) and in hindbrain neurons (Fig. 6.5*G*). So far we were not able to record specific neuronal responses in tectal cell bodies.

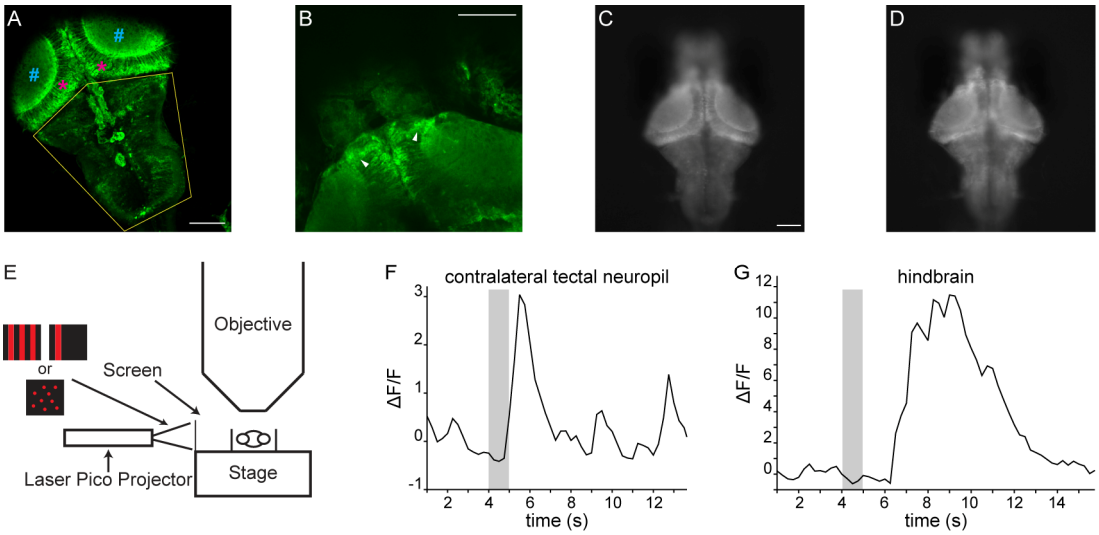


***Figure 6.5: Imaging of calcium activity in mitfa$^{-/-}$;Tg(elavl3:GCaMP5) larval brain upon visual stimulation.***
***A,*** *Maximum intensity projection of a confocal z-stack showing broad expression of GCaMP5 throughout the brain. Anterior is up oriented towards the left. Scale bar, 100 µm. # (blue) indicate the location of the tectal neuropil, asterisks (magenta) the location of the tectal cells. The yellow area corresponds to the hindbrain.* ***B,*** *Maximum intensity projection of a confocal z-stack showing expression of GCaMP5 in the pretectal region (arrowheads). Anterior is up oriented towards the left. Scale bar, 100 µm.* ***C,*** *Widefield fluorescence image of a mitfa$^{-/-}$;Tg(elavl3:GCaMP5) larva. Anterior is up. Scale bar, 100 µm.* ***D,*** *Same larva as in (**C**) at a different focal plane. The pretectal region is here in focus.* ***E,*** *Schematic illustration of the experimental setup. Movies (a moving grating pattern, a moving bar or moving random dots) were projected by a Laser Pico Projector onto a small screen in front of one larval eye while neuronal activity was recorded using a fluorescence widefield microscope.* ***F,*** *Example of fluorescence changes (ΔF/F) in a region of interest within the contralateral (left) tectal neuropil in response to a visual stimulus (a moving bar). Average from 5 trials. Grey bar represents time of visual stimulation of the right eye.* ***G,*** *Example of fluorescence changes (ΔF/F) in a region of interest in the hindbrain in response to a visual stimulus consisting of random dots. Average from 7 trials. Time of visual stimulation is indicated by the grey bar.*

Taken together, these data indicate that the *mitfa$^{-/-}$; Tg(elavl3:GCamp5)* line may be suitable for studying activation of neuronal circuits throughout the larval brain. However, as data are still highly variable and specific responses are often covered by spontaneous activity, the setup needs to be optimized. A highly sensitive camera would allow a higher frame rate and a more precise detection of fluorescence changes. The visual stimulus could be presented on a miniaturized LCD display as described in the literature (e.g. (Niell and Smith, 2005; Muto et al., 2013)) instead of being projected. Different stimuli could be tested since they may differ in their stimulation properties on tectal and hindbrain cells. To study neuronal activity in *bel* larvae, we crossed the transgenic line with heterozygous *bel* carriers generating a new *bel$^{+/-}$; mitfa$^{-/-}$; Tg(elavl3:GCamp5)* zebrafish line (*see* Materials and Methods).

## 6.5 Conclusions and Outlook

In this study, we described visually-driven postural instabilities in *bel* larvae with asymmetric innervations of optic nerve fibers to the two retinocipient brain hemispheres. The extent of asymmetric innervations correlated with the extent of postural instabilities, suggesting that misinterpretation of visual input due to an asymmetric distribution of afferents in the visual centers of the brain leads to postural instabilities. We proposed that

asymmetric innervations might lead to a stronger output from one brain hemisphere upon visual stimulation and as consequence to an imbalance of motor commands to the muscles during swimming.

The visually-driven postural instabilities described here have been observed in mutants with defects in either the vestibular or the somatosensory system (Granato et al., 1996; Whitfield et al., 1996; Nicolson et al., 1998), suggesting that the visual system is a component of the input system integrated by the brain for postural control. The phenotype was almost completely rescued in the dark, suggesting that visual input is not necessary to maintain balance and that the absence of vision can be compensated by inputs from vestibular and somatosensory systems. In contrast, the presence of postural instabilities under light conditions indicate that a wrong or misinterpreted visual input cannot be compensated by other sensory systems. Thus, a malfunctioning component of postural control can have more adverse effects than its absence.

To rule out any effect of an impaired vestibular or somatosensory system, a careful morphological and functional analysis of the inner ear and of the lateral line should be carried out in *bel* larvae. Morphology can be assessed by DIC images, fluorescein-phalloidin staining for actin in hair cell stereocilia and DASPEI live staining of lateral line hair cells as described by Whitfield et al. (Whitfield et al., 1996). Functionality of the inner ear and of the lateral line could be easily assessed by testing the Vibrational Startle Reflex, a response to water-borne vibrations (Nicolson et al., 1998): Tapping on the petri dish causes a quick escape of wt larvae. In *bel* mutant misrouting of optic nerve fibers has been well characterized. A whole-mount antibody staining against acetylated-tubulin would allow to visualize all axon tracts in order to rule out misrouting of additional fibers throughout the brain, which - on a theoretical basis - could play a role in postural control.

The conceptual model described above could be confirmed by calcium imaging experiments with the newly generated fish line *bel$^{+/-}$; mitfa$^{-/-}$; Tg(elavl3:GCamp5)*. The intensity of neuronal input reaching the two brain hemispheres can be quantified by measuring the change in mean fluorescence in the tectal neuropil upon binocular visual stimulation. If our model holds true, we expect to see a symmetric distribution of neuronal activity between the two neuropils in a wt larva but more activity in one neuropil in larvae with postural instabilities. The intensity of neuronal output can be quantified by measuring the change in mean fluorescence after visual stimulation in the tectal cells and in the hindbrain. The circuit involved in postural control is still unknown, but several neurons in the hindbrain projecting to the spinal cord drive basic motor patterns (Orger et al., 2008). Activity in the hindbrain is segregated on the two hemispheres depending on swimming direction (Ahrens et al., 2013). This segregation might be disrupted in larvae with postural instabilities.

## 6.6 References

Ahrens MB, Huang KH, Narayan S, Mensh BD, Engert F (2013) Two-photon calcium imaging during fictive navigation in virtual environments. Front Neural Circuits 7:104.

Akerboom J et al. (2012) Optimization of a GCaMP calcium indicator for neural activity imaging. J Neurosci 32:13819–13840.

Beck JC, Gilland E, Tank DW, Baker R (2004) Quantifying the ontogeny of optokinetic and vestibuloocular behaviors in zebrafish, medaka, and goldfish. J Neurophysiol 92:3546–3561.

Coombs S, Janssen J, Webb J (1988) Diversity of Lateral Line Systems. Evolutionary and Functional Considerations. In: Sensory Biology of Aquatic Animals (Atema J, Fay R, Popper A, Tavolga W, eds), pp 553–593. New York: Springer New York.

Cox KJ, Fetcho JR (1996) Labeling blastomeres with a calcium indicator. a non-invasive method of visualizing neuronal activity in zebrafish. J Neurosci Methods 68:185–191.

Gnuegge L, Schmid S, Neuhauss SC (2001) Analysis of the activity-deprived zebrafish mutant macho reveals an essential requirement of neuronal activity for the development of a fine-grained visuotopic map. J Neurosci 21:3542–3548.

Gobel W, Helmchen F (2007) In vivo calcium imaging of neural network function. Physiology (Bethesda) 22:358–365.

Granato M, van Eeden, F. J., Schach U, Trowe T, Brand M, Furutani-Seiki M, Haffter P, Hammerschmidt M, Heisenberg CP, Jiang YJ, Kane DA, Kelsh RN, Mullins MC, Odenthal J, Nusslein-Volhard C (1996) Genes controlling and mediating locomotion behavior of the zebrafish embryo and larva. Development 123:399–413.

Haffter P, Granato M, Brand M, Mullins MC, Hammerschmidt M, Kane DA, Odenthal J, van Eeden, F. J., Jiang YJ, Heisenberg CP, Kelsh RN, Furutani-Seiki M, Vogelsang E, Beuchle D, Schach U, Fabian C, Nusslein-Volhard C (1996) The identification of genes with unique and essential functions in the development of the zebrafish, Danio rerio. Development 123:1–36.

Huang Y, Tschopp M, Neuhauss, Stephan C F (2009) Illusionary self-motion perception in zebrafish. PLoS ONE 4:e6550.

Huber-Reggi SP, Chen CC, Grimm L, Straumann D, Neuhauss SC, Huang MY (2012) Severity of infantile nystagmus syndrome-like ocular motor phenotype is linked to the extent of the underlying optic nerve projection defect in zebrafish belladonna mutant. J Neurosci 32:18079–18086.

Karlstrom RO, Trowe T, Klostermann S, Baier H, Brand M, Crawford AD, Grunewald B, Haffter P, Hoffmann H, Meyer SU, Muller BK, Richter S, van Eeden, F. J., Nusslein-Volhard C, Bonhoeffer F (1996) Zebrafish mutations affecting retinotectal axon pathfinding. Development 123:427–438.

Lister JA, Robertson CP, Lepage T, Johnson SL, Raible DW (1999) nacre encodes a zebrafish microphthalmia-related protein that regulates neural-crest-derived pigment cell fate. Development 126:3757–3767.

Massion J (1994) Postural control system. Curr Opin Neurobiol 4:877–887.

Maurer C, Mergner T, Bolha B, Hlavacka F (2000) Vestibular, visual, and somatosensory contributions to human control of upright stance. Neurosci Lett 281:99–102.

Mullins MC, Hammerschmidt M, Haffter P, Nusslein-Volhard C (1994) Large-scale mutagenesis in the zebrafish: in search of genes controlling development in a vertebrate. Curr Biol 4:189-202.

Muto A, Ohkura M, Abe G, Nakai J, Kawakami K (2013) Real-time visualization of neuronal activity during perception. Curr Biol 23:307–311.

Nakai J, Ohkura M, Imoto K (2001) A high signal-to-noise Ca(2+) probe composed of a single green fluorescent protein. Nat. Biotechnol. 19:137–141.

Nicolson T (2005) The genetics of hearing and balance in zebrafish. Annu Rev Genet 39:9–22.

Nicolson T, Rusch A, Friedrich RW, Granato M, Ruppersberg JP, Nusslein-Volhard C (1998) Genetic analysis of vertebrate sensory hair cell mechanosensation. the zebrafish circler mutants. Neuron 20:271–283.

Niell CM, Smith SJ (2005) Functional imaging reveals rapid development of visual response properties in the zebrafish tectum. Neuron 45:941–951.

Nüsslein-Volhard C, Dahm R (2002) Zebrafish. A practical approach / edited by Christiane Nüsslein-Volhard and Ralf Dahm. Oxford: Oxford University Press.

O'Donovan M, Ho S, Sholomenko G, Yee W (1993) Real-time imaging of neurons retrogradely and anterogradely labelled with calcium-sensitive dyes. J Neurosci Methods 46:91–106.

Orger MB, Kampff AR, Severi KE, Bollmann JH, Engert F (2008) Control of visually guided behavior by distinct populations of spinal projection neurons. Nat Neurosci 11:327–333.

Park HC, Kim CH, Bae YK, Yeo SY, Kim SH, Hong SK, Shin J, Yoo KW, Hibi M, Hirano T, Miki N, Chitnis AB, Huh TL (2000) Analysis of upstream elements in the HuC promoter leads to the establishment of transgenic zebrafish with fluorescent neurons. Dev. Biol. 227:279–293.

Pineda RH, Heiser RA, Ribera AB (2005) Developmental, molecular, and genetic dissection of INa in vivo in embryonic zebrafish sensory neurons. J Neurophysiol 93:3582–3593.

Ramdya P, Engert F (2008) Emergence of binocular functional properties in a monocular neural circuit. Nat. Neurosci. 11:1083–1090.

Ribera AB, Nusslein-Volhard C (1998) Zebrafish touch-insensitive mutants reveal an essential role for the developmental regulation of sodium current. J Neurosci 18:9181–9191.

Rick JM, Horschke I, Neuhauss SC (2000) Optokinetic behavior is reversed in achiasmatic mutant zebrafish larvae. Curr Biol 10:595–598.

Simoneau G, Ulbrecht J, Derr J, Cavanagh P (1995) Role of somatsensory input in the control of human posture. Gait & Posture 3:115–122.

Straube A, Paulus W, Brandt T (1990) Influence of visual blur on object-motion detection, self-motion detection and postural balance. Behav Brain Res 40:1–6.

Straw AD (2008) Vision egg. an open-source library for realtime visual stimulus generation. Front Neuroinformatics 2:4.

Trowe T, Klostermann S, Baier H, Granato M, Crawford AD, Grunewald B, Hoffmann H, Karlstrom RO, Meyer SU, Muller B, Richter S, Nusslein-Volhard C, Bonhoeffer F (1996) Mutations disrupting the ordering and topographic mapping of axons in the retinotectal projection of the zebrafish, Danio rerio. Development 123:439–450.

Whitfield TT, Granato M, van Eeden, F J, Schach U, Brand M, Furutani-Seiki M, Haffter P, Hammerschmidt M, Heisenberg CP, Jiang YJ, Kane DA, Kelsh RN, Mullins MC, Odenthal J, Nüsslein-Volhard C (1996) Mutations affecting development of the zebrafish inner ear and lateral line. Development 123:241–254.

# Chapter 7

# General Discussion and Conclusion

## 7.1 Overview

A central goal of neuroscience is to understand sensory motor transformation: How sensory inputs are integrated and decoded by higher brain functions to produce an appropriate behavior in real time. Two forms of sensory information can be distinguished: An exafferent signal carrying information about the external world (e.g. about motion in the environment, odors or touching objects) and a reafferent signal about self-generated sensory stimuli (e.g. about own motion). Initially, exafferent signals elicit the behavioral response. Subsequently, both a copy of the motor command (the expected value) and the reafferent signal (the actual value) are sent back to the brain, where they are compared. If there is a difference between them, behavior is adapted accordingly. It is not surprisingly that miswiring of any involved neural circuit can affect those complex feedback loops leading to instabilities in motor behavior. In the present PhD Thesis, we have shown that miswiring of the retinotectal system (i.e. misprojection of the optic nerve) is associated with ocular motor (Chapters 3 to 5) and postural (Chapter 6) instabilities in zebrafish.

Key players in sensory motor transformation in the zebrafish are the pretectal region and the optic tectum, homologous to the mammalian superior colliculus, in which inputs from different sensory systems are integrated (Hall and Moschovakis, 2003). The architecture of the optic tectum is more complex compared to its mammalian homologue and it is likely that the tectum is involved in integration functions that would be accomplished by the neocortex in higher vertebrates (Friedrich et al., 2010). The retinotectal system converts moving visual inputs to an appropriate motor output (Nevin et al., 2010), thus perturbation of its wiring mechanisms may help understanding how visual inputs are integrated to produce a motor behavior. In the zebrafish mutant *belladonna* (*bel*) pathfinding of optic nerve fibers at the optic chiasm is downregulated, resulting in a variable fraction of fibers misprojecting to the wrong brain hemisphere. Whereas in wild-type (wt) zebrafish larvae all fibers cross at the optic chiasm and project to the contralateral tectal region, in *bel* some or all fibers run to the ipsilateral tectal region and project to the right position in the wrong hemisphere (Karlstrom et al., 1996; Neuhauss et al., 1999; Rick et al., 2000). In contrast to other pathfinding mutants, in *bel* miswiring is restricted to the forebrain and other commissures seem to project normally (Karlstrom et al., 1996). Thus, the effect of retinotectal miswiring on sensory motor control can be studied directly.

In this thesis, we performed correlation studies between different retinotectal projection phenotypes and motor behavior in *bel* larvae. In Chapter 4 we demonstrated that projection of the optic nerve fibers to the wrong brain hemisphere affects ocular motor behavior. Misprojection of some fibers leads to a reduction of the

optokinetic response (OKR) and misprojection of the majority of fibers leads to a reversal of the OKR. Those results confirmed our previously formulated hypothesis that optic nerve misrouting to the wrong hemisphere turns a negative feedback loop that would aim at stabilizing a moving environment on the retina, into a positive feedback loop which increases motion perception (Rick et al., 2000; Huang et al., 2006). Probably because of the positive feedback loop, larvae in which the majority of fibers are misprojecting display spontaneous eye oscillations (SOs) in the absence of a moving environment, a landmark of Infantile Nystagmus Syndrome (INS). INS is a congenital human disorder characterized by involuntary conjugate and mostly horizontal oscillations of the eyes, often accompanied by a poorly formed or even reversed OKR (CEMASWorkingGroup, 2001). The etiology of INS is still poorly understood but most likely many mechanisms can lead to SOs. We presented a mechanism that leads to SOs in zebrafish and that could play a role in human patients as well, since optic nerve pathfinding errors have been observed in some patients (McCarty et al., 1992; Apkarian et al., 1994; Jeffery, 1997; van Genderen et al., 2006). SOs in *bel* closely resemble oscillations in human patients and assume the same waveforms described by Dell'Osso and Daroff in humans (Dell'Osso and Daroff, 1975) (*see* Chapter 3). The etiology of single waveforms is unclear and a matter of debate (e.g. (Optican and Zee, 1984; Hertle and Dell'Osso, 1999; Jacobs and Dell'Osso, 2004; Dell'Osso, 2006; Dell'Osso et al., 2007; Akman et al., 2012)). In Chapter 5 we showed that in zebrafish *bel* mutant all waveforms often co-occurred in the same individual and were influenced by viewing conditions, suggesting that they are not indicative of the underlying morphological phenotype.

In Chapter 6, we described the effect of asymmetric visual input on postural control in *bel*. Those larvae in which more fibers projected to one brain hemisphere than to the other displayed visually-driven postural instabilities along the longitudinal body axis. We proposed that asymmetric innervations might lead to imbalance in outputs from the two hemispheres upon visual stimulation and thus to an imbalance of motor commands to the muscles during swimming.

## 7.2 *belladonna* as a disease model for Infantile Nystagmus Syndrome

The common feature in INS patients is the presence of spontaneous eye oscillations in the absence of movement in the surround. Those oscillations are frequently associated with additional congenital sensory disorders affecting the cornea, lens, retina or the optic nerve, but can also occur in the apparent absence of any other pathology (reviewed in (Khanna and Dell'Osso, 2006)). The etiology of the oscillations has been a matter of debate for decades and is still poorly understood. Some researchers suggested that the oscillations may be of motor nature and may result from a defect in the internal gain calibration of one of the ocular motor subsystems (Harris, 1995; Broomhead et al., 2000; Jacobs and Dell'Osso, 2004). Such a motor defect would not be related to concomitant sensory disorders which would be a separated entity (Dell'Osso, 2006). Other researchers consider INS as a developmental disorder in which sensory defects may interfere with the calibration of the visual system during intrauterine and early postnatal development. Thus, the oscillations could be an adaptive response to altered visual conditions during development (Tusa et al., 2002; Harris and Berry, 2006). Another model suggested that oscillations may be a direct consequence of abnormal positive feedback loops caused by neuronal miswiring (Optican and Zee, 1984). Most hypotheses are based on mathematical models, due to the absence of a suitable animal model. Until recently, the only animal model that displayed INS-like eye oscillations has been a

family of mutant Belgian Sheepdogs that exhibit achiasmia (Dell'Osso and Williams, 1995). However, dogs as model organisms have obvious problems related to breeding and life span. During the last years new possible animal models were introduced: Some albino mice strains described by Traber et al. (Traber et al., 2012) and the zebrafish mutant *belladonna* (Rick et al., 2000; Huang et al., 2006). All animal models display misrouting of optic nerve fibers, which has been suggested as the cause of eye oscillations (Dell'Osso and Williams, 1995; Rick et al., 2000; Huang et al., 2006; Traber et al., 2012). Here, we demonstrated that indeed misrouting of optic nerve fibers turns the normally negative feedback loop of the OKR into a positive one and leads to ocular motor instabilities in *bel*. In contrast, additional sensory defects present in *bel* were not related to ocular motor behavior (*see* Chapter 4). Many INS patients suffer from albinism (Sarvananthan et al., 2009), a condition characterized by hypopigmentation, fovea hypoplasia and misrouting of temporal optic nerve fibers (excessive crossing at the optic chiasm) (reviewed in (Summers, 2009)). Misrouting of optic nerve fibers has also been observed in other patients with INS-like eye oscillations, such as in congenital stationary night blindness (Tremblay et al., 1996), in the non-decussating retinal-fugal fiber syndrome (Apkarian et al., 1994) or in other forms of chiasmal misrouting not related to albinism (McCarty et al., 1992; van Genderen et al., 2006).

Optic nerve miswiring has not been described in other INS cases (e.g. (Apkarian and Shallo-Hoffmann, 1991; Shallo-Hoffmann and Apkarian, 1993)) suggesting that different mechanisms may lead to the same oscillations. On the other hand, optic nerve miswiring may be an under-diagnosed condition for two reasons. First, projection of the optic nerve is not routinely investigated during ophthalmic examination of INS patients. Second, the method of choice to diagnose a misrouting phenotype is nowadays the Visual Evoked Potential (VEP), which measures electrical potentials in the visual cortex that are triggered by short visual stimuli. VEP is an indirect way of detecting optic nerve pathway abnormalities and, although it works reliably for albinism, it may not detect other subtle forms of misprojection. Tractography of the optic chiasm may be a more reliable approach and, if used routinely, may help elucidate the real incidence of optic nerve fibers misrouting among INS patients.

In INS patients usually only a subset of optic nerve fibers misproject at the chiasm, while in *bel* only larvae with a large fraction of misprojecting fibers display a reversed OKR and SOs. Moreover, a reversed OKR is not always observed in human patients (e.g. (Halmagyi et al., 1980; Yee et al., 1980; Collewijn et al., 1985)). One possible explanation for this paradox lays in the full-field stimulation commonly used in the clinics. A stronger phenotype, incl. a reversed OKR, could be expected if only the portion of the retina is stimulated, where misrouting fibers originate from (e.g. the temporal retina in albino patients). This principle has nicely been demonstrated by Traber et al. in albino mice: During full-field stimulation, all albino strains showed a reduced but proper directed OKR, whereas during stimulation only of the anterior field (i.e. of the temporal retina), the OKR became reversed. Analogously, spontaneous eye oscillations in the presence of a stationary structured background increased in albino strains if the visual field was restricted (Traber et al., 2012).

The *bel* mutant as an animal model for INS has four main drawbacks. First, the visual system of zebrafish lacks a gaze-shifting mechanism, the smooth pursuit, which may interact with the OKR in higher vertebrates (Land, 1999; Schweigart et al., 1999; Delgado-García, 2000) and may be directly involved in the etiology of INS (Dell'Osso, 2006). The absence of smooth pursuit in zebrafish may be seen as an advantage since the role of the OKR can be studied without the interference of the smooth pursuit. However, the system may be oversimplified compared to the human condition. Hence, an important aspect possibly involved in the etiology of human INS is

missing in zebrafish. Second, in contrast to human INS, in *bel* larvae SOs are discontinued in darkness (Huang et al., 2006), as expected from a visually-driven behavior. This difference could be explained by adaptive mechanisms in humans during development. Thus, the larval zebrafish may miss an important component of human INS in spite of being a good model to study the origin of SOs without the complication of adaptive mechanisms. Adaptive mechanisms could be investigated by raising the larvae to adulthood and by following the disease throughout development. Third, see-saw nystagmus has been described in addition to INS-like horizontal nystagmus with classical waveforms in both non-decussating retinal-fugal fiber syndrome and achiasmatic Belgian Sheepdog (Dell'Osso and Daroff, 1998; Dell'Osso et al., 1998). See-saw nystagmus is characterized by conjugate torsional as well as disconjugate vertical eye movements that mimic the motion of a child's see-saw (Dell'Osso et al., 1998). We did not observe see-saw nystagmus in *bel* larvae but this may be due to the experimental conditions that make it difficult to detect torsional and vertical eye movements. Finally, the underlying genetic background (a mutation in the transcription factor *lhx2*) is most likely not informative since the phenotype in INS patients would be expected to be much more severe if they were carrying a mutation in the *lhx2* gene. *Lhx2* is essential for eye morphogenesis in mice and *Lhx2* knock-out mice mutants have a highly reduced telencephalon, no eyes and die *in utero* (Porter et al., 1997; Gordon et al., 2013; Roy et al., 2013). The relatively mild phenotype in *bel* may be due to redundancy with another transcription factor of the same family, *lhx9*, in most tissues (Ando et al., 2005; Peukert et al., 2011). Thus, *bel* is behaviorally comparable with INS but not genetically, as already pointed out previousy (Huang et al., 2006).

In spite of the different genetic background, *bel* larvae and INS patients might have an impairment in axonal growth in common. Recently, genetic studies have started to elucidate the molecular background of INS. Several genes have been related to INS, although most of them are indirectly related to INS (Proudlock and Gottlob, 2011). Few years ago, mutations in the FERM domain containing 7 (*FRMD7*) gene have been identified in idiopathic forms of INS (Tarpey et al., 2006). FRMD7 has been shown to be expressed in developing structures of the human embryo involved in the vestibular ocular response (VOR) and in the OKR such as the cerebellum, the vestibular apparatus and the retina, especially the developing optic nerve (Tarpey et al., 2006; Thomas et al., 2011). FRMD7 plays a role in neurite outgrowth and branching (Betts-Henderson et al., 2010), further suggesting that axonal growth during development may be involved in the pathogenesis of INS. Thomas et al. suggested that miswiring of developing OKR and VOR systems due to mutations in the *FRMD7* gene might predispose for INS (Thomas et al., 2011).

In summary, in this PhD Thesis we could demonstrate that a reversed visual input caused by misrouting of optic nerve fibers can directly trigger INS-like ocular motor abnormalities in an experimental animal model by turning a normally negative feedback loop into a positive one. Since visual pathway abnormalities are present in a subset of INS patients and are most likely under diagnosed, we suggest that the same mechanism may explain some cases of human INS. Moreover, any other mechanism that can lead to a reversal of the OKR feedback loop (such as miswiring of afferents from extraocular muscles (Optican and Zee, 1984)), may have a similar effect on ocular motor stability.

## 7.3 Visual postural control in zebrafish

Another intriguing behavior in *bel* mutants is a loss of postural control on the longitudinal body axis similar to corkscrew-like swimming patterns previously described in mutants with vestibular deficits (Granato et al., 1996; Whitfield et al., 1996). Postural instability in *bel* mutants are visually driven (*see* Chapter 6) and are, to our best knowledge, the first example of loss of balance due to a disrupted visual input in zebrafish. Huang et al. previously described another swimming behavior in *bel* larvae, best defined as looping around a central axis (Huang et al., 2009). However, in these larvae postural stability on the longitudinal body axis is not affected and looping is most likely caused by an illusionary self-motion perception in larvae with INS-like behavior (Huang et al., 2009).

Postural control is achieved by integration of inputs from different sensory systems that are partially redundant (Straube et al., 1990; Massion, 1994; Simoneau et al., 1995; Maurer et al., 2000). Thus, a blind patient is able to maintain posture with the help of vision independent cues. Zebrafish larvae are able to maintain balance in the absence of vision in complete darkness. In Chapter 6 of this PhD Thesis we could show that, in contrast to an absent visual input, a misleading visual input can affect postural control even in the presence of additional sensory information. We established a correlation between asymmetric innervations of the two brain hemispheres by optic nerve fibers and postural instabilities. Calcium imaging experiments will allow to measure neuronal activity and to investigate if asymmetric innervations indeed lead to asymmetric sensory input as well as asymmetric output to the motor centers. Future experiments need to visually stimulate the restrained larva and simultaneously measure calcium signals in both tectal neuropils (reflecting the afferent sensory signal), in the tectal cells, and in the hindbrain targets (reflecting motor command output). Recently, neural correlates of swimming bursts to the left and to the right have been imaged in the hindbrain: Ahrens et al. could elegantly show a left-right segregation of activity, depending on the swimming direction (Ahrens et al., 2013a). Asymmetric output to the motor centers in *bel* larvae may disrupt this segregation. The work presented in Chapter 6 on visual-postural control combined with functional imaging would set the basis to study the so far unknown circuit involved in visual-postural control.

## 7.4 Circuit neuroscience in zebrafish

The zebrafish started to become a popular model organism for *in vivo* calcium imaging during the last years. Compared to the mouse model, the zebrafish brain is easily accessible and its small size allows for simultaneously imaging of broad brain areas. The transparent larval brain is only 500 µm thick and 1.5 mm long, allowing imaging of internal structures, which would be covered by the neocortex in mammals. Many behaviors are stereotyped and are regulated by relatively simple circuits, making it comparably easy to study them. At the same time, the zebrafish shares neurochemistry and broad brain organization with higher vertebrates so that insights from zebrafish studies can be related to mammals. For reviews on possible advantages of zebrafish in circuit neuroscience *see* (Friedrich et al., 2010) and (Leung et al., 2013).

Neural activity in broad brain areas can be measured by means of pan-neuronally expressed genetically encoded calcium indicators (GECIs). GECIs with increasing sensitivity have been successfully developed in the

last years (Nakai et al., 2001; Tian et al., 2009; Muto et al., 2011; Akerboom et al., 2012; Chen et al., 2013; Muto et al., 2013) although most of them are still less sensitive than synthetic calcium indicators such as Oregon-Green-BAPTA-1 (Akerboom et al., 2012).

A challenging aspect of calcium imaging during behavior are the movement artifacts arising from the behaving larva. Successful imaging from freely swimming larvae has been reported recently by Muto and colleagues, who solved the problem by analyzing neural activity only when the larva did not move between bouts of swimming activity (Muto et al., 2013). An alternative approach to study neural circuits involved in visually induced locomotion is to work with partially restrained larvae whereby the trunk and the head are restrained in agarose, while the tail is free to move (Sumbre and Poo, 2013). However, this technique has a main drawback: Since the trunk is restrained, swimming behavior does not per se give rise to adaptation to a stimulus (e.g. a moving visual stimulus) and a closed-feedback loop cannot be generated. To overcome this problem, researchers mainly around Florian Engert have started to investigate behavior in a closed-loop virtuality setup, in which the reafferent signal recorded from the larva is used to adapt the stimulus (reviewed in (Engert, 2013)).

Ideally, the whole brain is imaged during behavior and neural activity is recorded at single cell resolution. Towards this ambitious goal, a number of technical aspects need to be considered (*see* (Muto and Kawakami, 2013) for a review on advantages and disadvantages of different imaging techniques). Although broad regions can be imaged with a fluorescence widefield microscope quite easily, resolution along the z-axis is low. In contrast, a two-photon microscope allows very good spatial resolution and deep penetration in a scattering tissue thanks to the excitation laser in the infra-red range, but has a low temporal resolution. The breakthrough towards the aim of whole brain imaging at single cell resolution came from further development of the laser scanning light sheet microscopy technology to allow high-speed three-dimensional recording. In light sheet microscopy, the excitation light is originating from a focused laser beam placed orthogonally to the detection system (reviewed in (Huisken and Stainier, 2009). Step-wise axial movement of either the detection objective and the light sheet or the sample allows fast scanning through the volume of the sample (Ahrens et al., 2013b; Panier et al., 2013). The drawback of light sheet microscopy, as any method using visible excitation light, is that the excitation light itself can activate the visual system leading to artifacts and therefore may interfere with visually driven behavior. A combination of light sheet microscopy with excitation in the infrared range could alleviate these problems (Truong et al., 2011).

To identify the imaged cells an anatomical annotation needs to be available. Although some databases exist already, they are far from being as complete as their counterparts in other model organisms (reviewed in (Arrenberg and Driever, 2013)). Therefore, the precise annotation of the identified neural circuits is still one of the biggest problems in zebrafish neuroscience. This may change in the near future due to much improved annotations, e.g. Virtual Brain Explorer for Zebrafish, a computational framework to align expression patterns to a reference brain (Ronneberger et al., 2012).

Taken together, the zebrafish is emerging as a great model organism for *in-vivo* circuit analysis in 4D, at cellular resolution and in the whole brain. This is made possible by the inherent advantages of the organism and by the constantly improvement of GECIs, genetic tools and imaging methods.

## 7.5 Concluding remarks

In the present thesis, we studied wiring mechanisms in the retinotectal system that allow visual input processing and motor behavior. We have shown the effects of axonal misrouting at the optic chiasm on ocular motor and postural control in the zebrafish larva, what not only helps to understand how the brain integrates sensory stimuli, but also gives insights on how the brain deals with contradictory and misleading inputs in health and disease. We now understand more deeply how miswiring to the wrong brain hemisphere affects ocular motor behavior and triggers INS in zebrafish. Additionally, the observation that miswiring can lead to postural instability - most likely because of an asymmetric distribution of motor commands - may be of relevance for further understanding of human disease. A combination of further characterization of miswiring phenotypes, genetics and functional *in vivo* imaging in the zebrafish will shape future neuroscience and will contribute to the characterization of basic mechanisms underlying behavior in health and disease.

## 7.6 References

Ahrens MB, Huang KH, Narayan S, Mensh BD, Engert F (2013a) Two-photon calcium imaging during fictive navigation in virtual environments. Front Neural Circuits 7:104.

Ahrens MB, Orger MB, Robson DN, Li JM, Keller PJ (2013b) Whole-brain functional imaging at cellular resolution using light-sheet microscopy. Nat Methods 10:413–420.

Akerboom J et al. (2012) Optimization of a GCaMP calcium indicator for neural activity imaging. J Neurosci 32:13819–13840.

Akman OE, Broomhead DS, Abadi RV, Clement RA (2012) Components of the neural signal underlying congenital nystagmus. Exp Brain Res 220:213–221.

Ando H, Kobayashi M, Tsubokawa T, Uyemura K, Furuta T, Okamoto H (2005) Lhx2 mediates the activity of Six3 in zebrafish forebrain growth. Dev Biol 287:456–468.

Apkarian P, Bour L, Barth PG (1994) A unique achiasmatic anomaly detected in non-albinos with misrouted retinal-fugal projections. Eur J Neurosci 6:501–507.

Apkarian P, Shallo-Hoffmann J (1991) VEP projections in congenital nystagmus; VEP asymmetry in albinism. a comparison study. Invest Ophthalmol Vis Sci 32:2653–2661.

Arrenberg AB, Driever W (2013) Integrating anatomy and function for zebrafish circuit analysis. Front Neural Circuits 7:74.

Betts-Henderson J, Bartesaghi S, Crosier M, Lindsay S, Chen HL, Salomoni P, Gottlob I, Nicotera P (2010) The nystagmus-associated FRMD7 gene regulates neuronal outgrowth and development. Hum Mol Genet 19:342–351.

Broomhead DS, Clement RA, Muldoon MR, Whittle JP, Scallan C, Abadi RV (2000) Modelling of congenital nystagmus waveforms produced by saccadic system abnormalities. Biol Cybern 82:391–399.

CEMASWorkingGroup (2001) A classification of eye movement abnormalities and strabismus (CEMAS). In: The National Eye Institute Publications: National Institutes of Health, National Eye Institute.

Chen T, Wardill, Trevor J., Sun Y, Pulver SR, Renninger SL, Baohan A, Schreiter ER, Kerr RA, Orger MB, Yayaraman V, Looger LL, Svoboda K, Kim DS (2013) Ultrasensitive fluorescent proteins for imaging neuronal activity. Nature 499:295–300.

Collewijn H, Apkarian P, Spekreijse H (1985) The oculomotor behaviour of human albinos. Brain 108 ( Pt 1):1–28.

Delgado-García JM (2000) Why move the eyes if we can move the head? Brain Res Bull 52:475–482.

Dell'Osso LF (2006) Biologically relevant models of infantile nystagmus syndrome. the requirement for behavioral ocular motor system models. Semin Ophthalmol 21:71–77.

Dell'Osso LF, Daroff RB (1975) Congenital nystagmus waveforms and foveation strategy. Doc Ophthalmol 39:155–182.

Dell'Osso LF, Daroff RB (1998) Two additional scenarios for see-saw nystagmus: achiasma and hemichiasma. J Neuroophthalmol 18:112–113.

Dell'Osso LF, Hertle RW, Daroff RB (2007) "Sensory" and "motor" nystagmus. erroneous and misleading terminology based on misinterpretation of David Cogan's observations. Arch Ophthalmol 125:1559–1561.

Dell'Osso LF, Williams RW (1995) Ocular motor abnormalities in achiasmatic mutant Belgian sheepdogs: unyoked eye movements in a mammal. Vision Res 35:109–116.

Dell'Osso LF, Williams RW, Jacobs JB, Erchul DM (1998) The congenital and see-saw nystagmus in the prototypical achiasma of canines: comparison to the human achiasmatic prototype. Vision Res 38:1629–1641.

Engert F (2013) Fish in the matrix: motor learning in a virtual world. Front Neural Circuits 6:125.

Friedrich RW, Jacobson GA, Zhu P (2010) Circuit neuroscience in zebrafish. Curr Biol 20:R371-81.

Gordon PJ, Yun S, Clark AM, Monuki ES, Murtaugh LC, Levine EM (2013) Lhx2 balances progenitor maintenance with neurogenic output and promotes competence state progression in the developing retina. J Neurosci 33:12197–12207.

Granato M, van Eeden, F. J., Schach U, Trowe T, Brand M, Furutani-Seiki M, Haffter P, Hammerschmidt M, Heisenberg CP, Jiang YJ, Kane DA, Kelsh RN, Mullins MC, Odenthal J, Nusslein-Volhard C (1996) Genes controlling and mediating locomotion behavior of the zebrafish embryo and larva. Development 123:399–413.

Hall WC, Moschovakis AK (2003) The Superior Colliculus. New Approaches for Studying. London: CRC Press.

Halmagyi GM, Gresty MA, Leech J (1980) Reversed optokinetic nystagmus (OKN). mechanism and clinical significance. Ann Neurol 7:429–435.

Harris C, Berry D (2006) A developmental model of infantile nystagmus. Semin Ophthalmol 21:63–69.

Harris CM (1995) Problems in modelling congenital nystagmus: towards a new model. In: Eye movement research: processes, mechanisms and applications (Findlay JM, Walker R, Kentridge RW, eds), pp 239–253. Amsterdam: Elsevier.

Hertle RW, Dell'Osso LF (1999) Clinical and ocular motor analysis of congenital nystagmus in infancy. J AAPOS 3:70–79.

Huang YY, Rinner O, Hedinger P, Liu SC, Neuhauss SC (2006) Oculomotor instabilities in zebrafish mutant belladonna. a behavioral model for congenital nystagmus caused by axonal misrouting. J Neurosci 26:9873–9880.

Huang YY, Tschopp M, Neuhauss SC (2009) Illusionary self-motion perception in zebrafish. PLoS One 4:e6550.

Huisken J, Stainier, Didier Y R (2009) Selective plane illumination microscopy techniques in developmental biology. Development 136:1963–1975.

Jacobs JB, Dell'Osso LF (2004) Congenital nystagmus. hypotheses for its genesis and complex waveforms within a behavioral ocular motor system model. J Vis 4:604–625.

Jeffery G (1997) The albino retina. an abnormality that provides insight into normal retinal development. Trends Neurosci 20:165–169.

Karlstrom RO, Trowe T, Klostermann S, Baier H, Brand M, Crawford AD, Grunewald B, Haffter P, Hoffmann H, Meyer SU, Muller BK, Richter S, van Eeden, F. J., Nusslein-Volhard C, Bonhoeffer F (1996) Zebrafish mutations affecting retinotectal axon pathfinding. Development 123:427–438.

Khanna S, Dell'Osso LF (2006) The diagnosis and treatment of infantile nystagmus syndrome (INS). ScientificWorldJournal 6:1385–1397.

Land MF (1999) Motion and vision: why animals move their eyes. J Comp Physiol A 185:341–352.

Leung LC, Wang GX, Mourrain P (2013) Imaging zebrafish neural circuit from whole brain to synapse. Front Neural Circuits 7:1–8.

Massion J (1994) Postural control system. Curr Opin Neurobiol 4:877–887.

Maurer C, Mergner T, Bolha B, Hlavacka F (2000) Vestibular, visual, and somatosensory contributions to human control of upright stance. Neurosci Lett 281:99–102.

McCarty JW, Demer JL, Hovis LA, Nuwer MR (1992) Ocular motility anomalies in developmental misdirection of the optic chiasm. Am J Ophthalmol 113:86–95.

Muto A, Kawakami K (2013) Prey capture in zebrafish larvae serves as a model to study cognitive functions. Front Neural Circuits 7:110.

Muto A, Ohkura M, Abe G, Nakai J, Kawakami K (2013) Real-time visualization of neuronal activity during perception. Curr Biol 23:307–311.

Muto A, Ohkura M, Kotani T, Higashijima S, Nakai J, Kawakami K (2011) Genetic visualization with an improved GCaMP calcium indicator reveals spatiotemporal activation of the spinal motor neurons in zebrafish. Proc Natl Acad Sci U S A 108:5425–5430.

Nakai J, Ohkura M, Imoto K (2001) A high signal-to-noise Ca(2+) probe composed of a single green fluorescent protein. Nat. Biotechnol. 19:137–141.

Neuhauss SC, Biehlmaier O, Seeliger MW, Das T, Kohler K, Harris WA, Baier H (1999) Genetic disorders of vision revealed by a behavioral screen of 400 essential loci in zebrafish. J Neurosci 19:8603–8615.

Nevin LM, Robles E, Baier H, Scott EK (2010) Focusing on optic tectum circuitry through the lens of genetics. BMC Biol 8:126.

Optican LM, Zee DS (1984) A hypothetical explanation of congenital nystagmus. Biol Cybern 50:119–134.

Panier T, Romano SA, Olive R, Pietri T, Sumbre G, Candelier R, Debrégeas G (2013) Fast functional imaging of multiple brain regions in intact zebrafish larvae using Selective Plane Illumination Microscopy. Front Neural Circuits 7.

Peukert D, Weber S, Lumsden A, Scholpp S (2011) Lhx2 and Lhx9 determine neuronal differentiation and compartition in the caudal forebrain by regulating Wnt signaling. PLoS Biol. 9:e1001218.

Porter FD, Drago J, Xu Y, Cheema SS, Wassif C, Huang SP, Lee E, Grinberg A, Massalas JS, Bodine D, Alt F, Westphal H (1997) Lhx2, a LIM homeobox gene, is required for eye, forebrain, and definitive erythrocyte development. Development 124:2935–2944.

Proudlock F, Gottlob I (2011) Foveal development and nystagmus. Ann N Y Acad Sci 1233:292–297.

Rick JM, Horschke I, Neuhauss SC (2000) Optokinetic behavior is reversed in achiasmatic mutant zebrafish larvae. Curr Biol 10:595–598.

Ronneberger O, Liu K, Rath M, Rueβ D, Mueller T, Skibbe H, Drayer B, Schmidt T, Filippi A, Nitschke R, Brox T, Burkhardt H, Driever W (2012) ViBE-Z: a framework for 3D virtual colocalization analysis in zebrafish larval brains. Nat Methods 9:735–742.

Roy A, Melo J de, Chaturvedi D, Thein T, Cabrera-Socorro A, Houart C, Meyer G, Blackshaw S, Tole S (2013) LHX2 is necessary for the maintenance of optic identity and for the progression of optic morphogenesis. J Neurosci 33:6877–6884.

Sarvananthan N, Surendran M, Roberts EO, Jain S, Thomas S, Shah N, Proudlock FA, Thompson JR, McLean RJ, Degg C, Woodruff G, Gottlob I (2009) The prevalence of nystagmus. the Leicestershire nystagmus survey. Invest Ophthalmol Vis Sci 50:5201–5206.

Schweigart G, Mergner T, Barnes G (1999) Eye movements during combined pursuit, optokinetic and vestibular stimulation in macaque monkey. Exp Brain Res 127:54–66.

Shallo-Hoffmann J, Apkarian P (1993) Visual evoked response asymmetry only in the albino member of a family with congenital nystagmus. Invest Ophthalmol Vis Sci 34:682–689.

Simoneau G, Ulbrecht J, Derr J, Cavanagh P (1995) Role of somatsensory input in the control of human posture. Gait & Posture 3:115–122.

Straube A, Paulus W, Brandt T (1990) Influence of visual blur on object-motion detection, self-motion detection and postural balance. Behav Brain Res 40:1–6.

Sumbre G, Poo MM (2013) Monitoring Tectal Neuronal Activities and Motor Behavior in Zebrafish Larvae. Cold Spring Harbor Protocols:873–879.

Summers CG (2009) Albinism: classification, clinical characteristics, and recent findings. Optom Vis Sci 86:659–662.

Tarpey P et al. (2006) Mutations in FRMD7, a newly identified member of the FERM family, cause X-linked idiopathic congenital nystagmus. Nat Genet 38:1242–1244.

Thomas MG, Crosier M, Lindsay S, Kumar A, Thomas S, Araki M, Talbot CJ, McLean RJ, Surendran M, Taylor K, Leroy BP, Moore AT, Hunter DG, Hertle RW, Tarpey P, Langmann A, Lindner S, Brandner M, Gottlob I (2011) The clinical and molecular genetic features of idiopathic infantile periodic alternating nystagmus. Brain 134:892–902.

Tian L, Hires SA, Mao T, Huber D, Chiappe ME, Chalasani SH, Petreanu L, Akerboom J, McKinney SA, Schreiter ER, Bargmann CI, Jayaraman V, Svoboda K, Looger LL (2009) Imaging neural activity in worms, flies and mice with improved GCaMP calcium indicators. Nat Methods 6:875–881.

Traber GL, Chen CC, Huang YY, Spoor M, Roos J, Frens MA, Straumann D, Grimm C (2012) Albino Mice as an Animal Model for Infantile Nystagmus Syndrome. Invest Ophthalmol Vis Sci 53:5737-5747.

Tremblay F, Becker I de, Cheung C, LaRoche GR (1996) Visual evoked potentials with crossed asymmetry in incomplete congenital stationary night blindness. Invest Ophthalmol Vis Sci 37:1783–1792.

Truong TV, Supatto W, Koos DS, Choi JM, Fraser SE (2011) Deep and fast live imaging with two-photon scanned light-sheet microscopy. Nat Methods 8:757–760.

Tusa RJ, Mustari MJ, Das VE, Boothe RG (2002) Animal models for visual deprivation-induced strabismus and nystagmus. Ann N Y Acad Sci 956:346–360.

van Genderen, M M, Riemslag, F C C, Schuil J, Hoeben FP, Stilma JS, Meire FM (2006) Chiasmal misrouting and foveal hypoplasia without albinism. Br J Ophthalmol 90:1098–1102.

Whitfield TT, Granato M, van Eeden, F. J., Schach U, Brand M, Furutani-Seiki M, Haffter P, Hammerschmidt M, Heisenberg CP, Jiang YJ, Kane DA, Kelsh RN, Mullins MC, Odenthal J, Nusslein-Volhard C (1996) Mutations affecting development of the zebrafish inner ear and lateral line. Development 123:241–254.

Yee RD, Baloh RW, Honrubia V (1980) Study of congenital nystagmus. optokinetic nystagmus. Br J Ophthalmol 64:926–932.

# *CURRICULUM VITAE*

## Personal Information


| | |
|---|---|
| Name: | Sabina Huber-Reggi |
| Present address: | Gässli 9, 5603 Staufen |
| Phone: | +41 62 891 25 60 |
| E-mail: | sabina.reggi@imls.uzh.ch |
| Date of birth: | 20.12.1984 |
| Place of birth: | Sorengo TI |
| Citizenship: | Switzerland |


## Academic Education

| | |
|---|---|
| since 04/2010 | PhD-Thesis in the Laboratory of Prof. Dr. Stephan Neuhauss at the Institute of Molecular Life Sciences, University of Zurich, Switzerland. Member of the PhD Program in Integrative Molecular Medicine (imMed) at the Life Science Zurich Graduate School. Title of the thesis: *Effects of Axonal Misrouting at the Optic Chiasm on Motor Behavior in Zebrafish Larvae.* |
| 06/2009 | Master in Cell Biology, ETH Zurich, Switzerland<br>Master Thesis in the Laboratory of Prof. Dr. Patrick Meraldi at the Institute of Biochemistry, ETH Zurich: *The Number of Centrosomes and Centrioles Affects Mitotic Progression in HeLa Cells.* |
| 2007 – 2009 | Graduate Studies in Cell Biology, ETH Zurich, Switzerland |
| 2004 – 2007 | Undergraduate Studies in Biology, ETH Zurich, Switzerland |
| 2000 – 2004 | Liceo Cantonale Lugano, Switzerland |
| 06/2004 | Matura with Major Subject ancient Greek |

## Professional Experience

| | |
|---|---|
| since 04/2010 | Teaching assistant, University of Zurich, Switzerland<br>Neurobiology courses for undergraduate students<br>Supervision of Research Projects of graduate students |
| 07/2012 - 07/2013 | Member of the Organizing Committee of the Vision 2020 seminar series, University of Zurich, Switzerland |
| 09/2009 - 02/2010 | Research assistant at the Division of Gastroenterology and Hepatology, University Hospital Zurich, Switzerland |

| | |
|---|---|
| 05/2009 - 07/2009 | Research assistant at the Institute of Biochemistry, ETH Zurich, Switzerland |
| 02/2007 - 03/2007 | Student research assistant at the Centre for Molecular Biology of Inflammation, Institute of Infectiology, Münster, Germany |

## Presentation at Meetings

| | |
|---|---|
| 08/2013 | 9th ZIHP Annual Symposium, Zurich, Switzerland<br>Poster: *Effect of asymmetric fiber crossing at the optic chiasm on visual-postural control in zebrafish larvae* |
| 07/2013 | 8th European Zebrafish Meeting, Barcelona, Spain<br>*Poster: Effect of asymmetric fiber crossing at the optic chiasm on visual-postural control in zebrafish larvae* |
| 04/2013 | 6th Swiss Zebrafish Meeting, Zurich, Switzerland<br>*Poster: Stimulus conditions determine waveform characteristics of eye oscillations in zebrafish with infantile nystagmus syndrome* |
| 08/2012 | 8th ZIHP Annual Symposium, Zurich, Switzerland<br>*Talk: Optic nerve misprojections in the zebrafish mutant belladonna: A disease model for infantile nystagmus syndrome* |
| 05/2012 | ARVO Annual Meeting, Fort Lauderdale, Florida, USA<br>*Talk: Optic nerve misprojections in the zebrafish mutant belladonna: A disease model for infantile nystagmus syndrome* |
| 01/2012 | Swiss Retina Meeting, Biel, Switzerland<br>*Talk: Optic nerve misprojections in the zebrafish mutant belladonna: A disease model for infantile nystagmus syndrome* |
| 08/2011 | 7th ZIHP Annual Symposium, Zurich, Switzerland<br>*Poster: Optokinetic response and eye oscillations in the zebrafish mutant belladonna: A disease model for infantile nystagmus syndrome* |
| 07/2011 | 7th European Zebrafish Meeting, Edinburgh, Scotland<br>*Poster: Optokinetic response and eye oscillations in the zebrafish mutant belladonna: A disease model for infantile nystagmus syndrome* |
| 06/2011 | imMed Annual Retreat, kleiner Scheidegg, Switzerland<br>Talk: *Optokinetic response and eye oscillations in the zebrafish mutant belladonna: A disease model for infantile nystagmus syndrome* |

## Scholarships

| | |
|---|---|
| 2012 | ARVO International Travel Grant |

## List of Publications

**Sabina P. Huber-Reggi**, Kaspar P. Mueller, Dominik Straumann, Melody YY Huang, Stephan C. Neuhauss
*Individual Zebrafish Larvae with Infantile Nystagmus Syndrome Display Multiple Nystagmus Waveforms, which Are Influenced by Viewing Conditions.*
Submitted for publication to *Investigative Ophthalmology & Visual Sciences*.

**Sabina P. Huber-Reggi**, Kaspar P. Mueller, Stephan C. Neuhauss
*Analysis of optokinetic response in zebrafish by computer based eye tracking.*
Published in *Ocular Molecular Biology, Retinal Degeneration: Methods and Protocols*, Methods in Molecular Biology, Humana Press, Vol 935 (2013).

**Sabina P. Huber-Reggi**, Chien-Cheng Chen, Lea Grimm, Dominik Straumann, Stephan C. Neuhauss, Melody YY. Huang
*Severity of Infantile Nystagmus Syndrome-Like Ocular Motor Phenotype Is Linked to the Extent of the Underlying Optic Nerve Projection Defect in Zebrafish belladonna Mutant.*
Published in *Journal of Neuroscience*, 32: 18079-18086 (2012).

Melody YY. Huang, Chien-Cheng Chen*, **Sabina P. Huber-Reggi***, Stephan C. Neuhauss, Dominik Straumann
*Comparison of infantile nystagmus syndrome in achiasmatic zebrafish and humans.*
** These authors contributed equally*
Published in *Annals of the New York Academy of Sciences*, 1233:285-291 (2011).

Claudio R. Thoma*, Alberto Toso*, Katrin L. Gutbrodt, **Sabina P. Reggi**, Ian J. Frew, Peter Schraml, Alexander Hergovich, Holger Moch, Patrick Meraldi, Wilhelm Krek
*VHL loss causes spindle misorientation and chromosome instability.*
** These authors contributed equally*
Published in *Nature Cell Biology*, 11:994-1001 (2009).

# *ACKNOWLEDGMENTS*

First and foremost I am very grateful to my mentor Dr Stephan Neuhauss for giving me the opportunity to do my PhD Thesis in his lab and for his constant support throughout all these years. I appreciate his way of supervision: Giving a lot of freedom but still keeping an eye on the activities and always being there for any support that is necessary. He transmits enthusiasm for research and helps us become independently-thinking scientists.

I would also like to thank the other members of my PhD Committee, Drs Christian Grimm, Dominik Straumann and Maarten Frens for all discussions, suggestions and critical questions during our meetings that helped me improve my work. I am grateful to Dr Melody Huang, my predecessor on the *belladonna* project, who initialized and coordinated our collaboration with the Neurology Department of the University Hospital Zurich within a bench-to-bed-side cooperative project. Thanks to her initiative I got the opportunity to participate in this project. I also would like to thank my fellow PhD student within the cooperative project, Chien-Cheng, for sharing his analysis software with me, and Fabian, my brother-in-law, for helping me modify some Matlab scripts.

Thanks to all present and former members of the Neuhauss-Lab for the great working atmosphere. It is an atmosphere of joy and enthusiasm for our work, and of motivation to do good research and to help each other. I appreciate the nice and funny time in the lab and at conferences or during journeys and free time activities. Special thanks go to Matthias, the boss's right-hand, for sharing his advices on many aspects of research and for critical reading of my manuscripts. My work would not have been possible without the help of Kara, who takes so much effort in keeping our fish healthy and happy and in maintaining order in the lab. Thank you Kara for everything! I am also grateful to Fränzi, Peter and the fishfeeders who support Kara in many ways. Special thanks go to Kaspar, who was always helpful whenever I needed some technical assistance or a new software for my experiments. It is amazing how efficiently he can help all of us besides his own research. Also many thanks to Marion for sharing many experiences during our life as PhD students, for the good conversations and for the nice time we have together. Thanks to both Marion and Dani for their help with the layout of my thesis. Last but not least, I would like to thank my students, Lea and Torben for their great contribution to my thesis. They did not only contribute to the scientific work, but also helped me grow as a person. I am specially thankful to Torben for his intellectual contribution that initiated our project on postural control.

I would like to take the opportunity to thank all my friends who made these years even more enjoyable. Special thanks go to Gaia for sharing and discussing many aspects of life and to the biologists from the "Ref'haus" (Basil, Josua, Pascale, and Stephanie). Without the constant mutual support and motivation we would not be where we are now.

I would like to express my gratitude to Dominique and his family, who always support me and share with me stressful and joyful moments. Last but not least, I would like to thank my grandmother for teaching me the courage to never give up and my family, my godfather, and his family for helping me in many ways and for being curious about my research.